CONSTRUCTION MATERIALS CONSULTANTS, INC.

Laboratory Analyses of A Stone & Masonry Mortars From Robert C Weaver Federal Building in Washington, D.C.

Robert C Weaver Federal Building (HUD)
451 7th Street SW
Washington, D.C.

March 25, 2020
CMC 0320114

TABLE OF CONTENTS

LABORATORY ANALYSES OF A STONE AND MASONRY MORTARS FROM ROBERT C WEAVER FEDERAL BUILDING IN WASHINTON, D.C.

EXECUTIVE SUMMARY

Located at 451 7th Street, SW in Washington, D.C. the Robert C. Weaver Federal Building is the headquarters of the U.S. Department of Housing and Urban Development (HUD). Constructed from 1965 to 1968 by the renowned architect Marcel Breuer, the building is recognized as the first federal building in the country to utilize precast concrete as the primary structural and exterior finish material, as well as the first fully modular design for a federal office building.

As part of the renovation process, two sets of masonry mortar samples were provided for detailed laboratory examinations. The first set comprises two samples from the original 1960s vintage, and the second set of two samples reportedly came from 2019 construction. The purpose of this laboratory examination is to determine the compositions and mix proportions of mortars from the original 1960s and recent 2019 constructions and evaluate their compatibilities and suitability for long-term performance of masonry walls. Additionally, a dark gray, dense hard crystalline stone masonry sample from the building was provided in two small pieces to determine the stone type.

Mortar samples were analyzed by comprehensive laboratory examinations following various industry standards, e.g., ASTM C 1324 and RILEM methods (Middendorf et al. 2004, 2005) starting with visual examinations, extensive optical microscopy, scanning electron microscopy and energy-dispersive X-ray microanalyses (SEM-EDS), followed by wet chemical (gravimetric) analyses, X-ray diffraction (XRD), energy-dispersive X-ray fluorescence spectroscopy (ED-XRF), thermal analyses (TGA, DTG, DSC), and, ion chromatography (IC) of water-soluble salts in mortars.

Visual examinations of mortar fragments from the original as well as recent construction showed apparent similarities in typical gray color tones of mortars found in many modern-day cement-lime or masonry cement mortars. Pieces in each mortar sample are reasonably dense, hard, and uniform in appearance confirming representative samples show no evidence of any contamination or odd-looking peace to indicate multiple pointing events. One of the two mortars (#5) from 2019 construction showed white efflorescence powder on a bedding face, which was subsequently determined by XRD studies to be calcium carbonate (calcite).

Optical microscopical examinations of mortars showed both similarities in basic ingredients across four mortars from original to recent constructions, as well as noticeable differences in sand and binder compositions. For the sand used in two original mortars from 1960s construction, both mortars (#2 and 3) showed use of compositionally similar sands, which are crushed siliceous sands consisting of major amounts of crushed silica (quartz) and minor amounts of quartzite, feldspar, and other siliceous components. Sands extracted from original mortars showed grain-size distributions having an abundance of finer grain sizes concentrated from crushing operations, which do not conform to grain size distribution of ASTM C 144 masonry sand. By contrast, sands used in the recent 2019 construction, though also siliceous, contain a noticeable amount of feldspar (albite), quartzite, mica and other siliceous components at subordinate amounts after quartz as the dominant siliceous constituents. Since sand constitutes the dominant volume fraction of mortars, such variabilities in and mineralogies between original and recent mortars is reflected in their bulk chemical (oxide) compositions as well. Grain size distribution of sand extracted from a recent 2019 mortar after acid digestion showed dominance of finer size fractions as also seen in the sands from the original mortars, having sand finer than the grain size distribution of sands recommended for ASTM C 144 masonry sands. Grain size distribution plots of sands from two original mortars and one recent mortar are very similar showing excessive fines and deviation of ranges of size distribution recommended for ASTM C 144 masonry sands. Excessive fines in the sands increases the water requirements of mortar, thereby increases the overall water-cementitious materials ratios, makes mortar more permeable to moisture, and reduces long-term moisture tightness of mortar joints. Sand particles are dense, hard, clear to off-

white to light brown, and present in sound conditions without any evidence of potentially deleterious alkali-aggregate reactions in the mortars.

Perhaps the most interesting similarities as well as differences between the two original (1960s) and two recent (2019) mortars are found in their binders. The two original mortars both used masonry cement as the binder, therefore, pastes in both mortars showed the characteristic carbonated nature, which is a hallmark microstructural feature of masonry cement mortars. Use of masonry cement was not uncommon in many 1960s masonry constructions, but the compositions of the masonry cements varied significantly. In mortar #2, masonry cement contained a significant amount of limestone fines, which has given an overall granular appearance of mortar as noticed in optical and electron microscopy. By contrast, masonry cement used in mortar #3 had major amount of dolomitic hydrated lime, which has given an overall very fine-grained porous and carbonated appearance of paste as opposed to coarser granular appearance from limestone fine particles seen in mortar #2. Besides this major difference in masonry cements' components, masonry cements in both mortars contained Portland cement as the main cementitious (hydraulic) phase, often detected by its residual cement particles leaving only dark brown skeletal remains of interstitial ferrite phases. Contrary to the abundant limestone fines in mortar #2, its presence is scarce in mortar #3, which, as mentioned, is dominated by hydrated lime. A trace amount of dark brown to black spherical fly ash particles are detected in the high-lime masonry cement paste in mortar #3 whose amount is less than that anticipated from intentional incorporation as in the blended cement, but enough to be detected in many areas of thin section to indicate perhaps it was accidentally incorporated either in the masonry cement during the manufacturing phase of cement and/or during the construction phase of the mortar.

Perhaps the most important difference between the two original mortars is in their air entrainment. Mortar #2 shows marginal air entrainment but has numerous irregular-shaped entrapped voids between sand particles as well as pore spaces between individual calcite grains of limestone fines, which have given an overall porous microstructure of this mortar susceptible to moisture penetration. By contrast, mortar #3 shows excellent air entrainment in having numerous fine, discrete, spherical and near-spherical entrained air voids of sizes 1 mm or less, as well as many coarse voids, all of which, in fact, have given an excessive air entrainment appearance in the mortar. Even though masonry cement mortars are characteristically air entrained in having 16 to 18 percent air, air content in mortar #3 is found to be at the high end of this range, which is detrimental to development of good bond to the adjacent masonry units. Abundant irregular-shaped voids and interstitial capillary pore spaces in mortar #2 and abundant spherical entrained air bubbles in mortar #3 are both detrimental to development of a good bond to adjacent masonry units as well as their resistance to moisture transmission. Therefore, both original mortars are found to be candidates to have weak bond to their adjacent masonry units and have high moisture permeabilities.

Contrary to the masonry cement binders in two original mortars, mortar #4 from the recent 2019 construction showed use of Portland cement and dolomitic hydrated lime as the two essential binder components. Therefore, paste in this mortar is non-carbonated, and contains abundant residual Portland cement particles, cement hydration products including coarser patches of calcium hydroxide crystals of cement hydration mixed with finer-grained porous hydrated lime, which is still not carbonated enough due to limited interaction with atmospheric carbon dioxide.

By contrast, mortar #5 from 2019 showed use of masonry cement as found in the original mortars, but the latest masonry cement was very different from 1960s masonry cements. In mortar #5, masonry cement does not show any noticeable abundance of either limestone fines (as found in #2) or hydrated lime (as found in #3) but more reasonable proportions of cement, lime, and limestone fines commonly found in many modern-day well-proportioned masonry cement mortars. Abundance of residual Portland cement particles in paste indicate a Portland cement-rich composition of the masonry cement, e.g., similar to an ASTM C 91 Type S masonry cement. Mortar #5 showed another difference in paste from the rest of the mortars in having a polymer component, which has densified the paste more than other mortars. Such polymer-induced added densification of paste beyond carbonated lime and cement hydration products is not only detected in optical microscopy but more so during

SEM-EDS studies. FTIR analysis of this mortar detected a latex-based polymer addition, consistent with reported latex-modified nature of this mortar.

SEM-EDS studies of paste *per se* in two original and two recent mortars showed overall enrichment of silica in siliceous sand grains and interstitial lime-based paste reflected in elemental (Ca-Si-Al-Mg-etc.) maps. Use of dolomitic lime in all mortars is reflected from the high magnesia contents of pastes in SEM-EDS studies. Cementation indices of paste (paste-CI after Eckel 1922) shows wide range within and between the mortars which is not unexpected considering proprietary mix composition of masonry mortars as well as variable degrees of mixing of cement, lime, and limestone fine components in the paste. A systematic trend in compositional plots of silica and lime contents of pastes against paste-CI from SEM-EDS studies demonstrated their lime, limestone fines, and Portland cement-based compositions of original binders.

Optical microscopy and scanning electron microscopy showed evidence of leaching of lime paste from around sand grains in mortar #2 from original mortar, which is responsible for overall porous microstructure of original mortar.

Compositional analyses of original and recent mortars by energy-dispersive X-ray fluorescence spectroscopy (ED-XRF) showed overall similar oxide compositions of two original mortars (despite their differences in compositions of masonry cements used), which are very different from the two recent mortars. Two recent mortars from 2019 construction showed overall similarities in oxide compositions. Two original mortars are found to be richer in silica mostly due to higher sand contents and quartz-rich composition of sands as opposed to many feldspar particles found in the sands in recent mortars, which are responsible for elevated alumina contents in the recent mortars compared to the original ones. High feldspar content of sand in the recent mortars also elevated the potassium contents in these mortars compared to the original ones. Since sand constitutes bulk volume of the mortar, changes in the sand mineralogies between the 1960s and 2019 mortars is reflected in their bulk chemistries. Oxide compositions of all four mortars reflect their similarities and differences in the mineralogies of sands used, as well as compositions of binder phases.

Mineralogical compositions of mortars determined from X-ray diffraction studies showed simple quartz-based mineralogy of sand in original mortars, more complex quartz-feldspar-mica based mineralogy of sand in recent mortars, dominance of quartz in the sand in all four mortars, and subordinate amount of calcite from carbonated paste and calcite fine particles of masonry cements. XRD studies of soft, white efflorescence powder on mortar #5 showed calcium carbonate (calcite) composition of the efflorescence due to moisture-induced leaching of lime and cement hydration products from mortar followed by evaporation, precipitation of dissolved salts on the mortar's outer surface, and atmospheric carbonation of precipitated salts.

Thermal analyses of all four mortars showed simple thermograms for original mortars mostly from the loss of free water and water in hydrate salts during heating up to 200ºC, polymorphic transition of quartz at 575ºC, and major endothermic peak from decarbonation of carbonated lime and calcite fine particles. Both original mortars showed very similar thermograms having a minimal loss of free water (<0.5%) and water from hydrated salts (<0.5%) at up to 200ºC followed by a measurable loss (2 to 2.2%) of hydrate water from 200ºC to 600ºC. Degrees of carbonation is higher in the #2 mortar (9.3% due to abundant limestone fine component along with hydrated lime) than 5.6% found in #3 mortar mostly from hydrated lime component in the latter. Quartz contents in both mortars are around 70 percent determined from polymorphic transition of quartz around 575ºC. Two recent mortars from 2019 construction, however, showed very different rather complex thermograms due to (i) the presence of noticeable structural water components in the 200ºC to 600ºC range, along with (ii) noticeably larger losses of free water and from hydrated salts at <200ºC, (iii) lower degree of carbonation than the original mortars, and (iv) lower quartz contents in the recent ones (<50%) compared to much higher quartz contents (70%) found in the original mortars.

FTIR studies of all four mortars (#2 to #4) showed the inorganic phases (e.g., quartz, calcite) that are already detected in microscopy and XRD studies but no polymer component in the mortars for which the study was done.

Mortar #5 from 2019 construction, however, showed absorbance peak from a latex-based polymer, which is consistent with its dense microstructure of paste found in optical and electron microscopy.

Ion chromatography (IC) of water-soluble salts showed negligible chloride contents in the original mortars (0.016% and 0.009% chlorides by mass of mortars in #2 and #3), which do not indicate ingress of any chloride salts or related distress. However, sulfate contents are noticeable and large variations in sulfate contents are found from 0.057% in #2 (limestone fine rich masonry cement) to 0.176% in #3 (hydrated lime rich masonry cement mortar). Chloride contents in the recent mortars are also negligible (0.018% and 0.021% chlorides by mass of mortars in #4 and #5) to confirm lack of any chloride salts or related distress. However, as in the original mortars, sulfate contents in 2019 mortars are noticeable (from 0.294% to 0.337%) which are higher than the maximum 0.176% sulfate found in #3 original mortar. Presence of Portland cement at a higher amount in the binders of the recent mortars is responsible for the high water-soluble sulfate contents. The highest Portland cement content detected from optical microscopy in mortar #5 correlated with its highest water-soluble sulfate from IC.

White efflorescence deposits on the surface of mortar #5 is determined to be calcium carbonate, which is a testament of moisture penetration through the masonry joints at the location of #5. This is rather unusual considering dense polymer-impregnated microstructure of #5 as well as its Portland cement-rich composition with the impression of the best mortar of all examined in this study. This indicates that other factors beyond the mortar type (compatibility with adjacent masonry units, design, improper flushing, etc.) are also important to control the overall moisture tightness of masonry facades.

Optical microscopy of the dense, hard, dark gray stone sample has determined its type to be diabase (also described in European literatures as dolerite), which is a medium-grained intrusive, basic igneous rock consisting of subhedral plagioclase feldspar laths, anhedral equant pyroxene grains, and small dark opaque minerals, where pyroxene crystals partially enclosed plagioclase laths to create the characteristic subophitic textural arrangement of crystals that are common in diabase.

Information obtained from: (a) petrographic examinations to determine the sand compositions, binder types, as well as overall mortar types, and (b) chemical analyses of mortars to determine the soluble silica contents, water contents, and insoluble residue contents are used to calculate volumetric proportions of mortars' ingredients. Mix calculations of mortars showed the two original mortars to be made using 1-part masonry cement to 2 to 3-part sand (mortar #3 has higher sand content than #2), whereas a recent cement-lime mortar (#4) was made using 1-part Portland cement to 1.1-part dolomitic hydrated lime to 6.6-part sand (which is 3.2 times the sum of separate volumes of cement and lime). All these proportions are indicative of use of ASTM C 270 Type N masonry cement for original mortar and Type N cement-lime mortar for the #4 recent mortar. Optical microscopy of mortar #5 from 2019 indicated a Portland cement-rich polymer-based binder, which is found to be more superior and more appropriate for the diabase stone masonry units than the other mortar types examined.

Based on the determined masonry mortar compositions of original mortars having 1-part masonry cement to 2 to 3-part sand similar to ASTM Type N masonry cement mortar, as well as the diabase stone composition of the masonry units, an appropriate masonry mortar should be an ASTM C 270 Type S or M cement-lime mortar, or, an ASTM C 270 Type S or M masonry/mortar cement mortar. A polymer-modified mortar, similar to mortar #5 would provide more flexibility to compensate increased brittleness from having a higher Portland cement content in the Type M or S mortar than the existing Type N that a dense stone masonry unit like diabase demands. A cement-lime mortar is preferable due to well-controlled proportions than a proprietary masonry cement binder. Air content of the mortar should be carefully controlled to provide the necessary workability and freeze-thaw durability without compromising the bond strength. Sand used should not be crushed too fine to increase the water demand of mortar mixes. Mortar ingredients should be in conformance to their respective ASTM specifications (e.g., ASTM C 91/C1329 for masonry/mortar cement, C 144 for sand, C 150 for Portland cement, C 207 for hydrated lime, etc.). Final choices of tuckpointing mortars should be decided from multiple mock-up batches to select the best match in compositions, properties, and appearances to the existing ones.

INTRODUCTION

Located at 451 7th Street, SW in Washington, D.C. the Robert C. Weaver Federal Building is the headquarters of the U.S. Department of Housing and Urban Development (HUD). Constructed from 1965 to 1968 by the renowned architect Marcel Breuer, the building is recognized as the first federal building in the country to utilize precast concrete as the primary structural and exterior finish material, as well as the first fully modular design for a federal office building.

Figure 1: Robert C Weaver Federal Building (HUD), Washington, D.C.

As part of the renovation process, two sets of masonry mortar samples were provided for detailed laboratory examinations. The first set comprises two samples from the original 1960s vintage, and the other set of two samples reportedly came from 2019 construction. The purpose of this laboratory examination is to determine the compositions and mix proportions of mortars from the original 1960s and latest 2019s constructions and evaluate their compatibilities and suitability for long-term performance of masonry walls. Additionally, a dark gray, dense hard crystalline stone sample from the building was provided in two small pieces to determine the stone type.

SAMPLES

Table 1 and Figure 2 show the stone and mortar samples received. Of the four mortars, two are from the original 1960s construction (marked as #2 and 3), whereas the remaining two (marked as #4 and 5) are from the recent 2019 construction.

Period	Sample Identification & Type	Weight (grams) and Dimensions of the largest piece (mm)	Appearance, Integrity, Figure	Figure
Original 1960s	Sample 1 HUD Stone	138.44g 80 mm × 40 mm × 10 mm	Two dark gray, crystalline, dense, hard rock fragments	2
	Sample 2 HUD SE-A-6-Vert. Face Mortar	29.2g 70 mm × 10 mm × 7 mm	Four (4) long strips of bed joint mortars	2
	Sample 3 HUD SE-A-6-Vert. Bed Mortar	33.33g 45 mm × 32 mm × 5 mm	Six (6) gray mortar pieces of variable sizes	2
2019	Sample 4 HUD SW-D-Edison-N Mortar	25.9g 75 mm × 26 mm × 7 mm	One (1) large & Three (3) small bed joint mortar pieces, gray, dense	2
	Sample 5 HUS SW-B-Edison-N Mortar (latex modified)	48.37g 88 mm × 22 mm × 7 mm	Two (2) long bed joint gray mortar strips Larger one has white efflorescence deposits	2

Table 1: Stone and mortar samples received from two periods of construction.

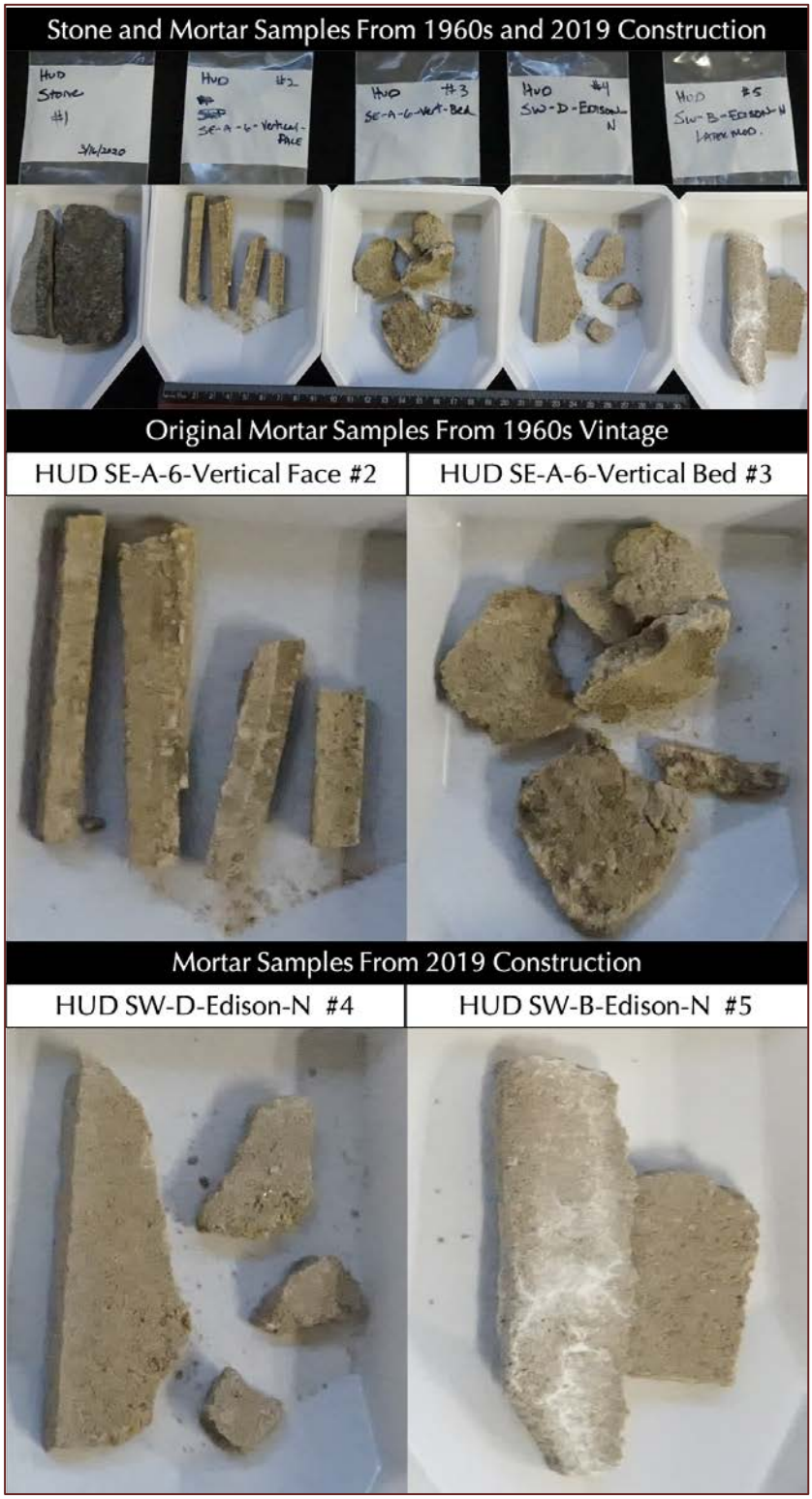

Figure 2: Stone and masonry mortar samples received. Of the four mortars, two are from the original 1960s construction (marked as #2 and 3), whereas the remaining two are from the recent 2019 construction.

METHODOLOGIES

The mortar samples were tested by following the methods of ASTM C 1324 "Standard Test Method for Examination and Analysis of Hardened Masonry Mortar," along with various analytical methods to test masonry mortars as described in various literatures, e.g., Erlin and Hime 1987, Doebley and Spitzer 1996, Chiari et al. 1996, Middendorf et al. 2005 a and b, Elsen 2006, Bartos et al. 2000, Valek et al. 2012, Jana 2005, 2006, and Goins 2001 and 2004. Details of various analytical techniques followed by CMC laboratories are provided in Appendix A. Also, visit www.cmc-concrete.com for details on analytical facilities for laboratory examinations of masonry mortars.

Petrographic examinations of stone sample were done by following the methods of ASTM C 295 and C 856.

RESULTS

Lapped Cross Sections & Micrographs of Lapped Cross Sections of Mortars

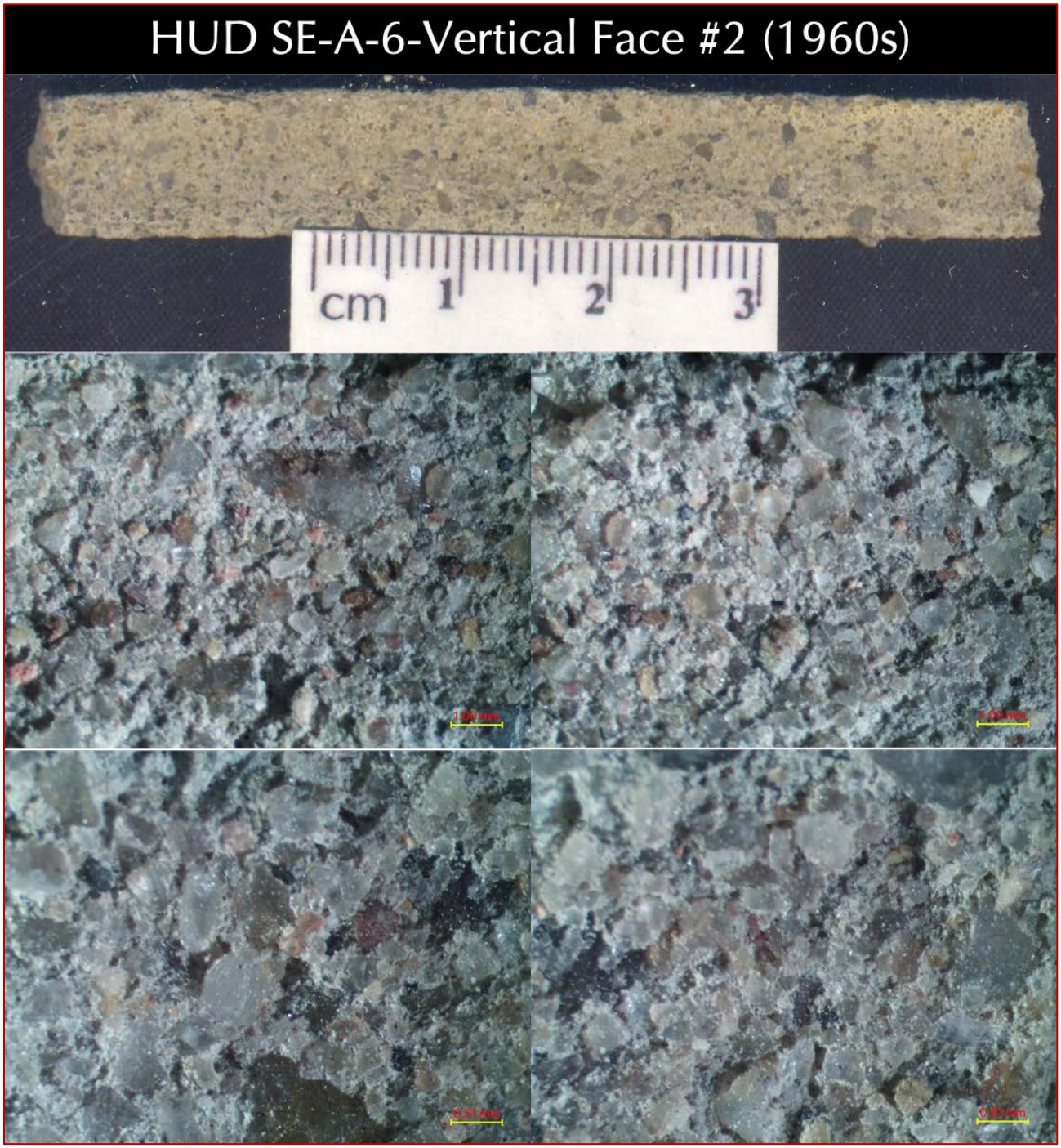

Figure 3: Top photo shows the exposed tooled joint face of the original mortar (#2) from 1960s construction showing the sand particles that are exposed relative to interstitial paste due to leaching of the paste from around sand grains. The middle row shows micrographs of tooled joint face of the mortar where sand grains are seen mostly comprising off-white to light gray colored well-graded and well-distributed silica sand particles. Bottom row shows micrographs of bedding face of the mortar where sand grains are seen along with interstitial paste. Scale bars in the photos are of 1 mm in the middle row and 0.5 mm in the bottom row.

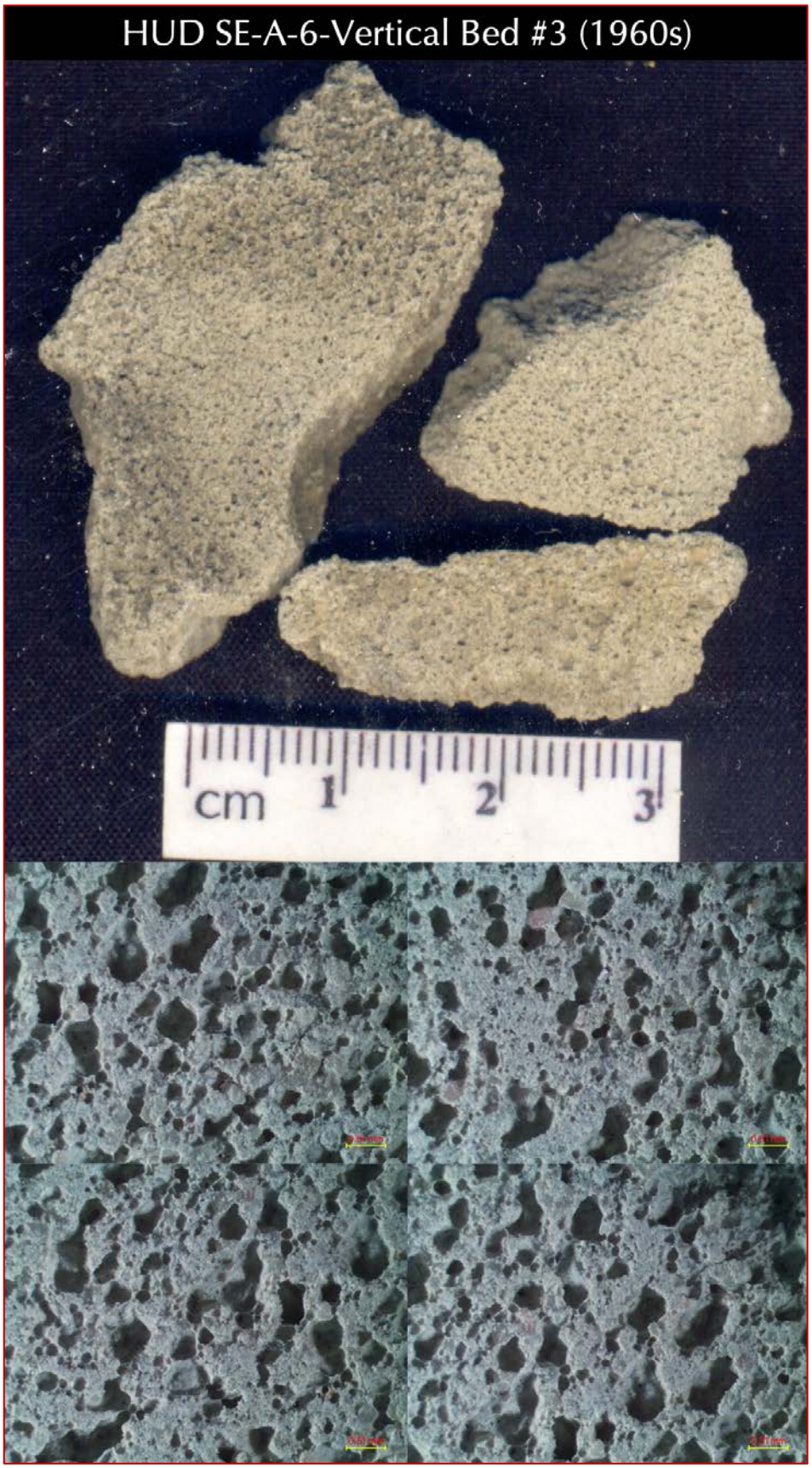

Figure 4: Top photo shows three pieces of the original mortar (#3) from 1960s construction. The middle and bottom row show micrographs of mortar pieces where sand grains are seen mostly comprising off-white to light gray colored well-graded and well-distributed silica sand particles.

The noticeable feature in the micrographs is excessive air entrainment and many coarse air voids that are detrimental to the interfacial bonds to adjacent masonry units.

Scale bars in the micrographs are of 0.5 mm.

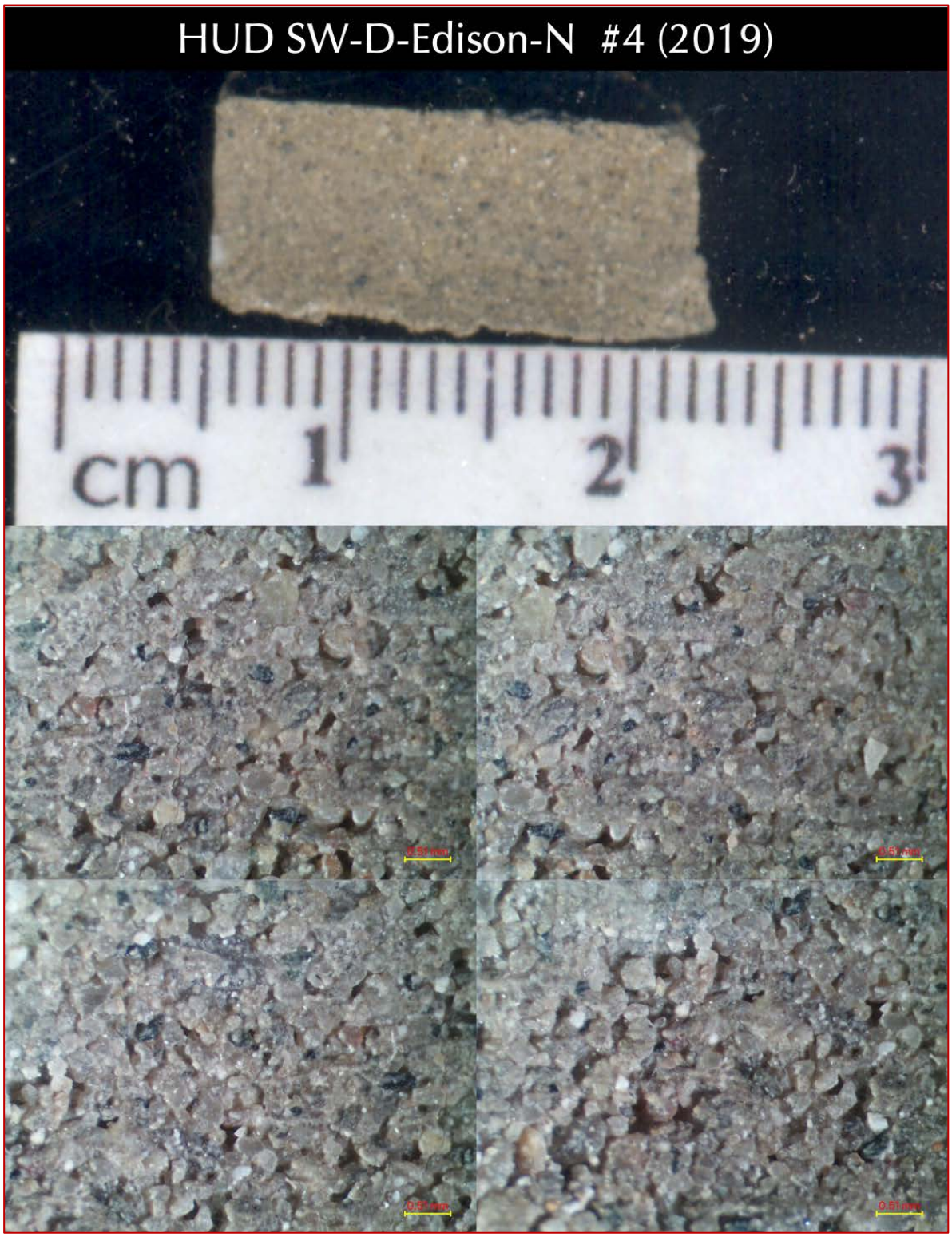

Figure 5: Top photo shows the exposed tooled joint face of the mortar (#4) from 2019 construction showing the sand particles that are exposed relative to interstitial paste. The middle row shows micrographs of tooled joint face of the mortar where sand grains are seen mostly comprising off-white to light gray colored well-graded and well-distributed silica sand particles. Bottom row shows photomicrographs of bedding face of the mortar where sand grains are seen along with interstitial paste. Scale bars in the micrographs are of 0.5 mm.

Figure 6: Top photo shows the bedding face of a piece of mortar (#5) from 2019 construction showing remains of white efflorescence deposits (after most of the deposits were scrapped off for X-ray diffraction study).

The next photo shows the exposed tooled joint face of the mortar.

The 3rd row shows micrographs of bedding face of the mortar where remains of soft, white powdery efflorescence deposits are seen along with sand grains that are mostly comprising off-white to light gray colored well-graded and well-distributed silica sand particles.

Bottom row shows photomicrographs of exposed tooled joint face of the mortar where sand grains are seen along with interstitial paste.

Scale bars in the micrographs are of 0.5 mm.

Grain-size Distribution of Sands in Masonry Mortars

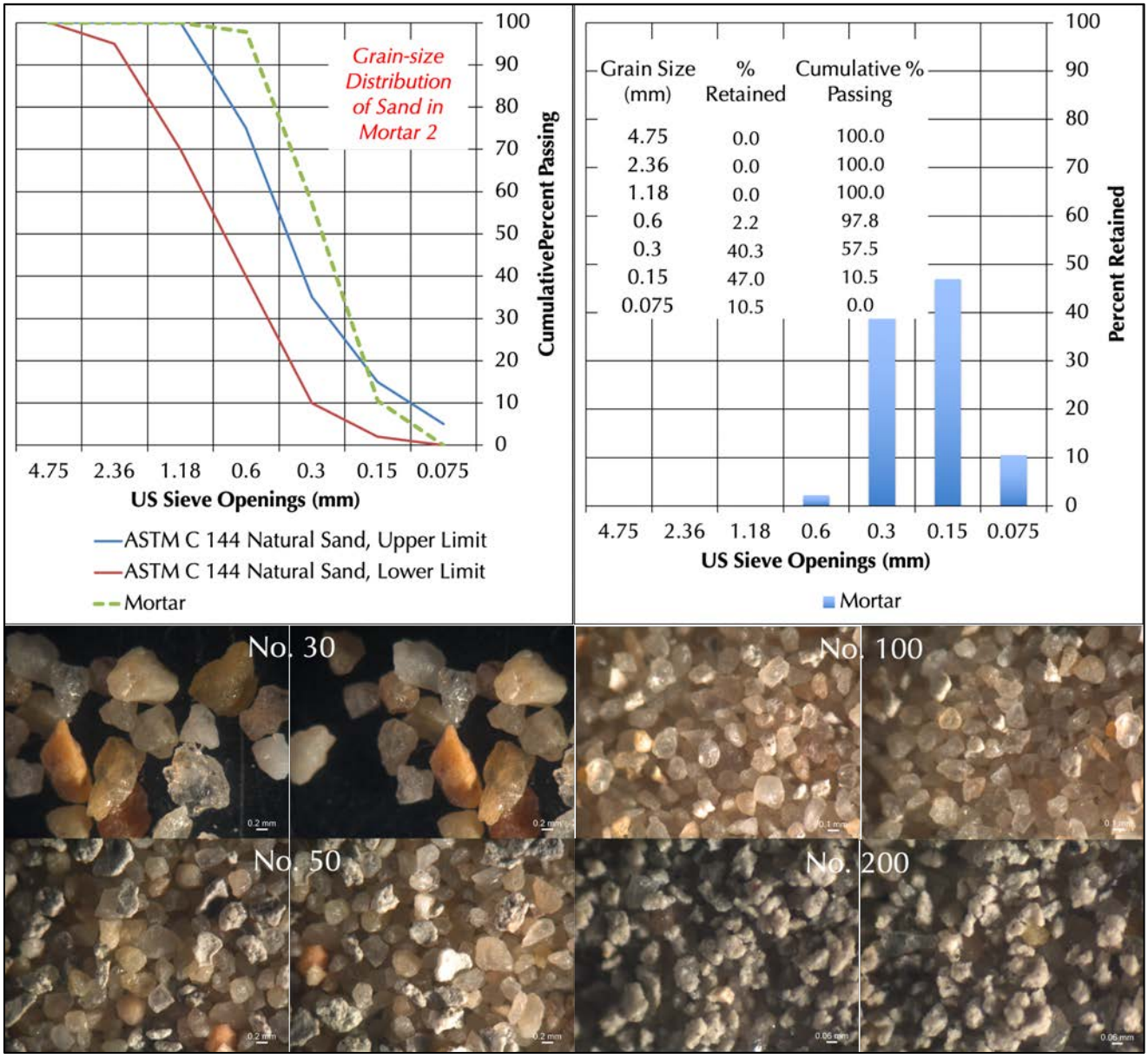

Figure 7: Grain-size distribution of sand extracted from an original mortar (# 2) from 1960s construction after acid digestion. In the top left plot, size distribution of sand is compared with upper and lower limits of natural sand in ASTM C 144 (blue and red lines, respectively). As seen in this plot, grain-size distribution of sand does not fall within the range of size distributions specified for ASTM C 144 masonry sand. The top right 'percent retained' histogram plot shows finer than 'normal' size distribution of sand with enrichment of fines. Bottom photos show stereo-micrographs of sand particles retained on various sieves, including size, shape, angularity, and color variations of sand particles. Note noticeably clear to light brown to off-white color tone of majority of sand particles. Subsequent optical microscopical examinations of sand determined its **siliceous composition**, and lack of any calcareous components. Therefore, sand extracted from acid digestion is determined to be the entire amount of sand without leaving any component and hence results provided here are representative of the bulk sand used.

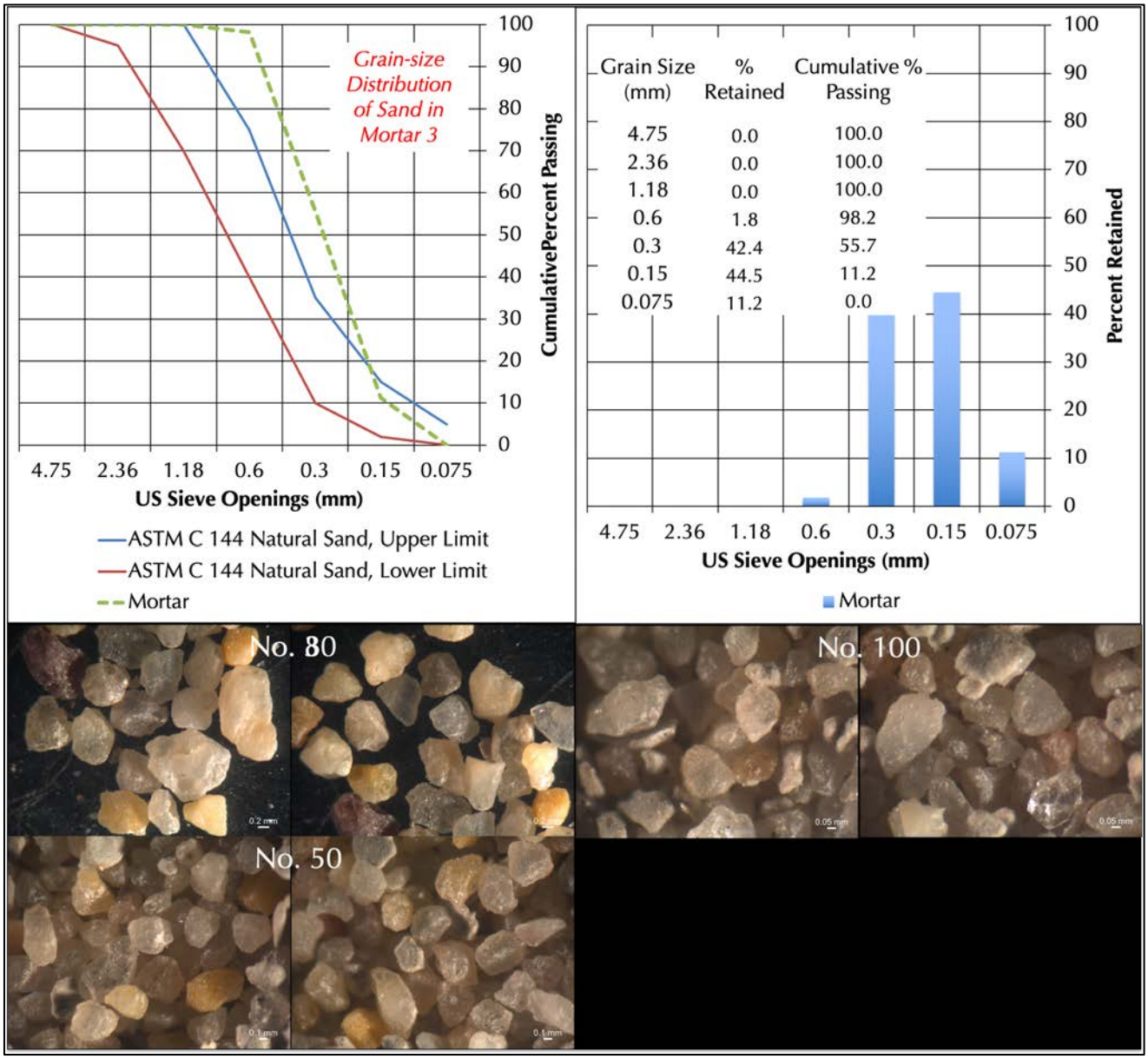

Figure 8: Grain-size distribution of sand extracted from an original mortar (# 3) from 1960s construction after acid digestion. In the top left plot, size distribution of sand is compared with upper and lower limits of natural sand in ASTM C 144 (blue and red lines, respectively). As seen in this plot, grain-size distribution of sand does not fall within the range of size distributions specified for ASTM C 144 masonry sand. The top right 'percent retained' histogram plot shows finer than 'normal' size distribution of sand with enrichment of fines. Bottom photos show stereo-micrographs of sand particles retained on various sieves, including size, shape, angularity, and color variations of sand particles. Note noticeably clear to light brown to off-white color tone of majority of sand particles. Subsequent optical microscopical examinations of sand determined its **siliceous composition**, and lack of any calcareous components. Therefore, sand extracted from acid digestion is determined to be the entire amount of sand without leaving any component and hence results provided here are representative of the bulk sand used.

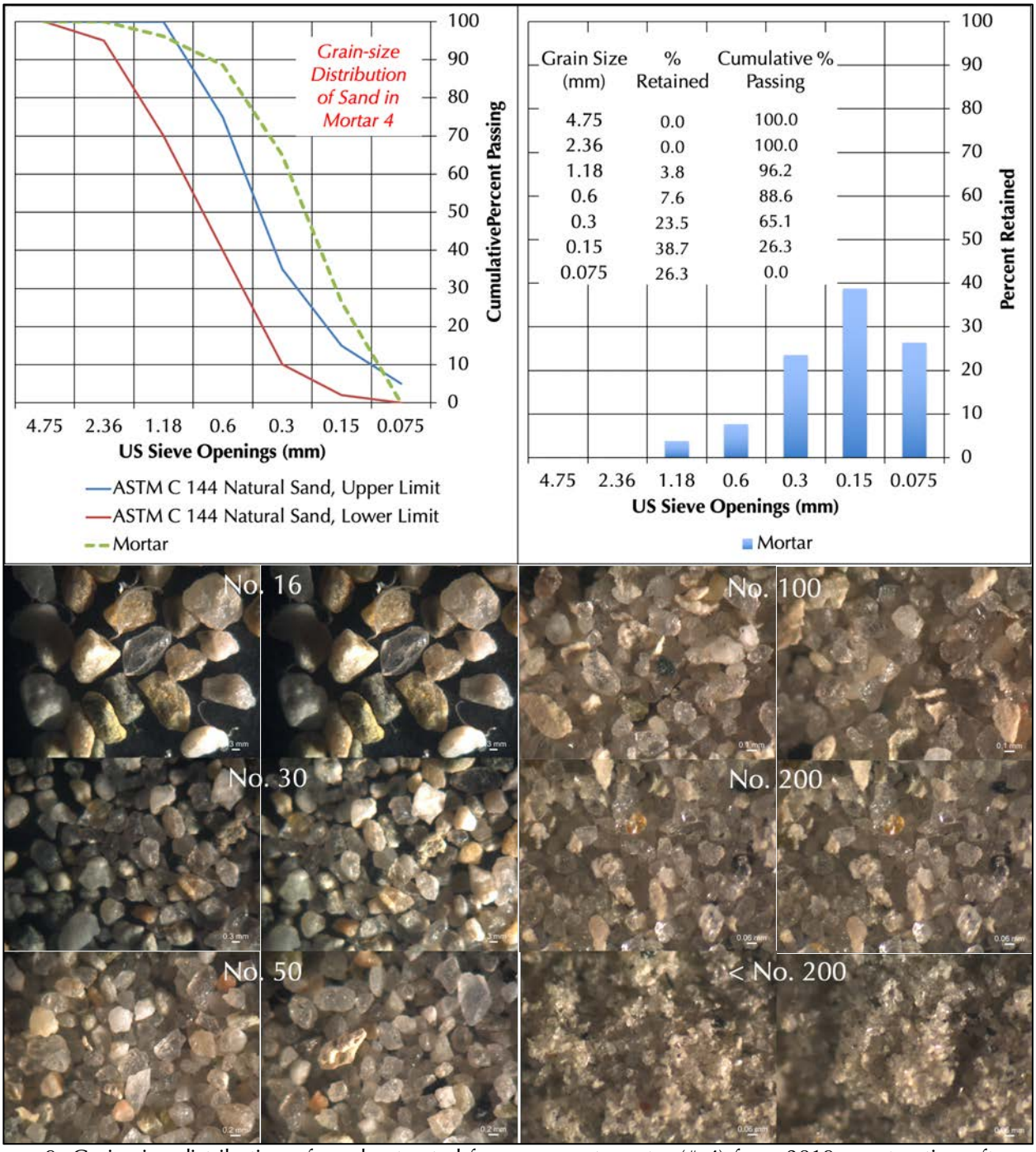

Figure 9: Grain-size distribution of sand extracted from a recent mortar (# 4) from 2019 construction after acid digestion. In the top left plot, size distribution of sand is compared with upper and lower limits of natural sand in ASTM C 144 (blue and red lines, respectively). As seen in this plot, grain-size distribution of sand does not fall within the range of size distributions specified for ASTM C 144 masonry sand. The top right 'percent retained' histogram plot shows finer than 'normal' size distribution of sand with enrichment of fines. Bottom photos show stereo-micrographs of sand particles retained on various sieves, including size, shape, angularity, and color variations of sand particles. Note noticeably clear to light brown to off-white color tone of majority of sand particles. Subsequent optical microscopical examinations of sand determined its **siliceous composition**, and lack of any calcareous components. Therefore, sand extracted from acid digestion is determined to be the entire amount of sand without leaving any component and hence results provided are representative of bulk sand used.

Thin Sections of Mortars

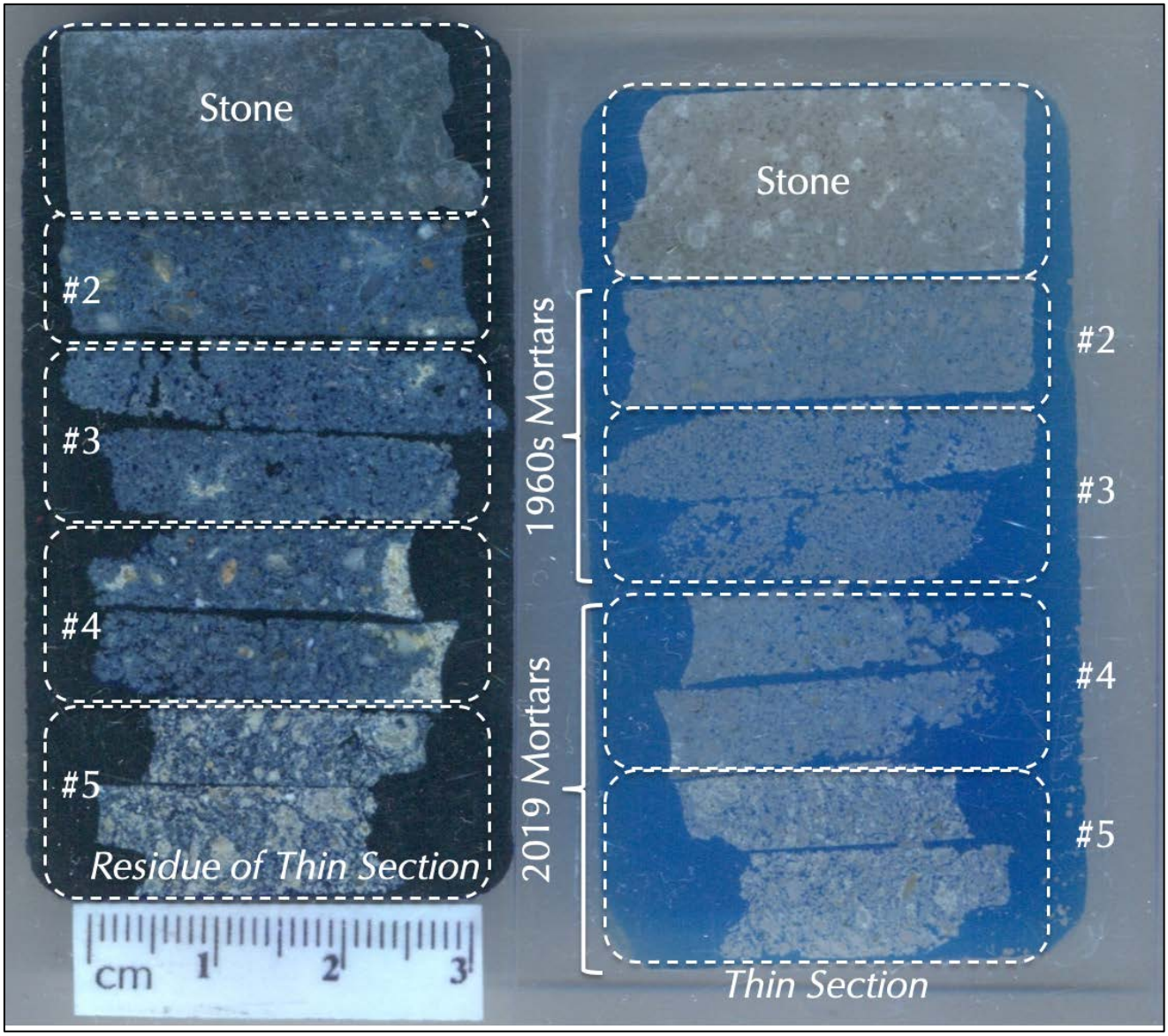

Figure 10: Blue dye-mixed epoxy-impregnated thin section of stone and mortar samples (right) and corresponding residue of epoxy-encapsulated block of samples left after thin section preparation (left). A representative portion of stone was sectioned and encapsulated for thin sectioning, which is shown at the very top of sequence of samples selected. Four mortar samples are arranged in order starting from two samples from 1960s construction, followed by remaining two from 2019 construction. The thin section at right was first used for detailed optical microscopical examinations of stone and mortar samples, after which the section was coated with a thin film of conductive gold alloy for subsequent examinations in a scanning electron microscope.

Optical Microscopy of Mortars From 1960s

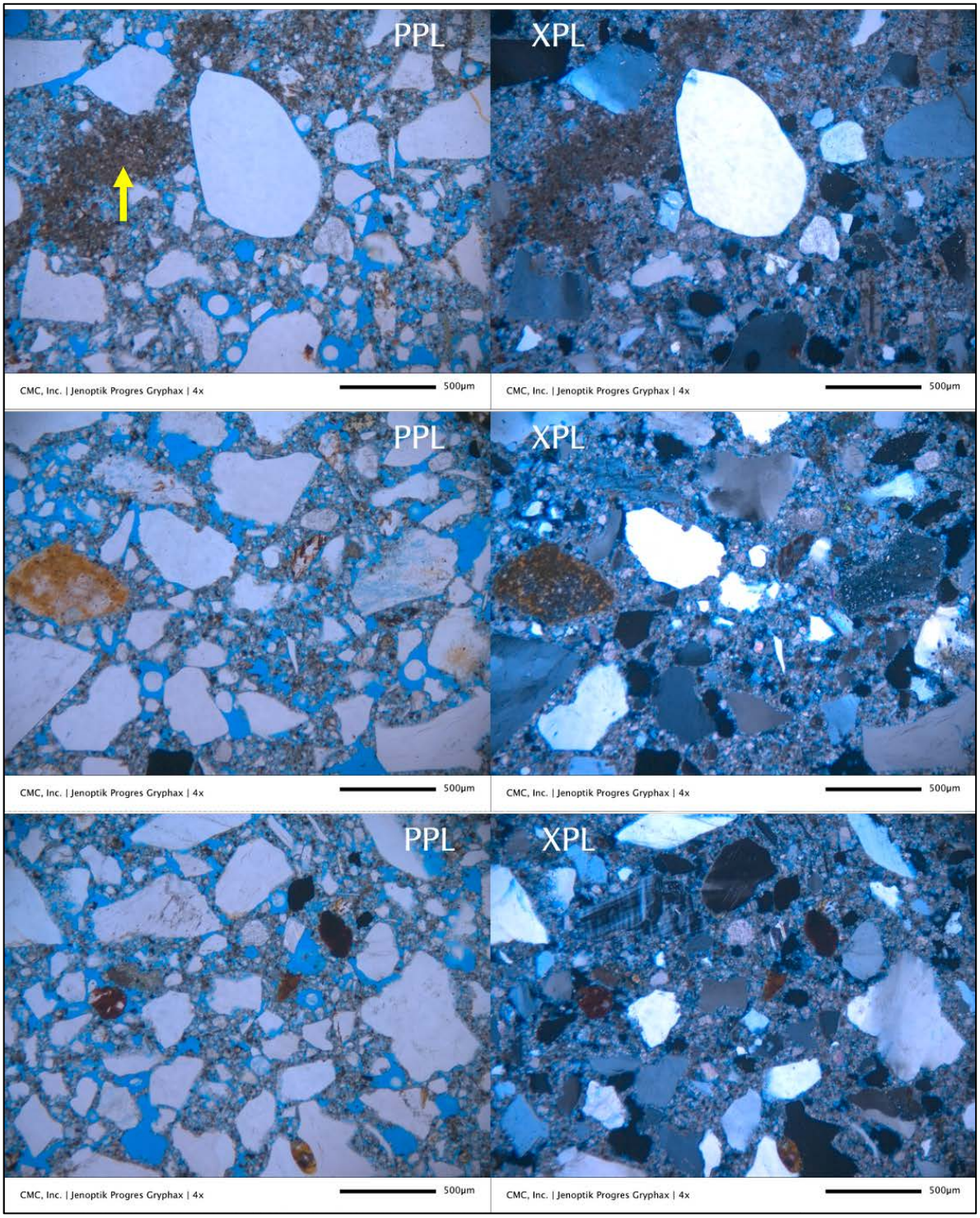

Figure 11: Optical micrographs of the original mortar (#2) from 1960s construction showing: (a) crushed silica sand consisting of major amount of variably strained quartz, and minor amount of quartzite, feldspar, and other siliceous particles (no carbonate components were found in the sand); (b) overall carbonated nature of the interstitial matrix between sand particles, which is a characterstic microstructure of many masonry cement mortars; however, (c) lack of good air-void system and air entrianment, which is also common in many masonry cement mortars.

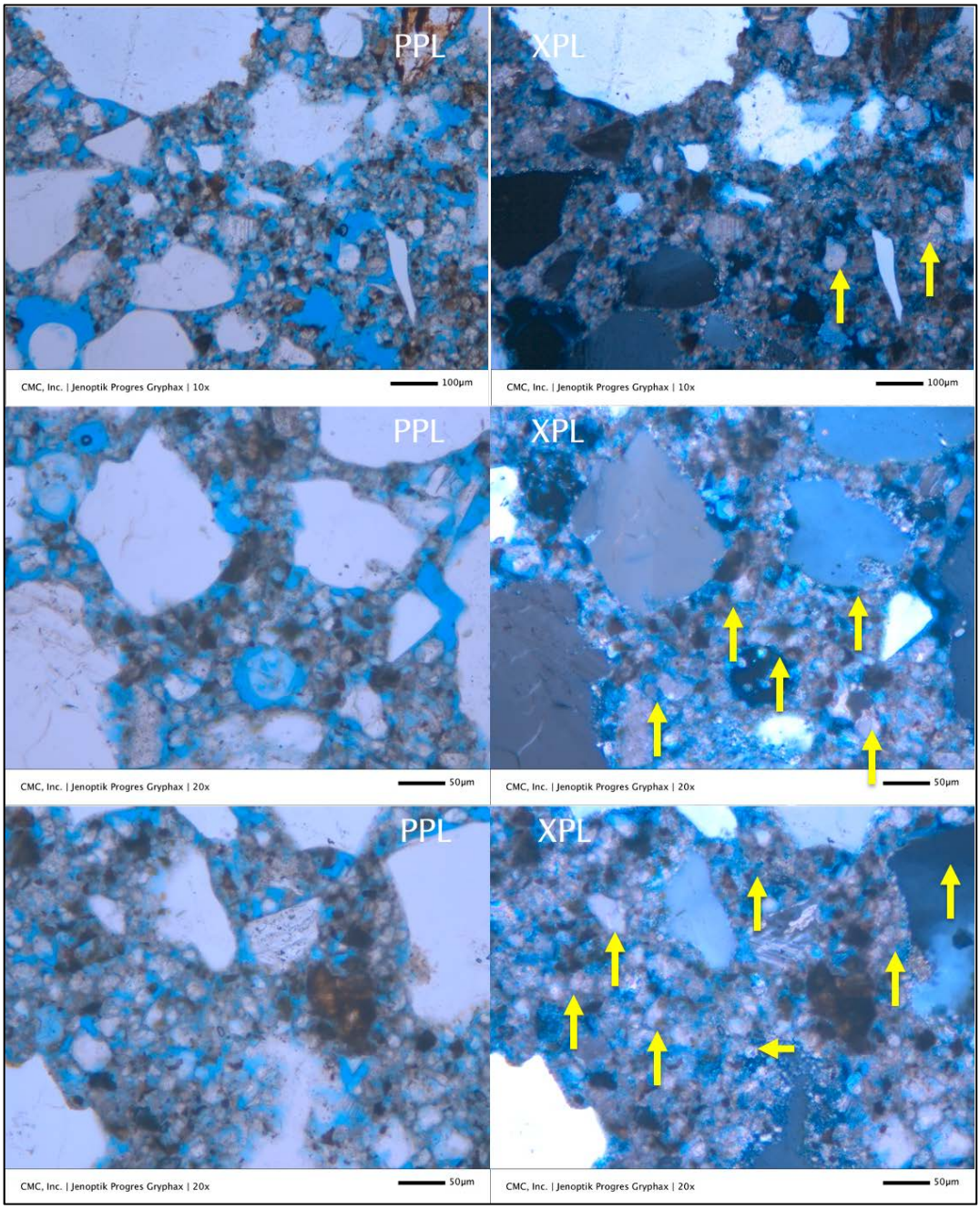

Figure 12: Optical micrographs of the original mortar (#2) from 1960s construction showing: (a) abundant void spaces between the sand and binder components in the matrix where many grains from finer fractions of sand and calcite fine particles from limestone fine component of the binder are not adequately coated to prevent moisture percolation through the mortar; these void spaces are highlighted by the blue epoxy that have filled all voids; (b) binder fraction in the interstitial matrix consisting of hydration products of Portland cement and a few residual and relic Portland cement particles consisting of dark ferrite remains, many hydrated lime remains of the binder mostly present as small clumps, and abundant calcite grains from limestone fine particles added as the main binder component of masonry cement used (many calcite grains are marked with arrows). The mortar shows an overall porous microstructure with characteristic carbonated nature of paste common in many masonry cement mortars, but not a clear air-void system that results in spherical air voids as seen in many masonry mortars. Notice remains of Portland cement particles are very few to detect except for a few dark brown ferrite remains of cement, indicating use of more limestone fines than cement in the original binder (proportions of binder components are similar to an ASTM C 270 Type N masonry cement mortar).

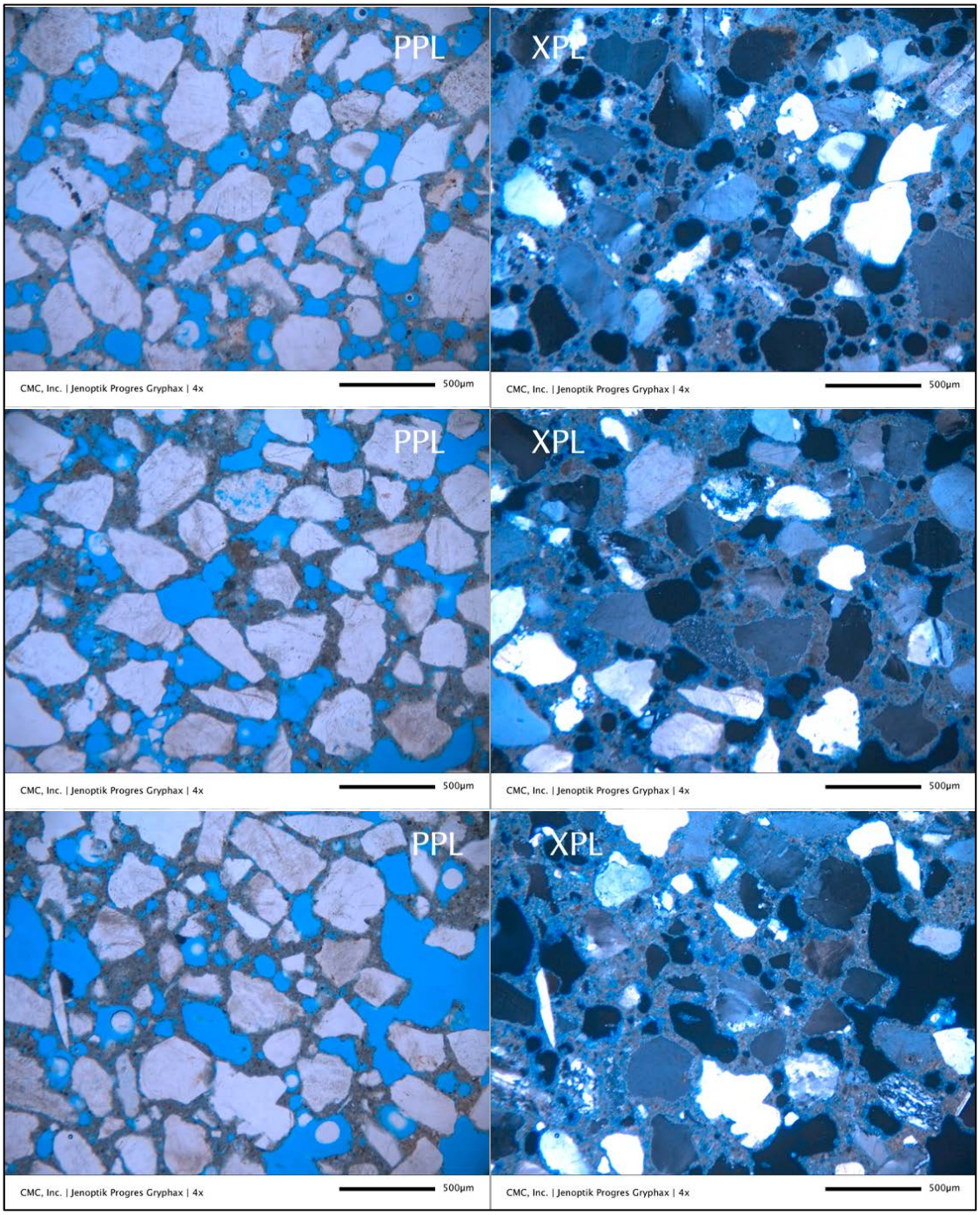

Figure 13: Optical micrographs of the original mortar (#3) from 1960s construction showing: (a) crushed silica sand consisting of major amount of variably strained quartz, and minor amount of quartzite, feldspar, and other siliceous particles (no carbonate components were found in the sand); (b) overall carbonated nature of the interstitial matrix between sand particles, which is a characterstic microstructure of many masonry cement mortars; and also (c) abundant fine, discrete, spherical and near-spherical entrained air voids (highlighted by blue epoxy), which is also common in many masonry cement mortars. The mortar appears to be excessively air-entrained and has too many air bubbles, which is detrimental to development of a good bond to adjacent masonry units. This mortar also appeared to be a masonry cement mortar as the original one (#2) but has abundant air entrainment and minor to trace amounts of limestone fines in the binder and major amount of hydrated lime contrary to lack of a good air entrainment, and abundant limestone fines found in the masonry mortar #2.

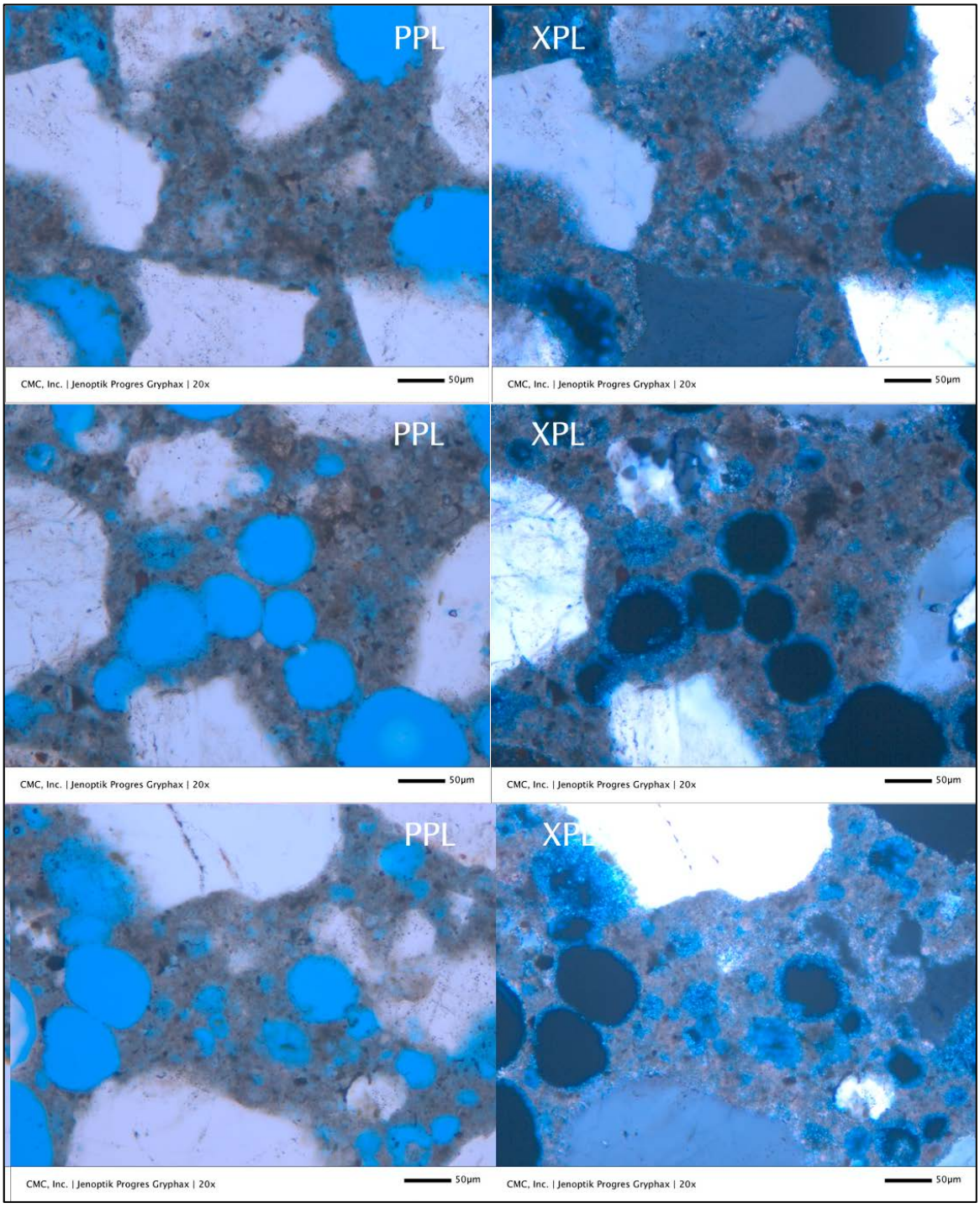

Figure 14: Optical micrographs of the original mortar (#3) from 1960s construction showing: (a) overall carbonated nature of the interstitial matrix between sand particles, which is a characterstic microstructure of many masonry cement mortars; (c) abundant fine discrete spherical and near-spherical entrained air voids (highlighted by blue epoxy), which is also common in many masonry cement mortars. This mortar also appeared to be a masonry cement mortar as the original one (#2) but has abundant air-entrainment and minor to trace amounts of limestone fines in the binder and major amount of hydrated lime contrary to lack of a good air entrainment, and abundant limestone fines found in the masonry mortar #2. Notice remains of Portland cement particles are very few to detect except for a few dark brown ferrite remains of cement, indicating use of more lime than cement in the original binder (proportions of binder components are similar to an ASTM C 270 Type N masonry cement mortar).

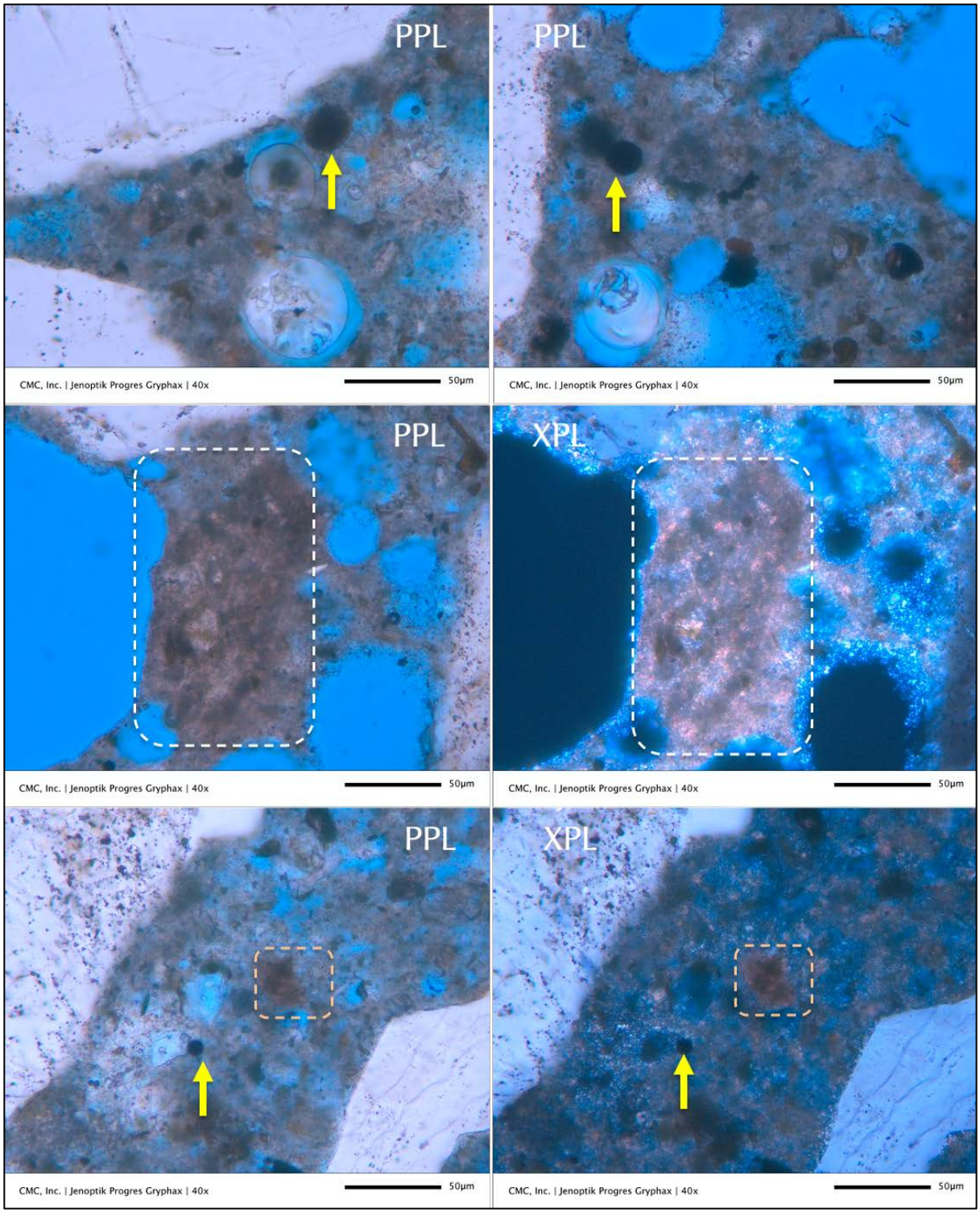

Figure 15: Optical micrographs of the original mortar (#3) from 1960s construction showing: trace amounts of dark brown to black spherical fly ash particles (marked with arrows) whose amount is lower than that anticipated from use of a blended cement and more representative of accidental contamination in the masonry cement. Boxed areas in the middle photo show a region that is denser than porous fine-grained carbonated lime based matrix, often occur as brown color tone that represents denser paste from cement hydration products. Small boxed areas in the bottom row show small patches of dolomitic hydrated lime that was added in the masonry cement binders.

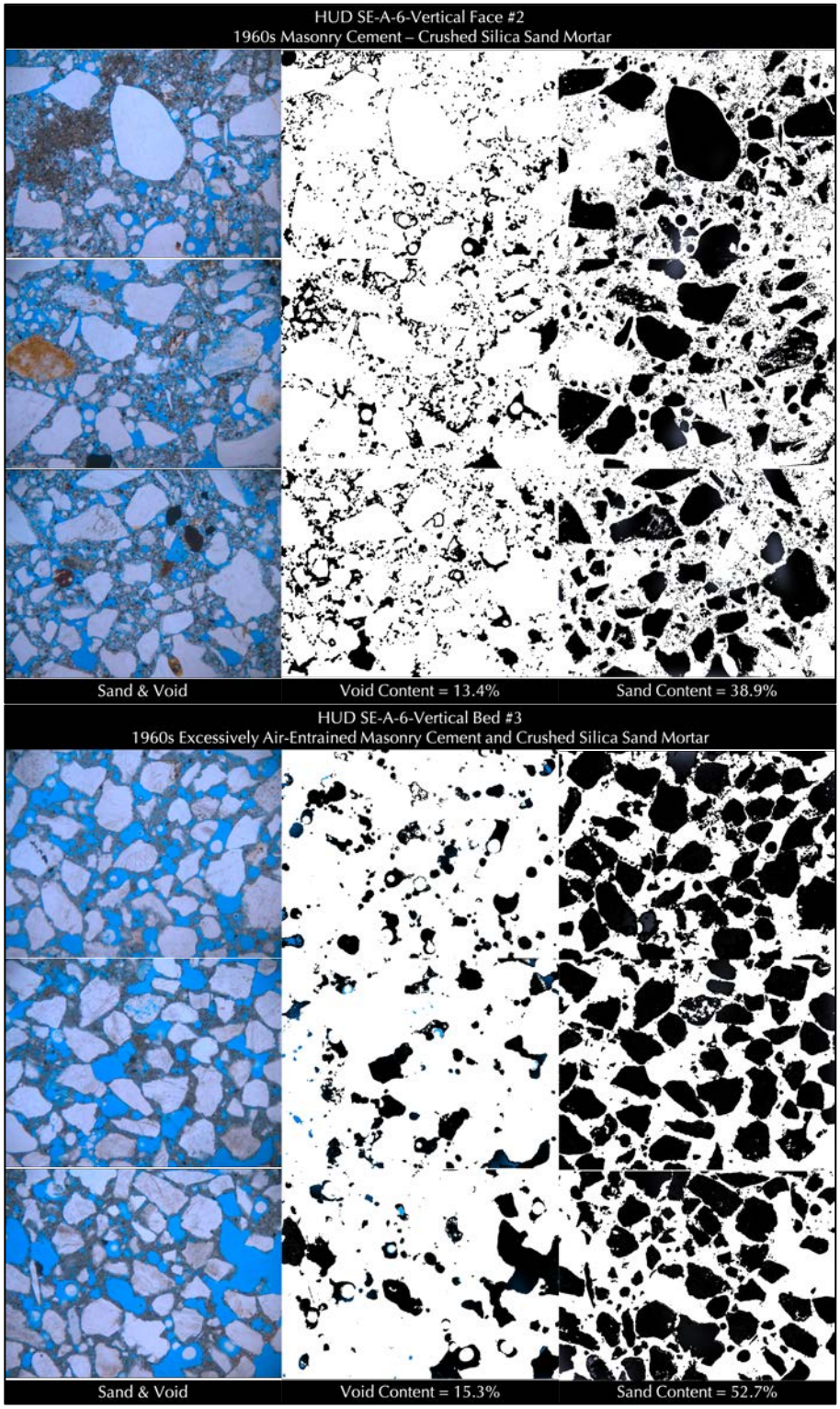

Figure 16: Image analyses (from Image J) to determine void and sand contents from optical micrographs of thin section of two original mortars. Left colum shows plane polarized light photos of distribution of sands and voids from which black and white contrast enhancements were done to highlight voids in black in the middle column and sand in the right column. Void and sand contents were subseuently determined from Image J open source image analysis software (https://imagej.nih.gov/ij).

Optical Microscopy of Mortars From 2019

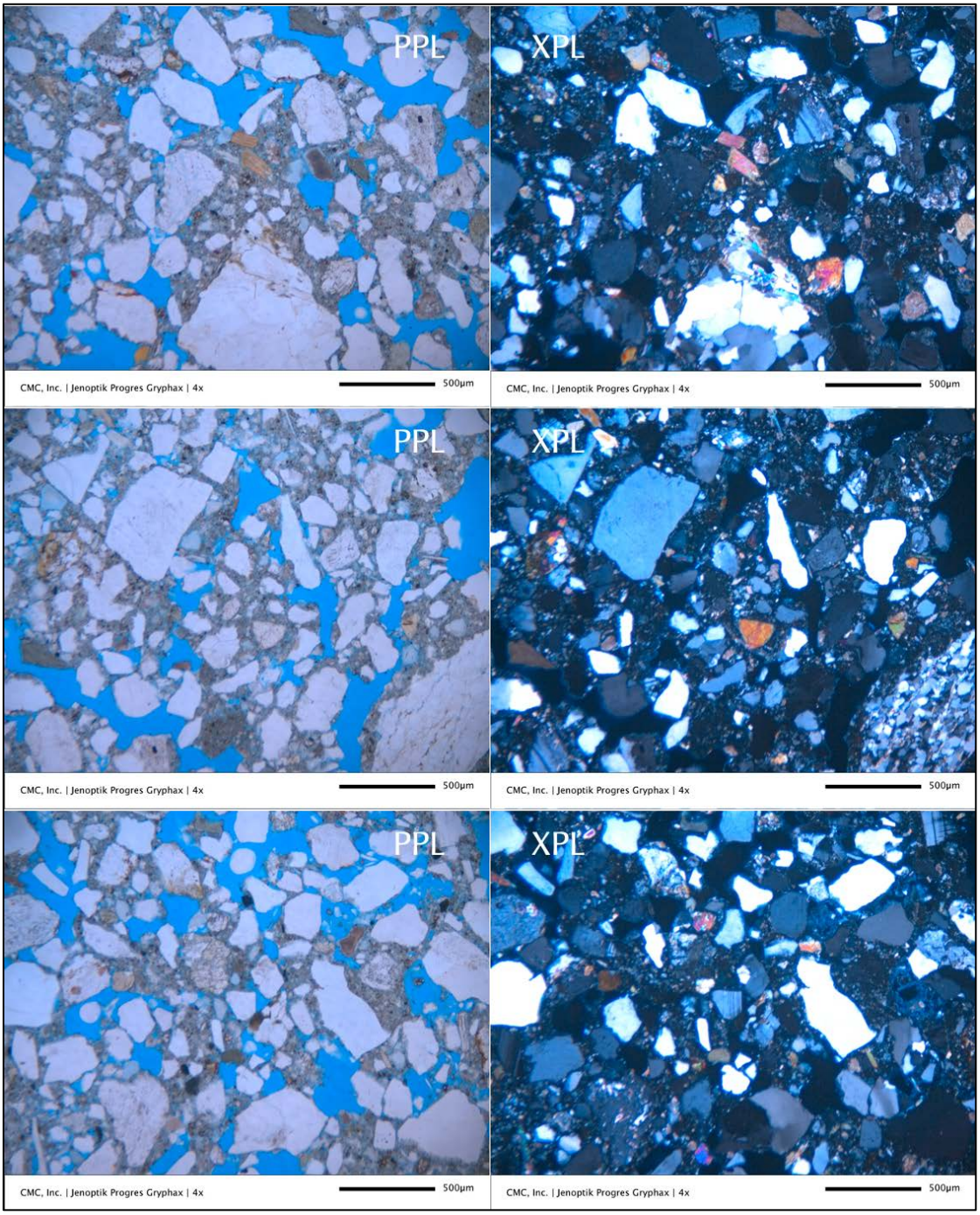

Figure 17: Optical micrographs of a recent mortar (#4) from 2019 construction showing: (a) crushed siliceous sand consisting of major amount of variably strained quartz, subordinate amount of quartzite, feldspar, schist, and other siliceous particles (no carbonate components were found in the sand, feldspar content of sand is higher than that found in the two original mortars); (b) overall non-carbonated nature of the interstitial matrix between sand particles, which is not a characterstic microstructure of masonry cement mortars found in the original mortars but more common of cement-lime mortars that have not been carbonated yet; (c) abundant irregularly-shaped air voids (highlighted by blue epoxy), giving an overall porous nature of the microstructure. The mortar appears to be a cement-lime mortar as opposed to two different types of masonry cement mortars (one with abundant lime and another with abundant limestone fines) found in the original 1960s construction.

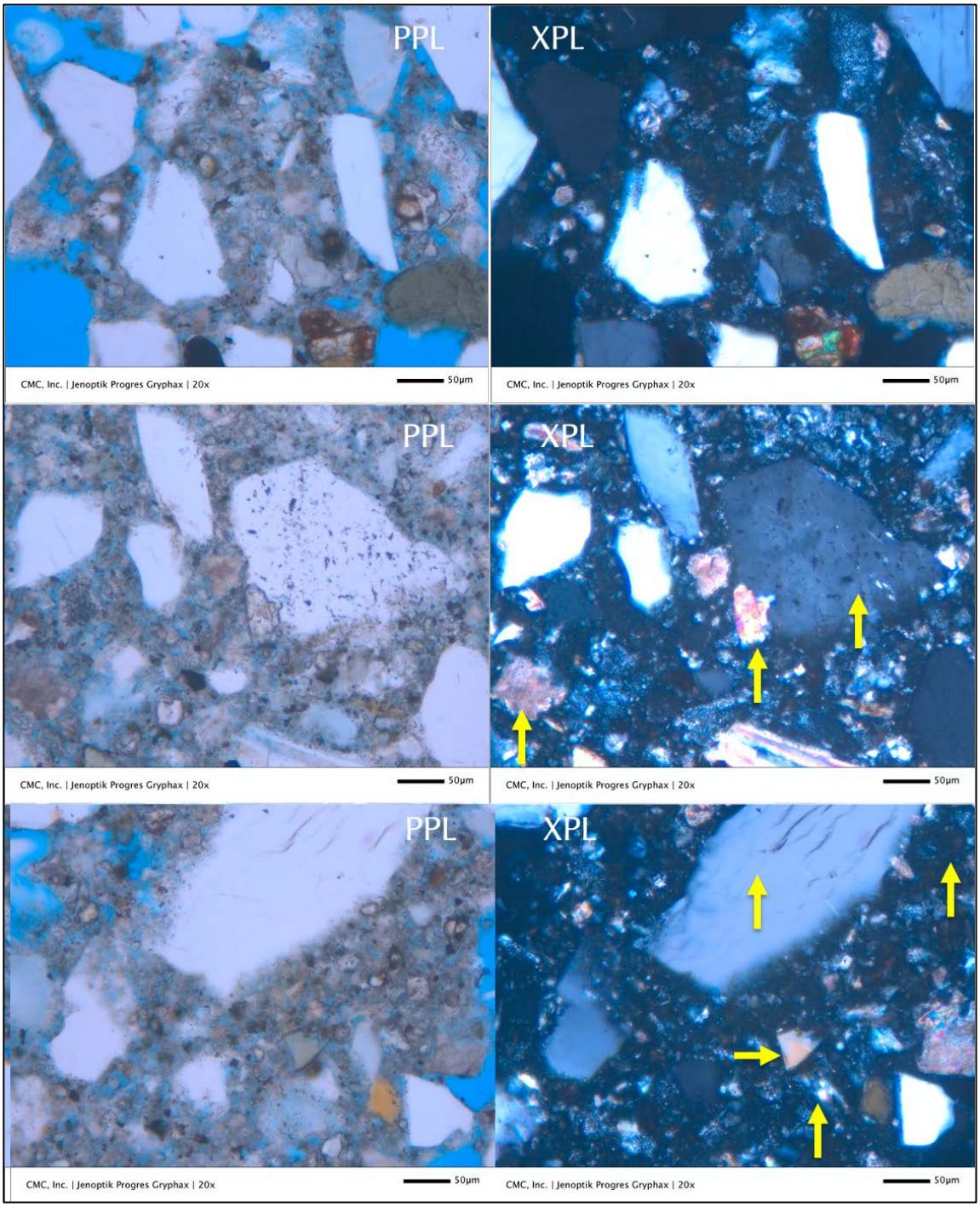

Figure 18: Optical micrographs of a recent mortar (#4) from 2019 construction showing: (a) crushed siliceous sand consisting of major amount of variably strained quartz, subordinate amounts of quartzite, feldspar, schist, and other siliceous particles (no carbonate components were found in the sand, feldspar content of sand is higher than that found in the two original mortars); (b) overall non-carbonated nature of the interstitial matrix between sand particles, which is not a characterstic microstructure of masonry cement mortars found in the original mortars but more common of cement-lime mortars that have not been carbonated yet; (c) hydration products of Portland cement and residual cement particles and a few clumps of hydrated lime and calcium hydroxide component of cement hydration (a few are marked with arrows) that are found in the denser paste fractions. The mortar appears to be a cement-lime mortar as opposed to two different types of masonry cement mortars (one with abundant lime and another with abundant limestone fines) found in the original 1960s construction.

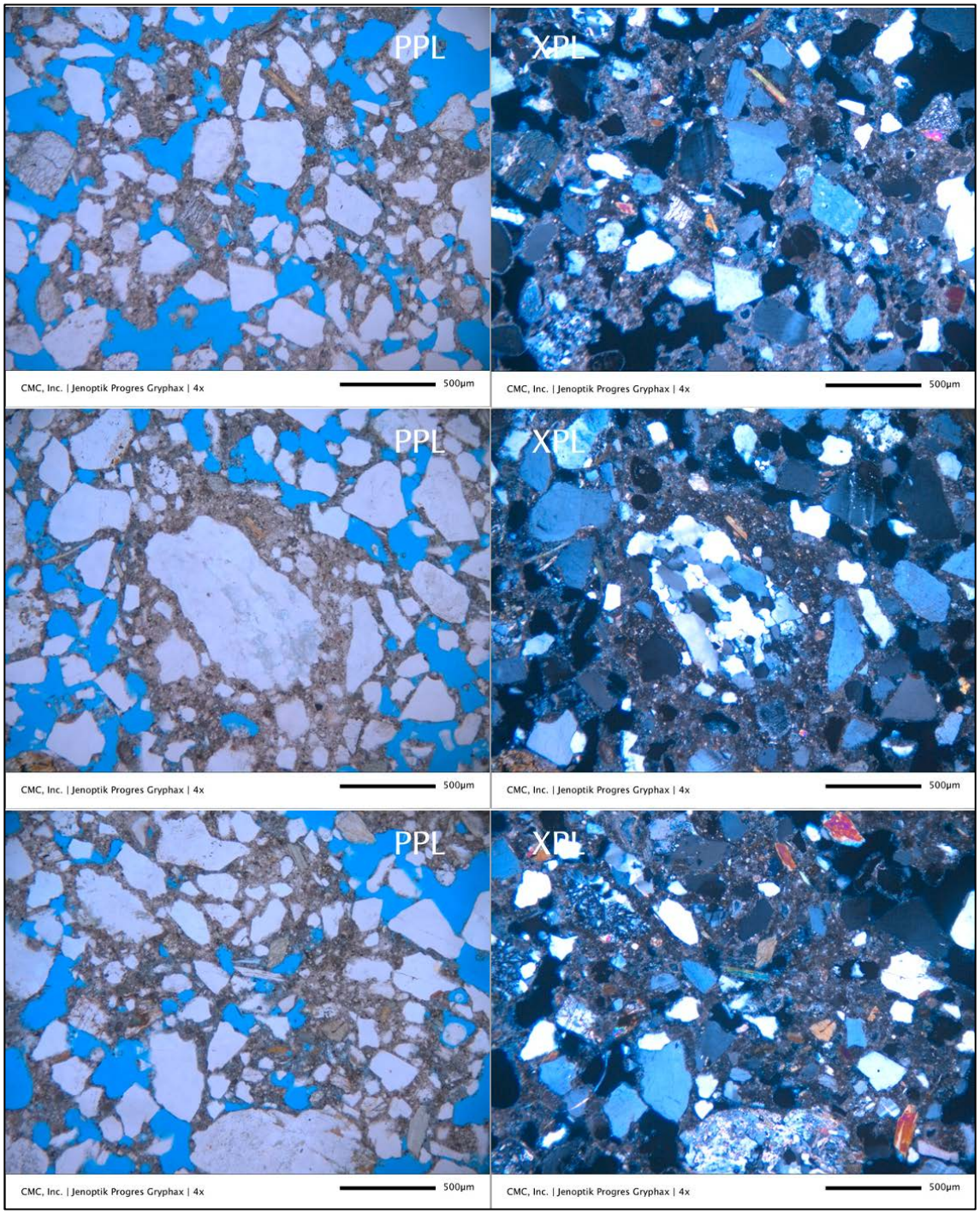

Figure 19: Optical micrographs of a recent mortar (#5) from 2019 construction showing: (a) crushed siliceous sand consisting of major amount of variably strained quartz, subordinate amount of quartzite, feldspar, schist, and other siliceous particles (no carbonate components were found in the sand, feldspar content of sand is higher than that found in the two original mortars); (b) overall carbonated nature of the interstitial matrix between sand particles, which is a characteristic microstructure of masonry cement mortars as found in the original mortars; (c) abundant irregularly-shaped air voids (highlighted by blue epoxy), giving an overall porous nature of the microstructure. The mortar appears to be a masonry cement mortar but not similar to the high-lime or high-limestone fine based masonry cement mortars found in the original 1960s construction since neither of those two binder components are found in levels higher than usually found in common ASTM C 270 Type M, S, or N masonry cement mortars.

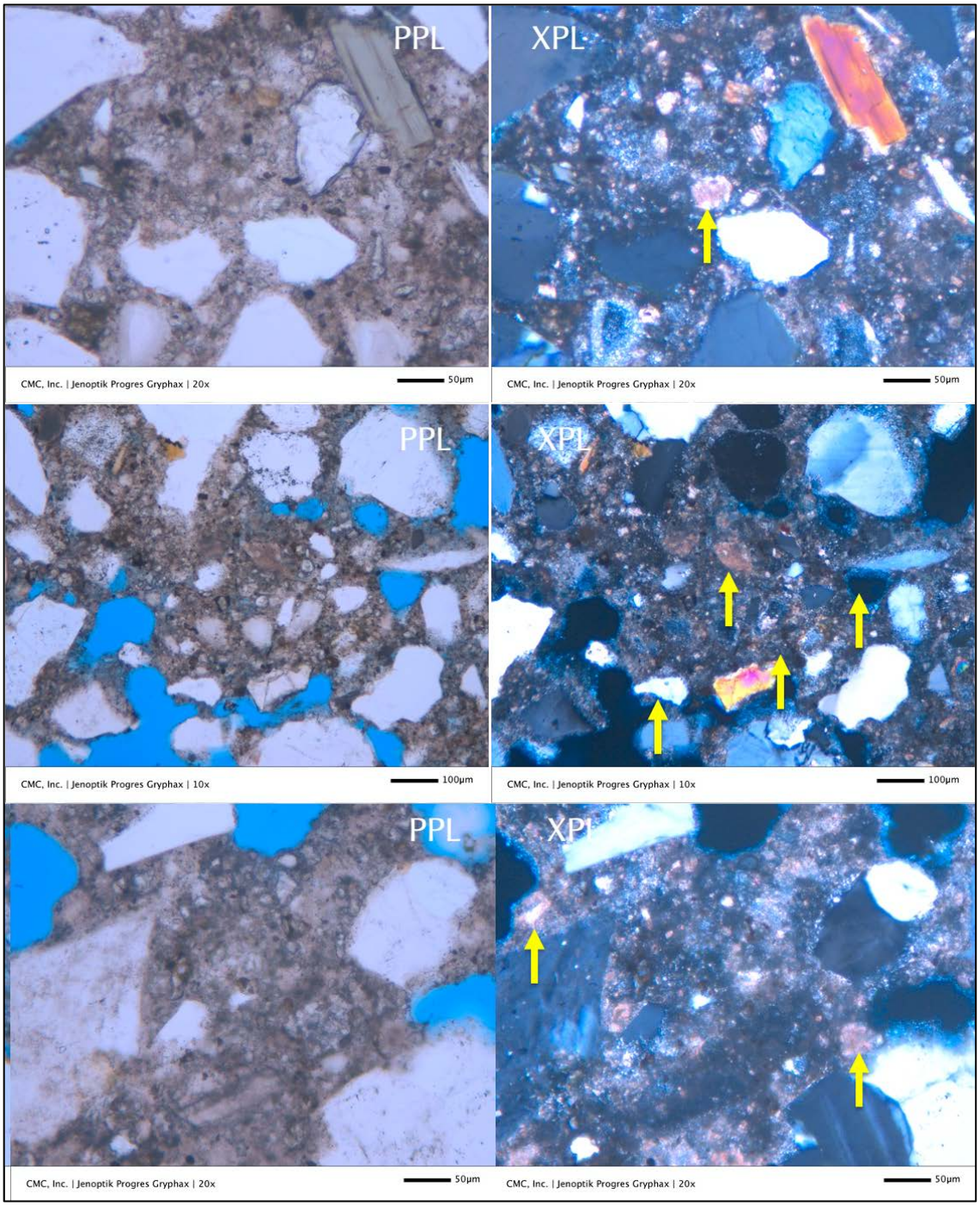

Figure 20: Optical micrographs of a recent mortar (#5) from 2019 construction showing: (a) crushed siliceous sand consisting of major amount of variably strained quartz, subordinate amount of quartzite, feldspar, schist, and other siliceous particles (no carbonate components were found in the sand, feldspar content of sand is higher than that found in the two original mortars); (b) overall carbonated nature of the interstitial matrix between sand particles, which is a characterstic microstructure of masonry cement mortars as found in the original mortars; (c) many patches of lime (some are marked with arrows) in the paste, which are mixed with limestone fines and abundant residual Portland cement particles. The mortar appears to be a masonry cement mortar but not similar to the high-lime or high-limestone fine based masonry cement mortars found in the original 1960s construction but in having more Portland cement than lime and limestone fine components (similar to an ASTM C 91 Type S masonry cment). The denser microstructure of paste is indicative of use of a polymer component in the mix.

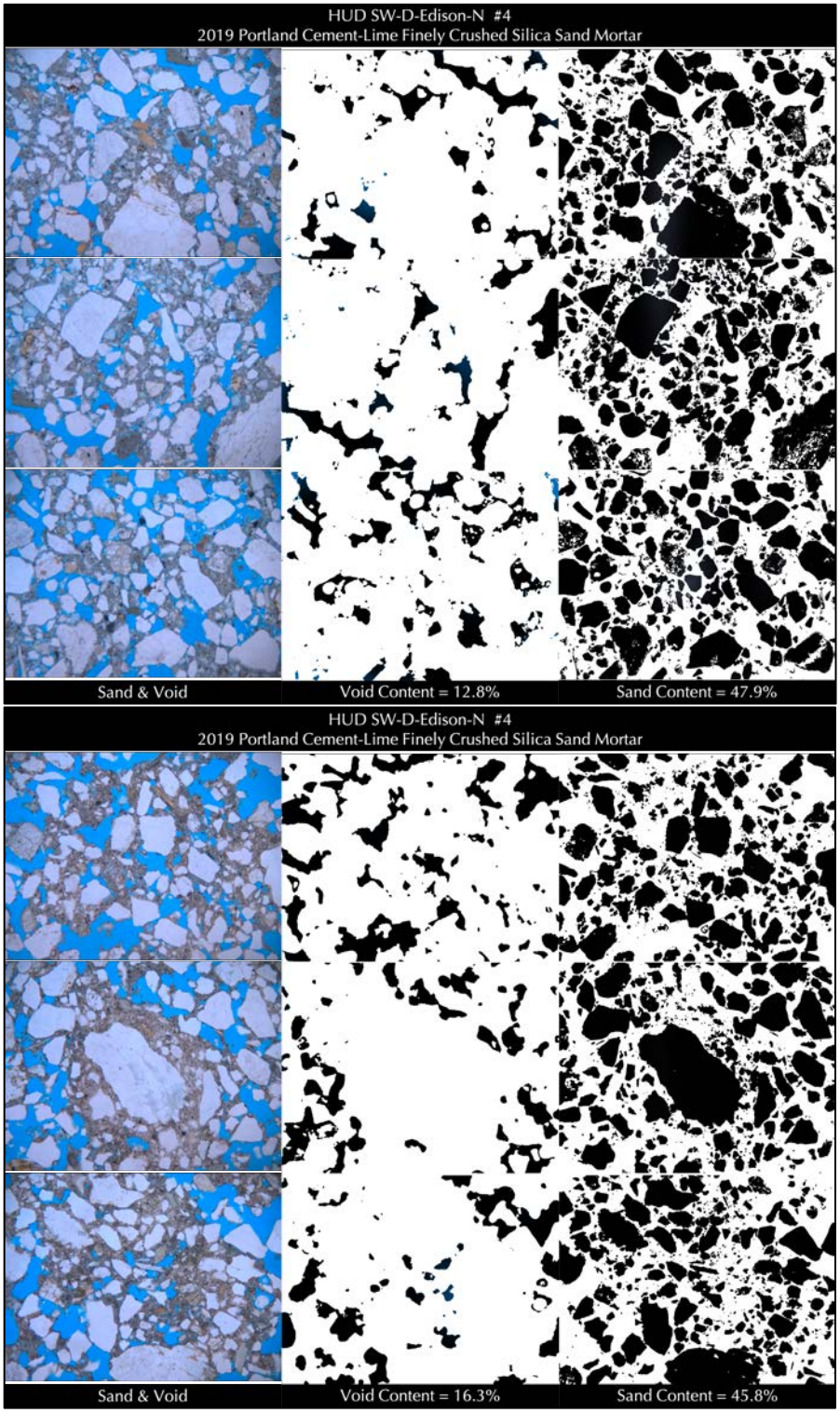

Figure 21: Image analyses (from Image J) to determine void and sand contents from optical micrographs of thin section of two recent mortars. Left column shows plane polarized light photos of distribution of sands and voids from which black and white contrast enhancements were done to highlight voids in black in the middle column and sand in the right column. Void and sand contents were subsequently determined from Image J open source image analysis software (https://imagej.nih.gov/ij).

Optical Microscopy of Stone

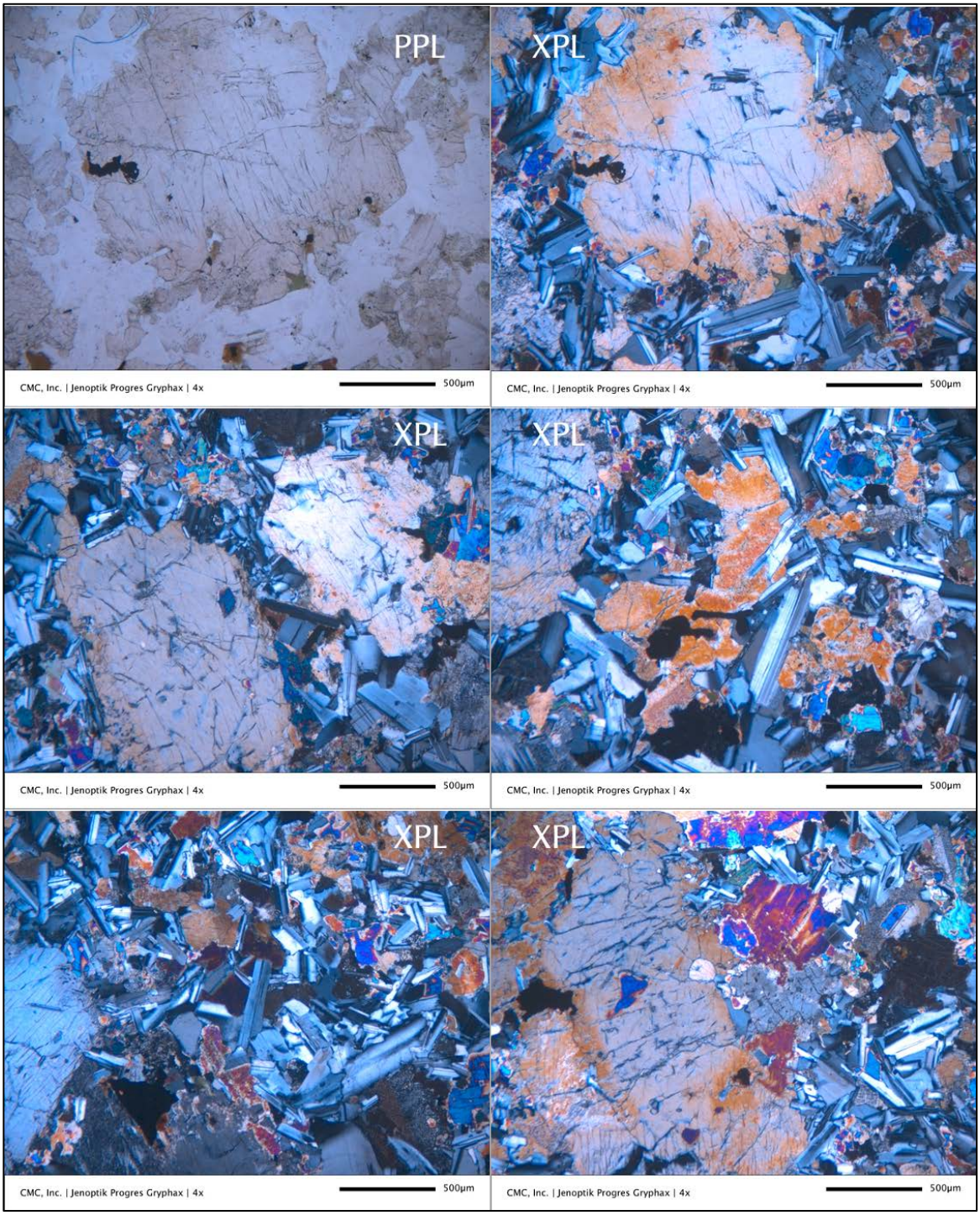

Figure 22: Optical micrographs of the stone sample showing medium-grained crystalline texture consisting of plagioclase feldspar laths and pyroxene crystals (ortho and clinopyroxenes) and a few dark mafic minerals in a subophitic textural arrangement due to partial enclosures of plagioclase laths by pyroxene crystals, which is typical mineralogy and texture of diabase, an intrusive basic igneous rock (also called dolerite in the European literatures), commonly found in many igneous sills (including the famous Palisades sill in New York).

SEM-EDS Compositional Variations of Pastes in Mortars From 1960s Vintage

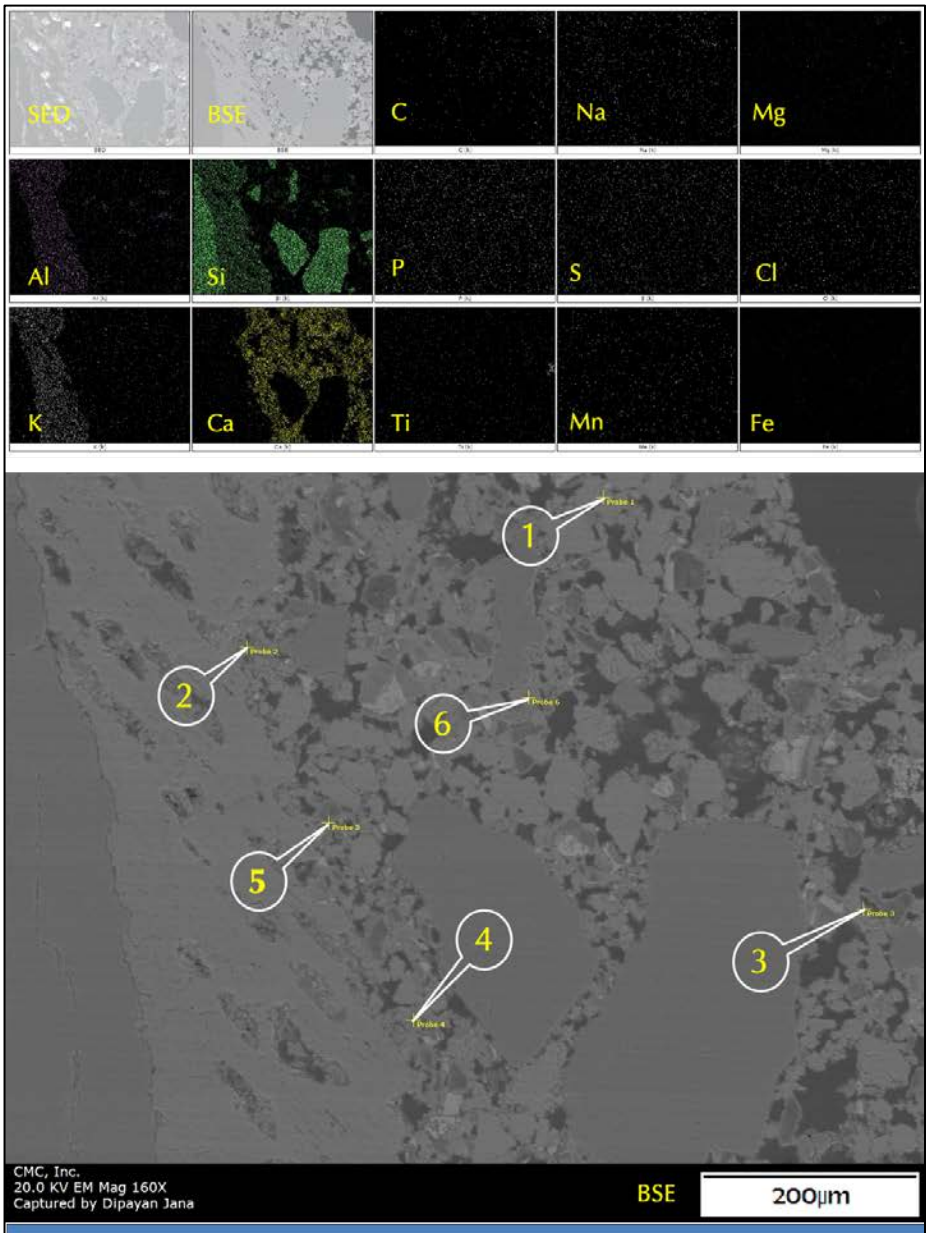

Probe	CaO	SiO2	Al2O3	Na2O	MgO	SO3	K2O	TiO2	FeO	P2O5	CO2	Total	Phase	Paste CI
1	94.85	0.07	0.00	0.00	0.00	0.31	0.00	0.06	0.01	0.54	4.15	99.99	Calcite	-
2	86.29	3.95	0.37	0.00	0.14	0.55	0.15	0.00	0.48	0.14	7.94	100.01	Calcite	-
3	89.06	1.67	2.64	0.00	0.00	0.66	0.13	0.18	0.13	0.77	4.76	100.00	Calcite	-
4	36.03	34.90	1.65	0.03	2.34	1.66	0.12	0.24	1.10	1.21	20.72	100.00	Paste	2.55
5	82.59	7.86	0.58	0.00	0.46	0.37	0.01	0.00	0.58	0.27	7.27	99.99	Calcite	-
6	73.73	11.11	2.32	0.00	0.83	1.36	0.12	0.18	2.26	0.09	8.00	100.00	Paste	0.47

Figure 23: SEM-EDS studies of the original mortar #2 from 1960s construction.

The top photo shows secondary electron image (SED), corresponding backscatter electron image (BSE), and X-ray elemental maps of carbon (C), sodium (Na), magnesium (Mg), aluminum (Al), silicon (Si), phosphorus (P), sulfur (S), chlorine (Cl), potassium (K), calcium (Ca), titanum (Ti), manganese (Mn), and iron (Fe) - showing characteristic enrichment of Si in siliceous sand particles and Ca in interstitial carbonated paste.

The middle photo shows microstructure of mortar in an BSE image. Tips of callouts on this image are areas that were measured by energy-dispersive X-ray fluorescence spectrometer attached to SEM. Results are tabulated below for each Probe#.

Paste CI (cementation index) in the last column is calculated after Eckel (1922) from [(2.8 SiO_2) + (1.1 Al_2O_3) + (0.7 Fe_2O_3)] / [(CaO) +(1.4MgO)], where higher paste-CIs indicate more hydraulic mortar (i.e. cement-based) and lower CI indicates less hydraulic (i.e. lime-based) mortars.

CIs are not calculated when a grain is encountered during compositional analyses as opposed to paste *per se*.

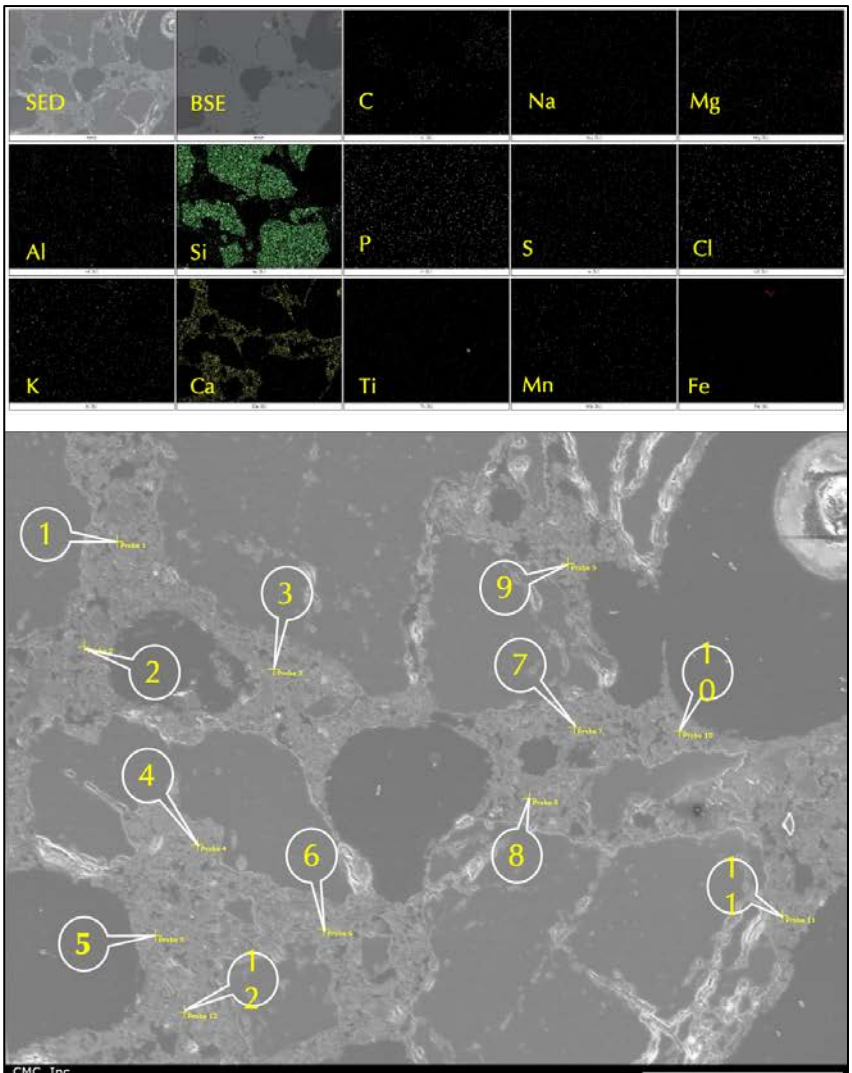

Probe	CaO	SiO2	Al2O3	Na2O	MgO	SO3	K2O	TiO2	FeO	P2O5	CO2	Total	Phase	Paste CI
1	53.62	14.06	2.45	0.15	3.16	1.47	0.12	0.01	1.46	0.75	22.76	100.0	Paste	0.74
2	33.12	34.34	7.60	0.00	3.83	2.84	0.30	0.23	0.77	1.24	15.75	100.0	Paste	2.73
3	29.37	22.45	6.63	0.05	3.85	1.68	0.24	0.28	2.76	0.74	31.98	100.0	Paste	2.07
4	1.00	0.76	0.00	0.00	0.00	0.91	0.07	0.00	0.17	1.88	95.20	99.99	Void	-
5	60.54	10.26	4.76	0.01	0.48	1.96	0.63	0.19	1.52	0.45	19.20	100.0	Paste	0.57
6	38.70	19.79	13.66	0.00	4.02	3.16	0.08	0.09	1.47	0.98	18.05	100.0	Paste	1.61
7	37.31	21.53	2.06	0.00	0.12	1.81	0.08	2.31	0.44	0.69	33.65	100.0	Paste	1.68
8	57.49	14.09	5.42	0.08	1.13	1.95	0.38	0.13	0.56	0.66	18.12	100.0	Paste	0.78
9	67.23	8.10	3.35	0.15	1.18	2.52	0.18	0.02	1.28	0.54	15.46	100.0	Paste	0.40
10	31.15	23.05	14.87	0.00	0.28	2.28	0.46	0.03	0.80	0.24	26.84	100.0	Paste	2.58
11	71.79	7.51	3.55	0.05	0.10	1.62	0.07	0.00	0.35	0.36	14.59	99.99	Paste	0.35
12	53.21	16.15	11.50	0.00	0.33	1.93	0.88	0.08	0.39	0.47	15.06	100.0	Paste	1.08

Figure 24: SEM-EDS studies of the original mortar #3 from 1960s construction.

The top photo shows secondary electron image (SED), corresponding backscatter electron image (BSE), and X-ray elemental maps of carbon (C), sodium (Na), magnesium (Mg), aluminum (Al), silicon (Si), phosphorus (P), sulfur (S), chlorine (Cl), potassium (K), calcium (Ca), titanum (Ti), manganese (Mn), and iron (Fe) - showing characteristic enrichment of Si in siliceous sand particles and Ca in interstitial carbonated paste.

The middle photo shows microstructure of mortar in an BSE image. Tips of callouts on this image are areas that were measured by energy-dispersive X-ray fluorescence spectrometer attached to SEM.

Results are tabulated below for each Probe#. Paste CI (cementation index) in the last column is calculated after Eckel (1922) from [(2.8 SiO_2) + (1.1 Al_2O_3) + (0.7 Fe_2O_3)] / [(CaO) +(1.4MgO)], where higher paste-CIs indicate more hydraulic mortar (i.e. cement-based) and lower CI indicates less hydraulic (i.e. lime-based) mortars.

Paste-CIs are not calculated when a grain is encountered during compositional analyses as opposed to paste *per se*.

SEM-EDS Compositional Variations of Pastes in Mortars From 2019

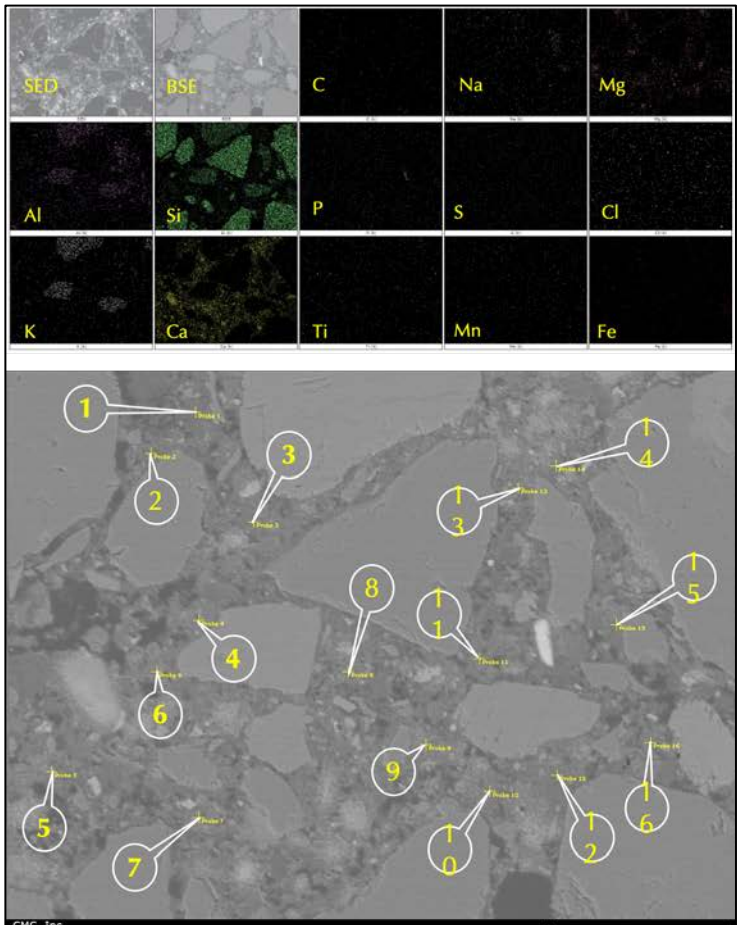

Probe	CaO	SiO2	Al2O3	Na2O	MgO	SO3	K2O	TiO2	FeO	P2O5	CO2	Total	Phase	Paste CI
1	23.37	6.51	3.34	0.00	34.54	1.11	0.05	0.00	0.41	0.97	29.70	100.0	Paste	0.31
2	18.21	11.53	7.53	0.05	29.73	0.78	0.00	0.04	0.21	0.26	31.65	100.0	Paste	0.68
3	27.81	24.43	4.20	0.00	5.53	2.81	0.06	0.04	2.61	1.06	31.45	100.0	Paste	2.11
4	57.89	19.85	2.10	0.00	1.03	0.17	0.01	0.09	2.19	0.87	15.81	100.0	Paste	1.00
5	21.05	36.34	12.06	1.52	7.87	0.57	0.11	0.09	1.15	0.45	18.79	100.0	Paste	3.61
6	31.24	27.80	3.46	0.00	5.63	1.97	0.02	0.26	2.36	0.59	26.67	100.0	Paste	2.13
7	27.41	23.32	4.95	0.08	6.89	1.76	0.00	0.02	3.59	0.29	31.70	100.0	Paste	1.98
8	28.52	25.08	3.46	0.00	6.94	1.70	0.01	0.29	1.27	0.93	31.80	100.0	Paste	1.96
9	32.81	17.06	5.25	0.00	8.94	4.13	0.02	0.11	0.56	0.65	30.47	100.0	Paste	1.19
10	23.98	19.89	3.94	0.00	10.33	1.02	0.03	0.04	0.27	0.31	40.18	100.0	Paste	1.57
11	30.26	22.91	2.98	0.00	5.08	2.22	0.07	0.06	2.01	0.15	34.25	100.0	Paste	1.84
12	16.85	9.46	5.85	0.06	37.13	1.64	0.00	0.00	0.76	0.90	27.35	100.0	Paste	0.49
13	33.47	16.17	2.96	0.00	14.13	1.20	0.06	0.16	0.49	0.95	30.40	100.0	Paste	0.92
14	28.27	16.44	2.86	0.00	5.20	1.79	0.04	0.08	0.00	0.04	45.27	100.0	Paste	1.38
15	9.78	57.49	5.10	0.00	4.32	0.37	0.00	0.08	0.84	0.35	21.67	100.0	-	-
16	10.01	10.09	7.11	0.19	20.84	0.81	0.08	0.00	0.28	0.18	50.40	100.0	Paste	0.93

Figure 25: SEM-EDS studies of the recent mortar #4 from 2019 construction.

The top photo shows secondary electron image (SED), corresponding backscatter electron image (BSE), and X-ray elemental maps of carbon (C), sodium (Na), magnesium (Mg), aluminum (Al), silicon (Si), phosphorus (P), sulfur (S), chlorine (Cl), potassium (K), calcium (Ca), titanum (Ti), manganese (Mn), and iron (Fe) - showing characteristic enrichment of Si in siliceous sand particles and Ca in interstitial carbonated paste.

The middle photo shows microstructure of mortar in an BSE image. Tips of callouts on this image are areas that were measured by energy-dispersive X-ray fluorescence spectrometer attached to SEM.

Results are tabulated below for each Probe#. Paste CI (cementation index) at the last column is calculated after Eckel (1922) from [(2.8 SiO_2) + (1.1 Al_2O_3) + (0.7 Fe_2O_3)] / [(CaO) +(1.4MgO)], where higher paste-CIs indicate more hydraulic mortar (i.e. cement-based) and lower CI indicates less hydraulic (i.e. lime-based) mortars.

Paste-CIs are not calculated when a grain is encountered during compositional analyses as opposed to paste *per se*.

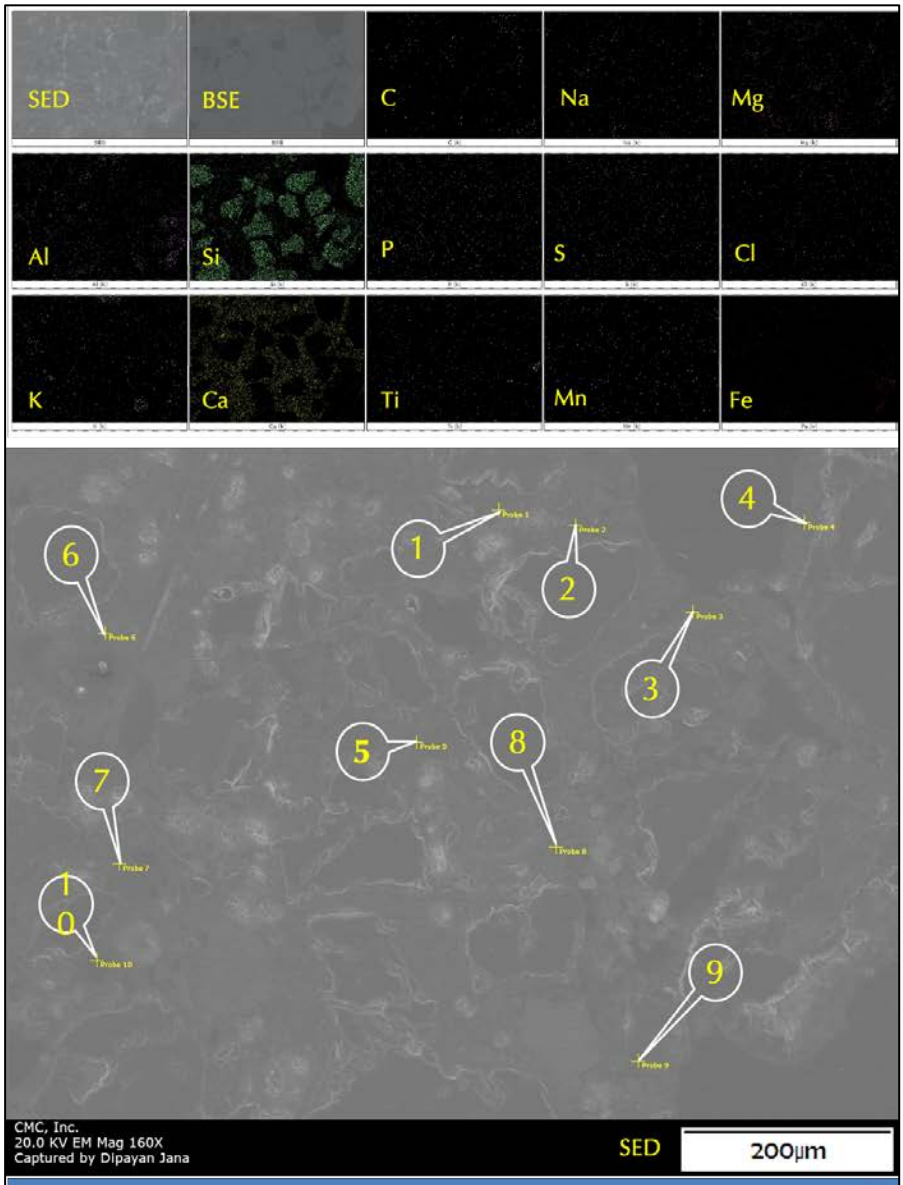

Probe	CaO	SiO2	Al2O3	Na2O	MgO	SO3	K2O	TiO2	FeO	P2O5	CO2	Total	Phase	Paste CI
1	11.26	6.16	3.79	0.48	25.49	0.84	0.00	0.02	0.29	0.35	51.32	100.0	Paste	0.46
2	36.68	16.14	1.20	0.02	7.01	0.80	0.02	0.19	0.34	0.64	36.96	100.0	Paste	1.01
3	37.39	6.55	1.17	0.08	4.56	0.00	0.04	0.06	0.10	0.20	49.85	100.0	Paste	0.45
4	52.51	6.11	0.61	0.00	19.62	0.21	0.02	0.00	0.62	0.36	19.92	100.0	Paste	0.23
5	37.53	12.62	2.35	0.00	17.44	0.69	0.05	0.16	0.46	0.58	28.11	100.0	Paste	0.62
6	50.99	2.70	0.02	0.01	21.37	0.57	0.00	0.00	0.00	0.18	24.15	100.0	Paste	0.09
7	12.42	62.71	0.99	0.00	1.06	0.11	0.00	0.00	0.31	0.61	21.79	100.0	-	-
8	40.35	4.15	0.46	0.00	13.10	0.51	0.01	0.06	0.34	0.30	40.72	100.0	Paste	0.21
9	36.29	15.97	4.03	0.16	2.24	2.59	0.06	0.00	0.42	0.37	37.86	100.0	Paste	1.25
10	15.18	4.72	0.16	0.05	0.14	1.66	0.00	0.09	0.70	0.17	77.14	100.0	Paste	0.90

Figure 26: SEM-EDS studies of the recent mortar #5 from 2019 construction.

The top photo shows secondary electron image (SED), corresponding backscatter electron image (BSE), and X-ray elemental maps of carbon (C), sodium (Na), magnesium (Mg), aluminum (Al), silicon (Si), phosphorus (P), sulfur (S), chlorine (Cl), potassium (K), calcium (Ca), titanium (Ti), manganese (Mn), and iron (Fe) - showing characteristic enrichment of Si in siliceous sand particles and Ca in interstitial carbonated paste.

The middle photo shows microstructure of mortar in an SED image. Tips of callouts on this image are areas that were measured by energy-dispersive X-ray fluorescence spectrometer attached to SEM.

Results are tabulated below for each Probe#. Paste CI (cementation index) in the last column is calculated after Eckel (1922) from [(2.8 SiO_2) + (1.1 Al_2O_3) + (0.7 Fe_2O_3)] / [(CaO) +(1.4MgO)], where higher paste-CIs indicate more hydraulic mortar (i.e. cement-based) and lower CI indicates less hydraulic (i.e. lime-based) mortars.

Paste-CIs are not calculated when a grain is encountered during compositional analyses as opposed to paste *per se*.

Notice the overall denser microstructure of paste compared to other mortars due to incorporation of a polymer component in the mix.

SEM-EDS Studies Binder Fractions of Mortars From 1960s and 2019 – A comparison

	Probe#	CaO	SiO2	Al2O3	Na2O	MgO	SO3	K2O	TiO2	FeO	P2O5	CO2	Total	Phase	Paste CI
Mortar 2	4	36.03	34.90	1.65	0.03	2.34	1.66	0.12	0.24	1.10	1.21	20.72	100	Paste	2.55
Mortar 2	6	73.73	11.11	2.32	0.00	0.83	1.36	0.12	0.18	2.26	0.09	8.00	100	Paste	0.47
Mortar 3	1	53.62	14.06	2.45	0.15	3.16	1.47	0.12	0.01	1.46	0.75	22.76	100	Paste	0.74
Mortar 3	2	33.12	34.34	7.60	0.00	3.83	2.84	0.30	0.23	0.77	1.24	15.75	100	Paste	2.73
Mortar 3	3	29.37	22.45	6.63	0.05	3.85	1.68	0.24	0.28	2.76	0.74	31.98	100	Paste	2.07
Mortar 3	5	60.54	10.26	4.76	0.01	0.48	1.96	0.63	0.19	1.52	0.45	19.20	100	Paste	0.57
Mortar 3	6	38.70	19.79	13.66	0.00	4.02	3.16	0.08	0.09	1.47	0.98	18.05	100	Paste	1.61
Mortar 3	7	37.31	21.53	2.06	0.00	0.12	1.81	0.08	2.31	0.44	0.69	33.65	100	Paste	1.68
Mortar 3	8	57.49	14.09	5.42	0.08	1.13	1.95	0.38	0.13	0.56	0.66	18.12	100	Paste	0.78
Mortar 3	9	67.23	8.10	3.35	0.15	1.18	2.52	0.18	0.02	1.28	0.54	15.46	100	Paste	0.40
Mortar 3	10	31.15	23.05	14.87	0.00	0.28	2.28	0.46	0.03	0.80	0.24	26.84	100	Paste	2.58
Mortar 3	11	71.79	7.51	3.55	0.05	0.10	1.62	0.07	0.00	0.35	0.36	14.59	100	Paste	0.35
Mortar 3	12	53.21	16.15	11.50	0.00	0.33	1.93	0.88	0.08	0.39	0.47	15.06	100	Paste	1.08
Mortar 4	1	23.37	6.51	3.34	0.00	34.54	1.11	0.05	0.00	0.41	0.97	29.70	100	Paste	0.31
Mortar 4	2	18.21	11.53	7.53	0.05	29.73	0.78	0.00	0.04	0.21	0.26	31.65	100	Paste	0.68
Mortar 4	3	27.81	24.43	4.20	0.00	5.53	2.81	0.06	0.04	2.61	1.06	31.45	100	Paste	2.11
Mortar 4	4	57.89	19.85	2.10	0.00	1.03	0.17	0.01	0.09	2.19	0.87	15.81	100	Paste	1.00
Mortar 4	5	21.05	36.34	12.06	1.52	7.87	0.57	0.11	0.09	1.15	0.45	18.79	100	Paste	3.61
Mortar 4	6	31.24	27.80	3.46	0.00	5.63	1.97	0.02	0.26	2.36	0.59	26.67	100	Paste	2.13
Mortar 4	7	27.41	23.32	4.95	0.08	6.89	1.76	0.00	0.02	3.59	0.29	31.70	100	Paste	1.98
Mortar 4	8	28.52	25.08	3.46	0.00	6.94	1.70	0.01	0.29	1.27	0.93	31.80	100	Paste	1.96
Mortar 4	9	32.81	17.06	5.25	0.00	8.94	4.13	0.02	0.11	0.56	0.65	30.47	100	Paste	1.19
Mortar 4	10	23.98	19.89	3.94	0.00	10.33	1.02	0.03	0.04	0.27	0.31	40.18	100	Paste	1.57
Mortar 4	11	30.26	22.91	2.98	0.00	5.08	2.22	0.07	0.06	2.01	0.15	34.25	100	Paste	1.84
Mortar 4	12	16.85	9.46	5.85	0.06	37.13	1.64	0.00	0.00	0.76	0.90	27.35	100	Paste	0.49
Mortar 4	13	33.47	16.17	2.96	0.00	14.13	1.20	0.06	0.16	0.49	0.95	30.40	100	Paste	0.92
Mortar 4	14	28.27	16.44	2.86	0.00	5.20	1.79	0.04	0.08	0.00	0.04	45.27	100	Paste	1.38
Mortar 4	16	10.01	10.09	7.11	0.19	20.84	0.81	0.08	0.00	0.28	0.18	50.40	100	Paste	0.93
Mortar 5	1	11.26	6.16	3.79	0.48	25.49	0.84	0.00	0.02	0.29	0.35	51.32	100	Paste	0.46
Mortar 5	2	36.68	16.14	1.20	0.02	7.01	0.80	0.02	0.19	0.34	0.64	36.96	100	Paste	1.01
Mortar 5	3	37.39	6.55	1.17	0.08	4.56	0.00	0.04	0.06	0.10	0.20	49.85	100	Paste	0.45
Mortar 5	4	52.51	6.11	0.61	0.00	19.62	0.21	0.02	0.00	0.62	0.36	19.92	100	Paste	0.23
Mortar 5	5	37.53	12.62	2.35	0.00	17.44	0.69	0.05	0.16	0.46	0.58	28.11	100	Paste	0.62
Mortar 5	6	50.99	2.70	0.02	0.01	21.37	0.57	0.00	0.00	0.00	0.18	24.15	100	Paste	0.09
Mortar 5	8	40.35	4.15	0.46	0.00	13.10	0.51	0.01	0.06	0.34	0.30	40.72	100	Paste	0.21
Mortar 5	9	36.29	15.97	4.03	0.16	2.24	2.59	0.06	0.00	0.42	0.37	37.86	100	Paste	1.25
Mortar 5	10	15.18	4.72	0.16	0.05	0.14	1.66	0.00	0.09	0.70	0.17	77.14	100	Paste	0.90

Table 2: SEM-EDS oxide compositional variations of pastes from original (1960s) and recent (2019) mortar samples encompassing original masonry cement mortars in # 2 and 3, followed by recent cement-lime mortar in #4 and masonry cement mortar in #5. Paste CI (cementation index) in the last column is calculated after Eckel (1922) from [(2.8 SiO_2) + (1.1 Al_2O_3) + (0.7 Fe_2O_3)] / [(CaO) +(1.4MgO)], where higher paste-CIs indicate more hydraulic mortar (i.e. cement-based) and lower CI indicates less hydraulic (i.e. lime-based) mortars. These results are used in the plots of compositional variations of pastes shown in Figures 24 and 25.

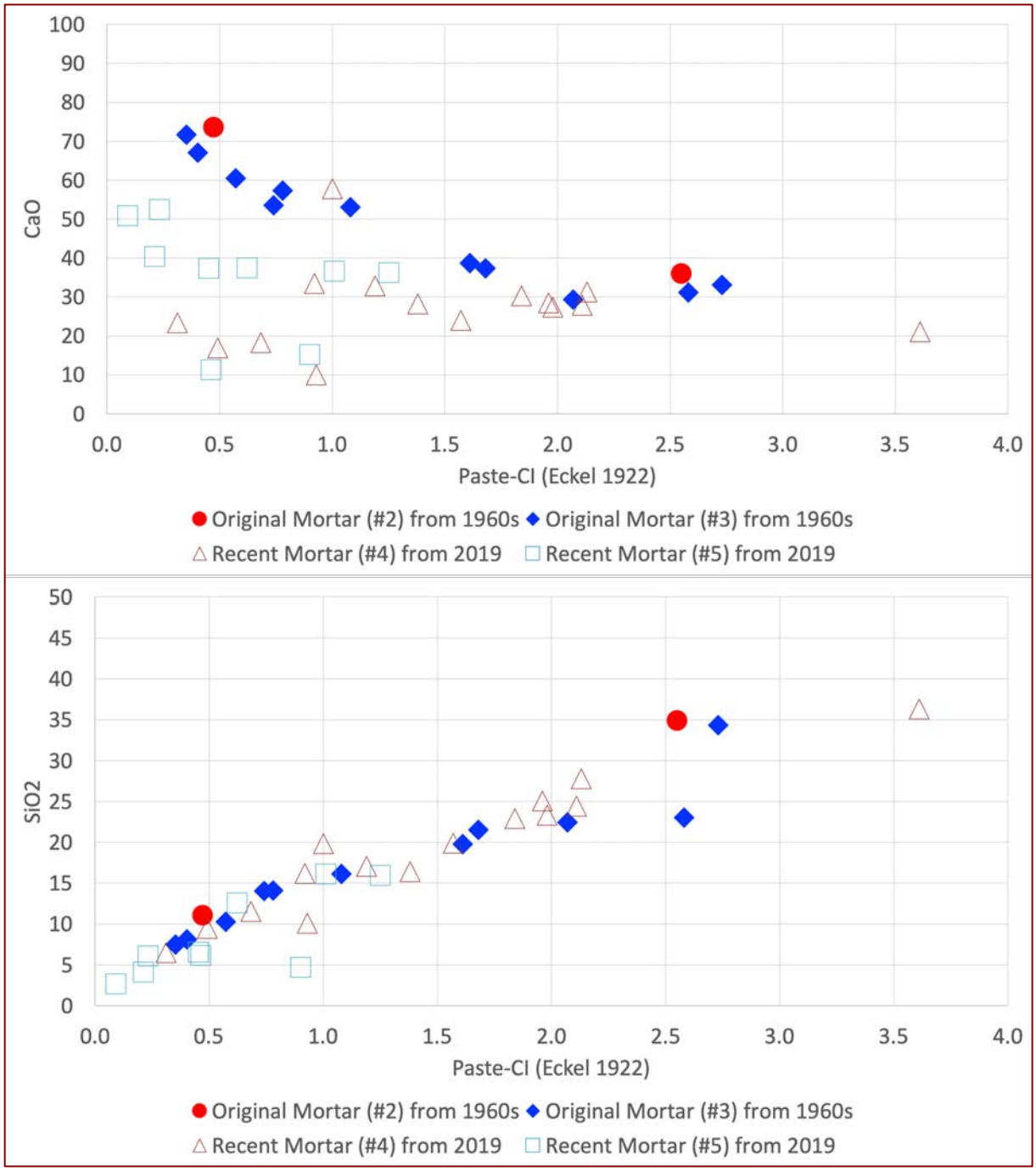

Figure 27: Variations in lime and silica contents of pastes plotted against paste-CIs from the original (1960s) mortars #2 (filled red circle) and #3(filled blue diamond), and recent (2019) mortars #4 (open triangle) and #5 (open square). Results show a very typical characteristic trend of increasing silica content of paste with decreasing lime content resulting in increasing paste-CI. A modern cement-lime mortar shows similar trends of lime and silica contents against paste-CI due to variations in lime and cement contents. Trends as seen here are due to multiple factors from various binder types used in these mortars from Portland cement to lime to limestone fines along with various degrees of alterations during service that also alters the paste-CI, e.g., from lime leaching. Paste-CIs for most plots are results of such alterations, rather than pristine binder compositions (which are usually <1 for non-hydraulic lime binders, 1 to 1.5 for cement-lime binders, and 1.5 to 2 for cement-rich binders).

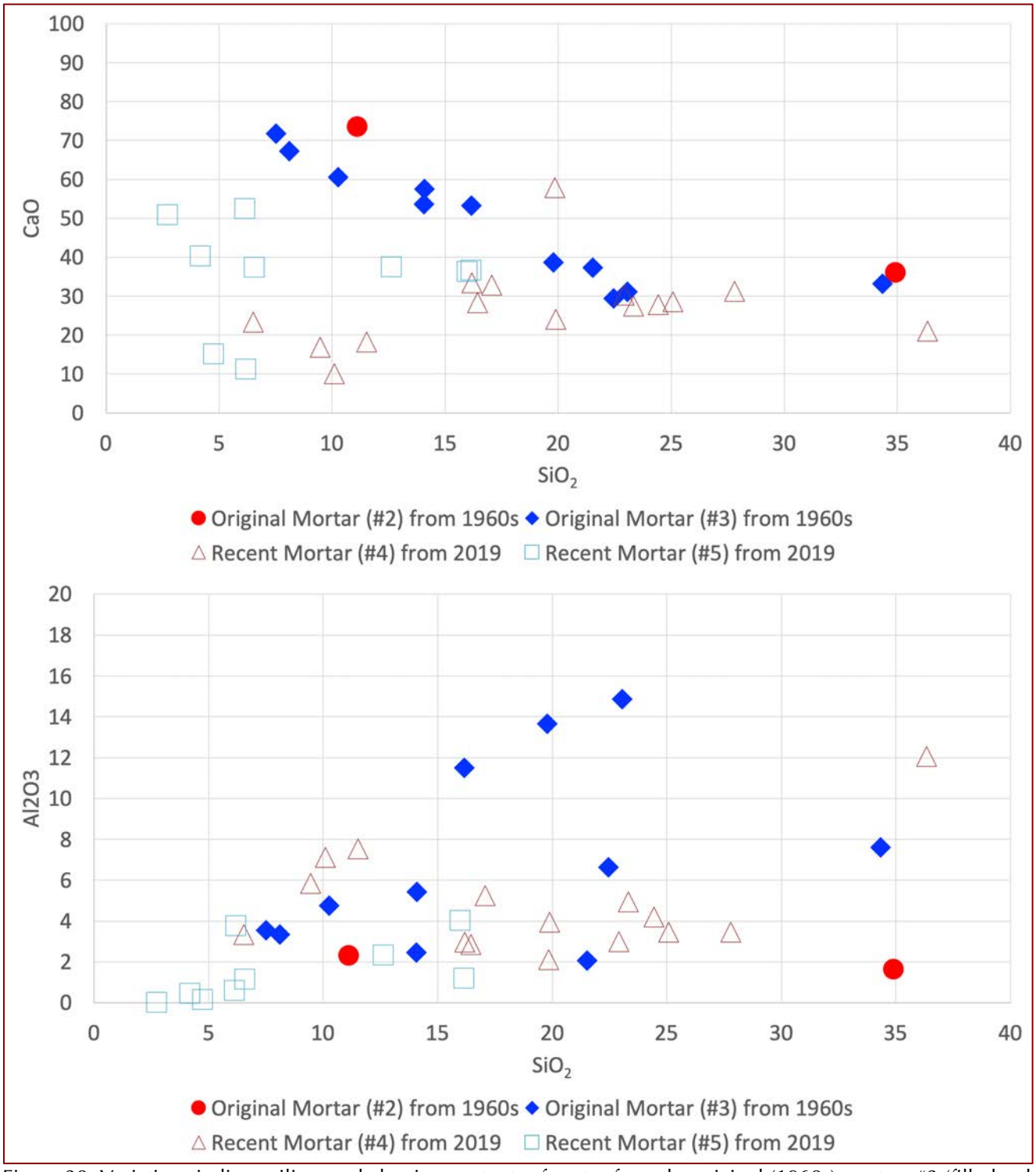

Figure 28: Variations in lime, silica, and alumina contents of pastes from the original (1960s) mortars #2 (filled red circle) and #3(filled blue diamond), and recent (2019) mortars #4 (open triangle) and #5 (open square).

Mortar Types from Optical & Electron Microscopy

Mortars	Type	Sand	Binder	Comments
HUD #2 from 1960s construction	Masonry cement mortar	Crushed silica sand made using • Major amount of quartz • Minor amounts of quartzite, feldspar, and • Trace amounts of other siliceous components	Masonry cement made using • Major amount of limestone fines • Subordinate amount of lime, and • Minor amount of Portland cement	• Abundant interstitial voids between finer sand particles and calcite grains of limestone fine resulting in an overall porous microstructure of mortar • Overall carbonated nature of paste is characteristic of many masonry cement mortars • However, unlike many masonry cement mortars, which are characteristically air-entrained, the present mortar does not show good air void system of fine discrete spherical entrained air bubbles instead of mostly irregular-shaped voids between particles
HUD #3 from 1960s construction	Masonry cement mortar	Crushed silica sand made using • Major amount of quartz • Minor amounts of quartzite, feldspar, and • Trace amounts of other siliceous components • Sand is compositionally similar to the sand found in the original mortar in #2	Masonry cement made using • Major amount of dolomitic hydrated lime, • Minor amount of Portland cement, • Minor amount of limestone fines, and • Trace amount of spherical fly ash particles	• Overall paste porosity is less than that found in the original mortar from #2 • Overall much finer-grained carbonated lime microstructure of paste due to dominance of lime in the binder than the granular appearance of paste from limestone fines in the #2 mortar • Overall carbonated nature of paste is characteristic of many masonry cement mortars • However, unlike many masonry cement mortars, which are characteristically air-entrained, the present mortar does not show good air-void system of fine discrete spherical entrained air bubbles instead of mostly irregular-shaped voids between particles
HUD #4 from 2019 construction	Portland cement-dolomitic hydrated lime mortar	Crushed silica sand made using • Major amount of quartz • Minor amounts of quartzite, feldspar, and • Trace amounts of other siliceous components	Portland cement and dolomitic hydrated lime	• Overall non-carbonated nature of the paste due to cement-lime composition of binders and lack of atmospheric carbonation of cement hydration products or lime as opposed to carbonated nature found in three other mortars all of which are masonry cement mortars • Calcium hydroxide patches from cement hydration along with clustered finer grained lime patches
HUD #5 from 2019 construction	Masonry cement mortar	Crushed silica sand made using • Major amount of quartz • Subordinate amounts of quartzite, feldspar, and • Minor amounts of other siliceous components (e.g., schist)	Masonry cement made using major amount of Portland cement, subordinate hydrated lime, and minor limestone fines, similar to an ASTM C 91 Type S masonry cement	• Overall carbonated nature of paste is characteristic of many masonry cement mortars • However, unlike many masonry cement mortars, which are characteristically air-entrained, the present mortar does not show good air-void system of fine discrete spherical entrained air bubbles instead of mostly irregular-shaped voids between particles

Table 3: Summary of compositional information of four mortars from 1960s and 2019 construction determined from optical and electron microscopy.

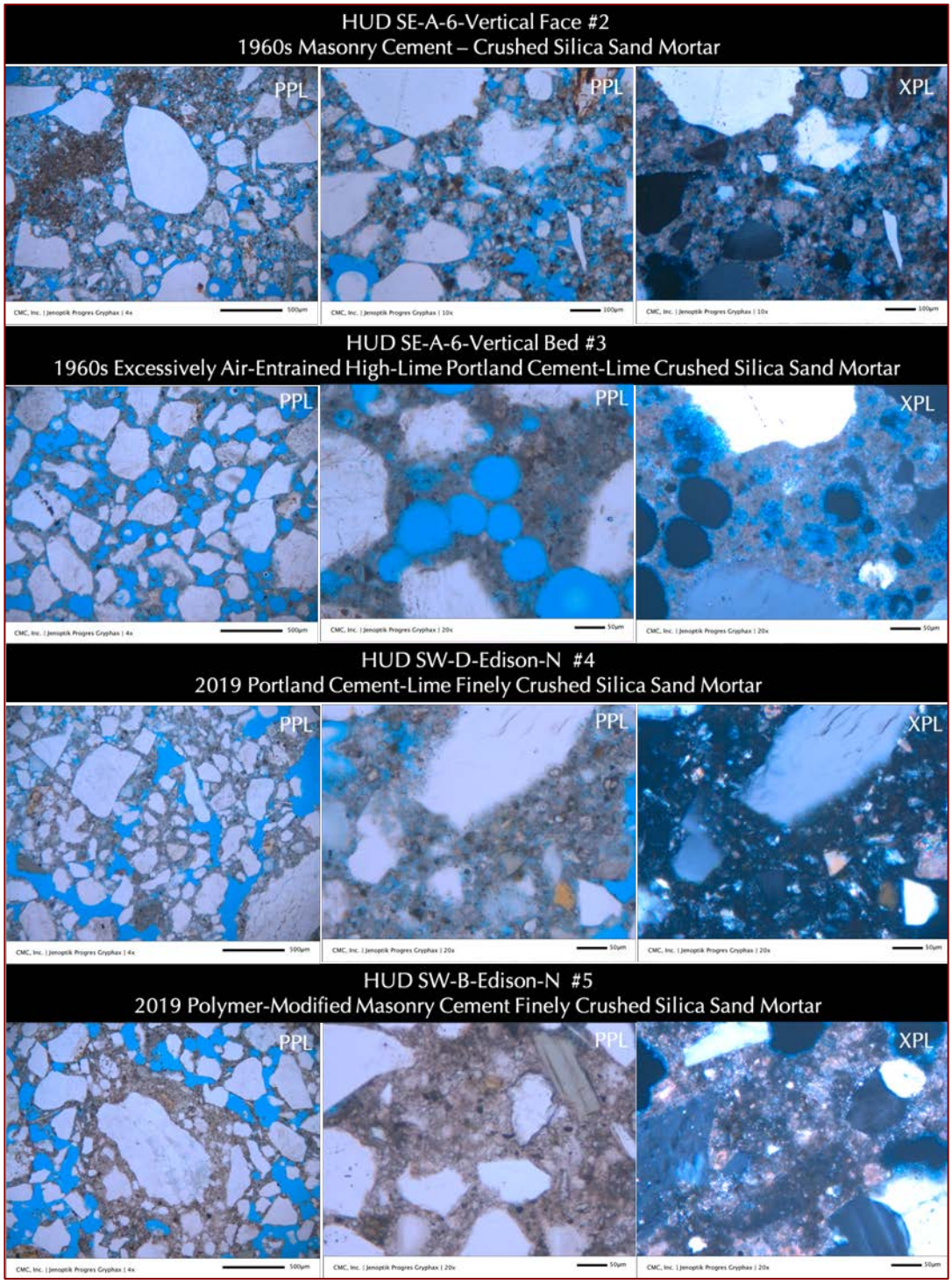

Figure 29: Summary of optical micrographs of four mortar types showing:

(a) Overall crushed nature of sand used in all mortars from the overall angularities of sand particles, along with silcieous nature of sand used, which are dominantly silica (quartz) based on the original mortars but quartzote-quartzite-feldspar based in the recent mortars;

(b) Abundant interstitial voids between sand particles in mortars from #2, 4, and 5 which are all non-air-entrained to marginally air-entrained whereas abunant air entrainment in the original mortar from #3 which shows interstitial voids from excessive air-entrainment, which is detrimental to bonds of this mortar to adjacent masonry units;

(c) Overall carbonated natures of mortars from #2, 3, and 5 due to use of masonry cements (though of variable compositions) in these mortars, whereas non-carbonated nature of paste in the mortar from #4 due to use of cement-lime binders;

(d) Abundant limestone fine components in the masonry mortar from #2 compared to masonry mortars from # 3 (which has abundant dolomitic hydrated lime) or #5 which has reasonable cement and lime components as found in other masonry mortars).

Mineralogical Compositions of 1960s Mortars from X-Ray Diffraction (XRD)

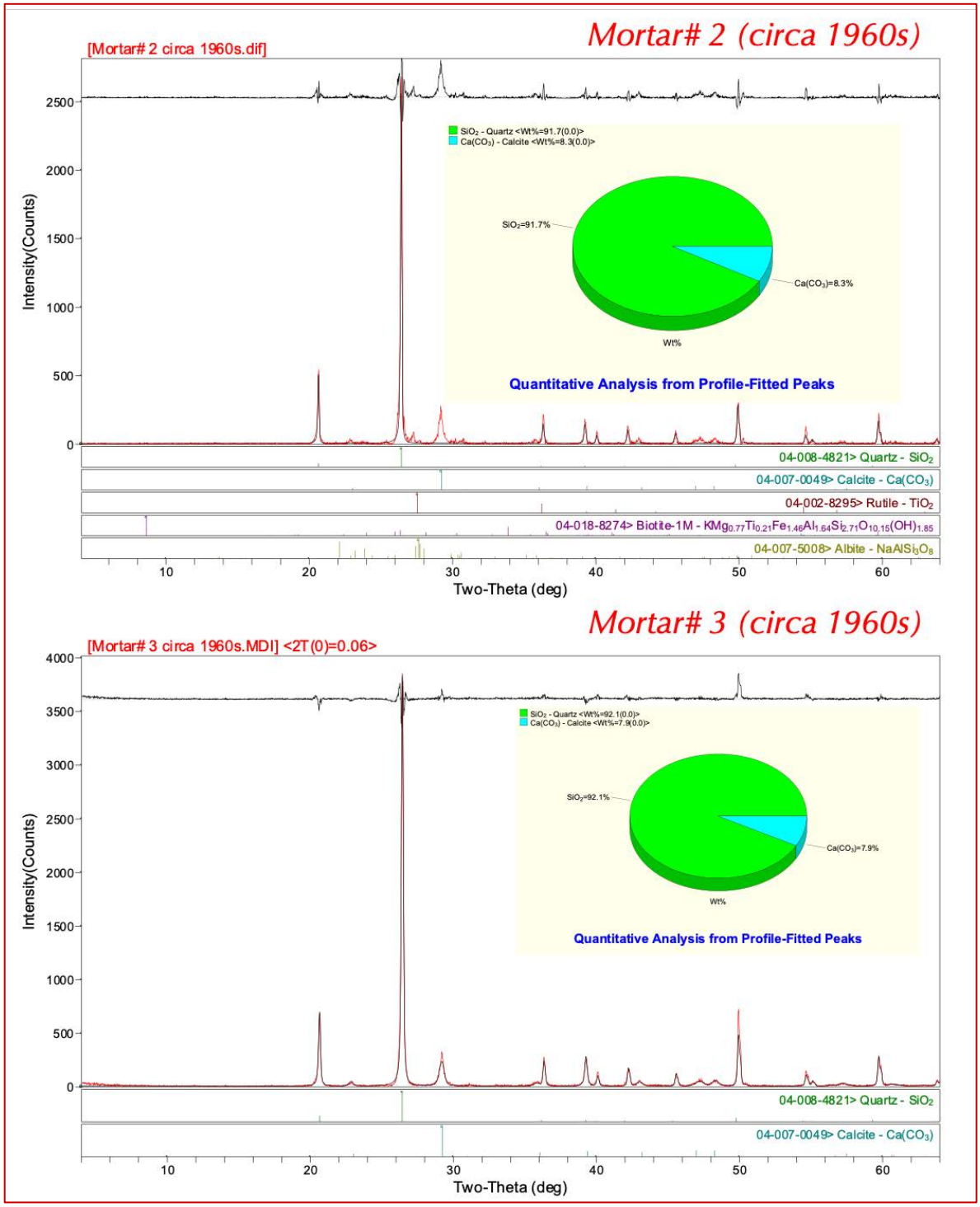

Figure 30: X-ray diffraction patterns of two original mortars from 1960s construction from #2 (top) and #3 (bottom) showing dominance of quartz in the silica sand, and, subordinate calcite from finely crystalline fine-grained carbonated lime matrix in both mortars, and additionally calcite grains from the dominant limestone fine component of masonry cement in #2 mortar. Quartz contents from XRD, after corrections for acid-insoluble residue contents, show good matches to the quartz contents determined from DSC (thermal) studies.

Mineralogical Compositions of a 2019 Mortar & Efflorescence Deposits from X-Ray Diffraction (XRD)

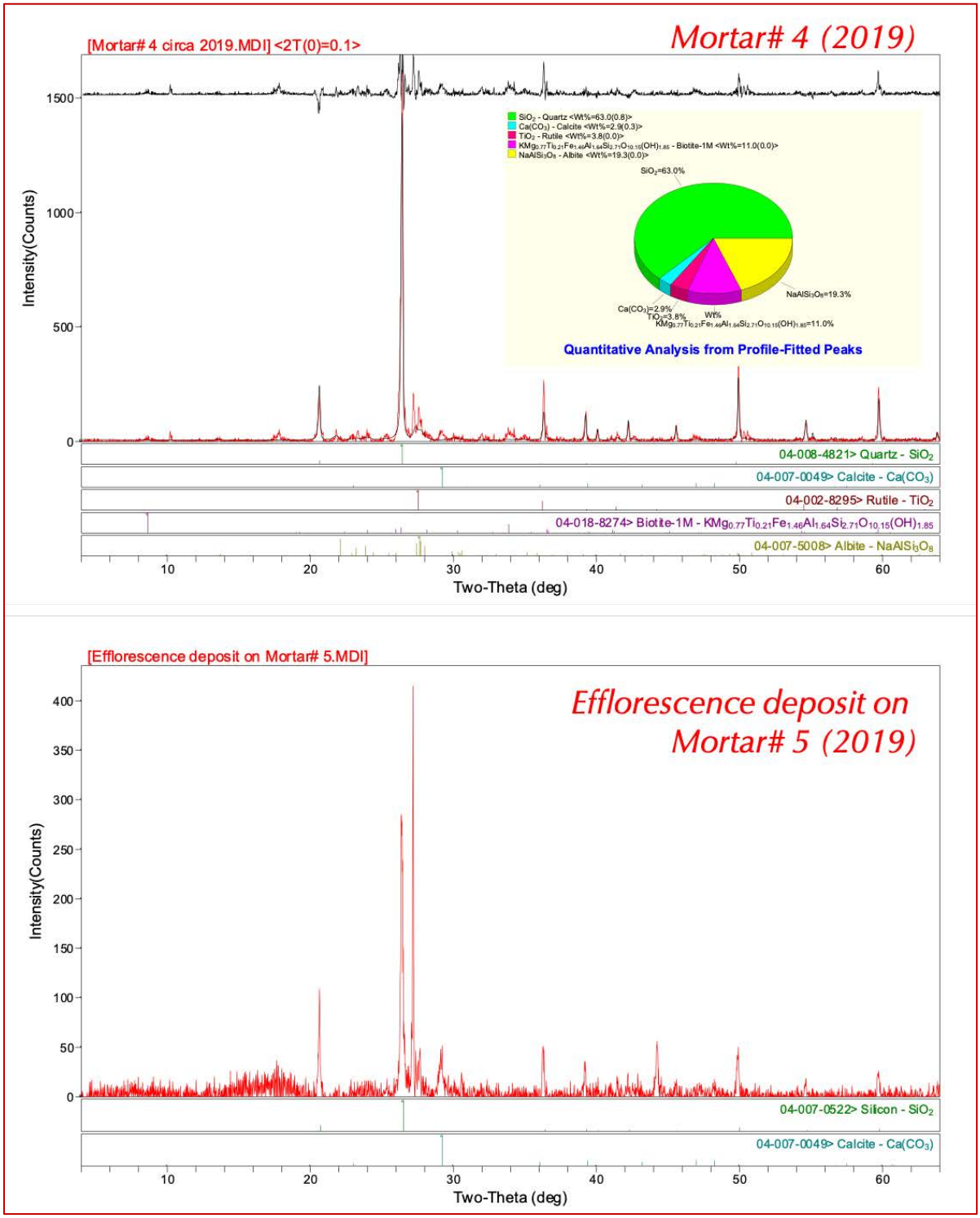

Figure 31: X-ray diffraction patterns of a recent mortar #4 from 2019 construction (top), and, white efflorescence deposits scrapped off from the surface of mortar #5 (bottom) showing dominance of quartz in the silicesous sand, followed by subordinate feldspar (albite) and mica in the sand in mortar #4. Efflorescence deposit on the surface of mortar #5 shows calcium carbonate (calcite) as the only salt (besides quartz from mortar's sand). Quartz content in mortar #4 from XRD, after corrections for acid-insoluble residue contents, show good matches to the quartz content determined from DSC (thermal) studies.

Chemical Compositions of Mortars from X-Ray Fluorescence (XRF)

Bulk Chemical Compositions of Mortars From XRF

Mortars	SiO_2	Al_2O_3	Fe_2O_3	CaO	MgO	Na_2O	K_2O	TiO_2	P_2O_3	SO_3	Balance (LOI)	Total
Masonry cement Mortar# 2 circa 1960s	70.0	2.64	2.61	14.70	1.100	0.183	1.11	0.608	0.0836	ND	7.11	100
AE Cement-Lime Mortar# 3 circa 1960s	79.7	1.46	2.01	9.35	0.672	ND	0.132	0.141	0.0518	0.0192	6.55	100
Cement-lime Mortar# 4 2019	64.1	6.59	3.21	11.40	2.450	1.410	1.90	0.199	0.0893	0.0626	8.59	100
Masonry cement Mortar# 5 2019	63.7	6.11	3.04	11.60	2.220	1.430	1.86	0.200	0.0983	0.0077	9.71	100

Mortar Types	Binder Types	Characteristic Chemical Compositions
Masonry cement Mortar# 2 circa 1960s	Portland cement, hydrated lime, limestone fine, similar to a modern equivalent of ASTM C 270 Type N masonry cement mortars	• Highest lime for contribution from limestone fine besides cement and lime • High potassium is from alkali salt and minor contribution from minor feldspar in the sand • Sulfate undetectable due to low cement content
AE Masonry Cement Mortar# 3 circa 1960s	Abundant dolomitic hydrated lime, subordinate Portland cement, minor fly ash, similar to a modern equivalent between ASTM C 270 Type N and O masonry cement mortars	• Highest silica for highest silica sand content • Lowest alumina for low feldspar in sand • Lowest lime despite high lime content of cement-lime mortar • Sulfate undetectable due to low cement content
Cement-lime Mortar# 4 2019	Cement-Lime Mortar	• Overall similar bulk compositions of both mortars from 2019 despite their different binder compositions where #4 is a cement-lime mix whereas #5 is a proprietary masonry cement mortar • High magnesia from use of dolomitic lime • High alkalis from noticeable feldspar in sand • Lowest silica from lowest quartz content in the sand
Masonry cement Mortar# 5 2019	Masonry cement Mortar	

Table 4: Chemical (oxide) compositions of bulk mortars determined from X-ray fluorescence spectroscopy. Balance represents loss on ignition (volatiles, e.g., water, CO_2) parts of mortars. Results in red show the characteristic chemical signatures of mortars based on which (along with textural properties) mortars are classified in four different types, two from the original mortars of 1960s construction are found to be two different masonry cement mortars, whereas two recent mortars from 2019 construction showed use of cement-lime mortar for #4 and masonry cement mortar for #5.

Chemical Compositions of Mortars from Gravimetry

Volatiles & Acid-Insoluble Residue Contents of Mortars From Gravimetry				
Mortars	**LOI at 110°C**	**LOI at 550°C**	**LOI at 950°C**	**Acid-Insoluble Residue**
Masonry cement Mortar# 2 circa 1960s	0.40	1.90	10.10	67.6 Mostly quartz
AE Cement-Lime Mortar# 3 circa 1960s	1.60	2.10	6.30	74.8 Mostly quartz
Cement-lime Mortar# 4 2019	3.60	3.10 Higher hydrate water than 1960s mortars	2.50 Noticeably lower carbonation than 1960s mortars	68.8 Quartz, feldspar, mica

Table 5: Loss on ignition and acid-insoluble residue contents of mortars.

Following detailed petrographic examinations of mortars from optical and electron microscopy, and mineralogical compositions from X-ray diffraction studies, chemical compositions of mortars were determined from

a. Bulk chemical compositions in terms of oxide components of mortars from energy-dispersive X-ray fluorescence spectroscopy (XRF)
b. Hydrochloric acid-insoluble residue contents of mortars to determine the proportion of siliceous components in the mortars, which, based on petrographic examinations are determined to be representative of sand contents since sands contain no calcareous (acid-soluble) components.
c. Losses on ignition after igniting a gram of pulverized mortar in a muffle furnace in a step-wise manner from ambient to 110ºC, followed by 110ºC to 550ºC, and finally from 550ºC to 950ºC to determine the proportion of free water, combined (hydrate) water, and, degree of carbonation of mortars, respectively.

Bulk chemical compositions of mortars from XRF studies show similarities in overall bulk chemical compositions of two recent mortars from 2019 despite their very different binder types (cement-lime versus masonry cement). The recent mortars differed in bulk chemistry from the mortars from 1960s vintage where the original mortars are richer in silica mostly due to higher sand contents and quartz-rich composition of sands as opposed to many feldspar particles found in the sands in recent mortars, which are responsible for elevated alumina contents in the recent mortars compared to the original ones. High feldspar content of sand in the recent mortars also elevated the potassium contents in these mortars compared to the original ones. Since sand constitutes bulk volume of the mortar, changes in the sand mineralogies between the 1960s and 2019 mortars is reflected in their bulk chemistries.

Based on petrographic examinations and chemical analyses, mortars are classified into four types depending on the binder types present (masonry cement versus cement-lime), variations in masonry cement compositions (lime-rich versus limestone fine-rich), air entrainment versus lack of adequate air entrainment, etc.

Results from loss on ignition, particularly losses from 110ºC to 550ºC represents amount of hydrate water, which, in turn, determines relative hydraulicities of binders where hydrate water content in mortar increases with increasing hydraulicities of mortars resulting in higher amount of calcium silicate aluminate hydrate phases in the paste. Results from 550ºC to 950ºC determines degree of carbonation from lime content, limestone fine content, and degree of carbonation of pastes.

Thermal Analyses

Milligrams of mortars from 1960s and 2019 construction were subjected to controlled heating experiments in a Mettler-Toledo TGA/DSC simultaneous thermogravimetric and differential scanning calorimetry unit to detect the presence of various hydrous, sulfate, and carbonate phases in these mortars and their relative abundances. Figures 32 through 36 show TGA (in bold black), DSC (in dotted red), and DTG (in dashed blue) curves of mortars showing losses in weight due to decompositions (loss of water and carbon dioxide) of various phases during controlled heating in a Mettler-Toledo's simultaneous TGA/DSC 1 unit from 30ºC to 1000ºC in a ceramic crucible (alumina 70µl, no lid) at a heating rate of 10ºC/min in a nitrogen purge at a rate of 75 mL/min. Dehydration and decarbonation reactions are marked as endothermic peaks in the DTG curve, whereas alpha to beta-form polymorphic transition of quartz is marked at the characteristic temperature of 575 ºC in the DSC curve.

In the DTG curve, successive losses in weights are detected at (i) up to 120ºC from losses of free and combined water, (ii) from 120ºC to 200ºC for water from hydrated salts, (iii) from 200ºC to 600ºC for dihydroxylation of structural/hydrate water in various hydraulic components, and (iv) from 600ºC to 950ºC for decomposition of carbonate phases from limestone fines and fine-grained calcite in carbonated pastes. DSC curve shows polymorphic transition from alpha to beta form of quartz around 575ºC from silica (quartz) sand.

Figures 32 and 33 show very similar thermograms of two original mortars showing a minimal loss of free water (<0.5%) and water from hydrated salts (<0.5%) at up to 200ºC followed by a measurable loss (2 to 2.2%) of hydrate water from 200ºC to 600ºC. Degrees of carbonation is higher in the #2 mortar (9.3% due to abundant limestone fine component along with hydrated lime) than 5.6% found in #3 mortar mostly from hydrated lime component on the latter. Quartz contents in both mortars are around 70 percent determined from polymorphic transition of quartz around 575ºC.

Two recent mortars from 2019 construction, however, showed very different rather complex thermograms in Figures 34 through 36 due to (i) the presence of noticeable structural water components in the 200ºC to 600ºC range, along with (ii) noticeably larger losses of free water and from hydrated salts at <200ºC, (iii) lower degree of carbonation than the original mortars, and (iv) lower quartz contents in the recent ones (<50%) compared to much higher quartz contents (70%) found in the original mortars.

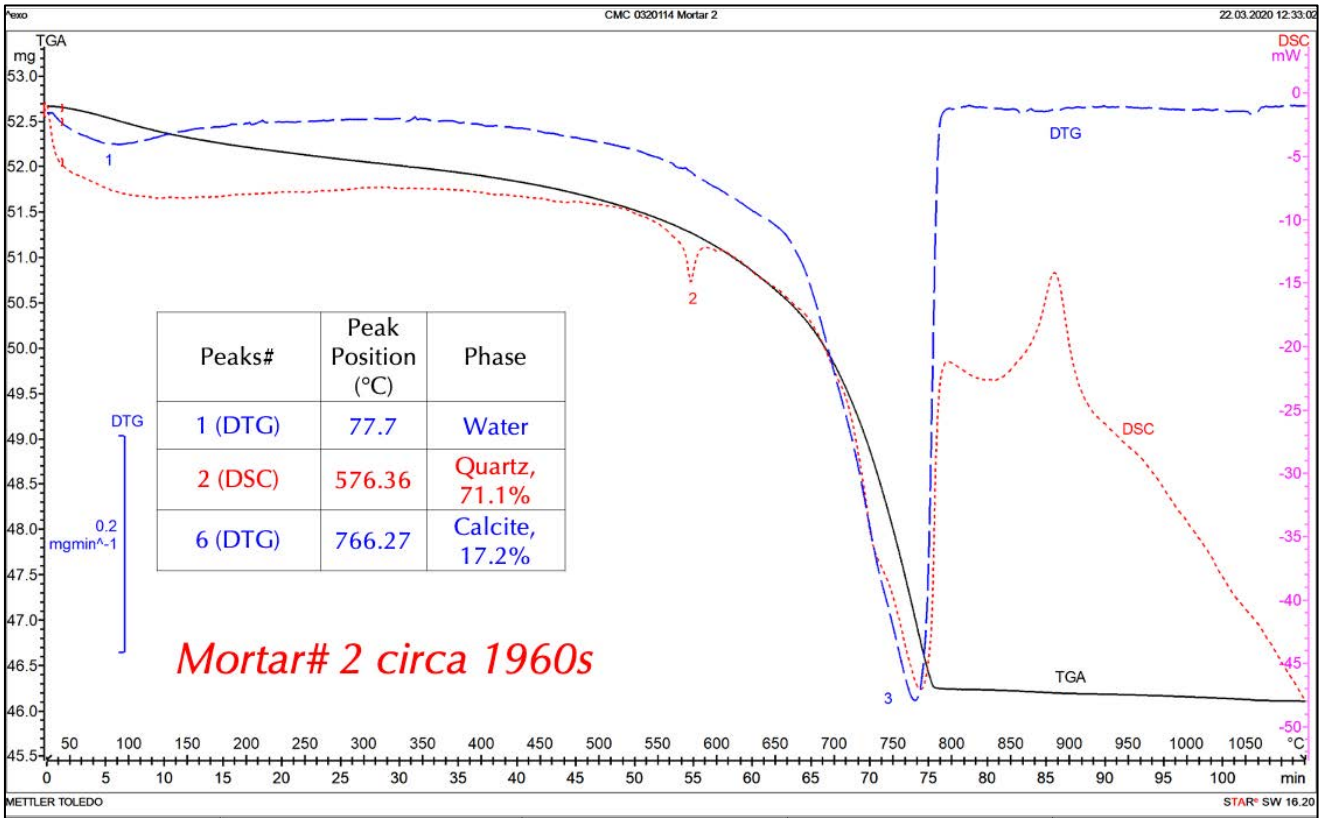

T(°C)	Up to 120°C	120°C to 200°C	200°C to 600°C	> 600°C
Phases	Hygroscopic Water	Water from Hydrated Salts	Structural Water From Hydraulic Components	CO_2 from decomposition of carbonates
Mass Loss (%) from TGA	0.47	0.37	2.08	9.35

Figure 32: TGA (bold black), DSC (dotted red), and DTG (dashed blue) curves of mortar from 1960s construction showing losses in weight due to various decompositions (loss of water and carbon dioxide) during controlled heating in a Mettler-Toledo's simultaneous TGA/DSC 1 unit from 30ºC to 1000ºC in a ceramic crucible (alumina 70µl, no lid) at a heating rate of 10ºC/min in a nitrogen purge at a rate of 75 mL/min.

Original mortar #2 from 1960s construction showed a rather simple thermogram in Figure 32, which is unusual considering masonry cement composition of the binder. The main endotherm found is at 766.27ºC from decarbonation of major amount of limestone fines and subordinate amount of hydrated lime components of the binder. Polymorphic transition of quartz sand at 576.36ºC showed about 70 percent quartz, which shows a good resemblance to the quartz content determined (after correction for insoluble residue content) from XRD.

Loss of masses from heating (i) up to 120ºC is 0.47%, which represents losses of free and combined water, (ii) from 120ºC to 200ºC is 0.37%, which represents loss of water from hydrated salts, (iii) from 200ºC to 600ºC is 2.08%, which represents dihydroxylation of structural/hydrate water in various hydraulic components, and finally (iv) 9.35% from 600ºC to 950ºC for decomposition of carbonate phases from limestone fines and fine-grained calcite in carbonated pastes.

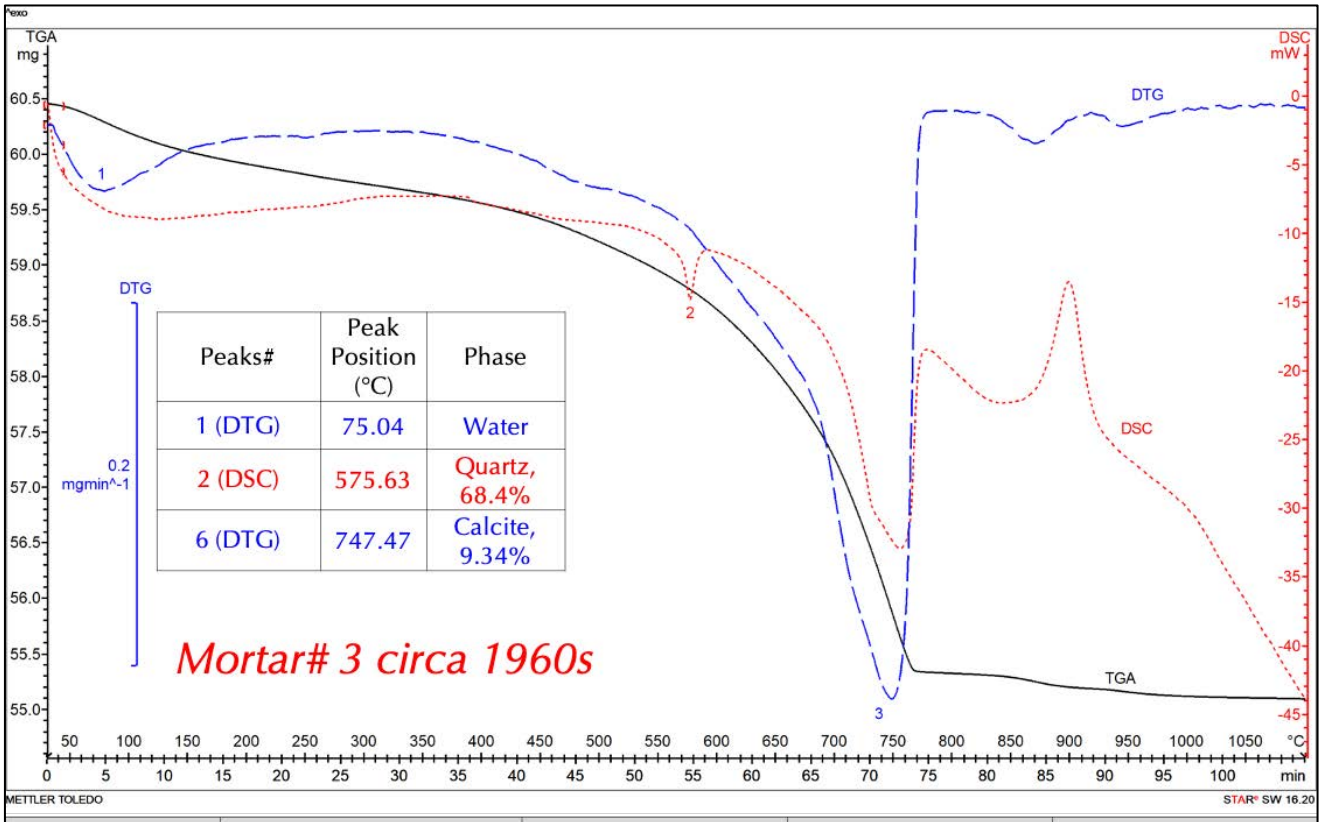

Peaks#	Peak Position (°C)	Phase
1 (DTG)	75.04	Water
2 (DSC)	575.63	Quartz, 68.4%
6 (DTG)	747.47	Calcite, 9.34%

T(°C)	Up to 120°C	120°C to 200°C	200°C to 600°C	> 600°C
Phases	Hygroscopic Water	Water from Hydrated Salts	Structural Water From Hydraulic Components	CO_2 from decomposition of carbonates
Mass Loss (%) from TGA	0.46	0.35	2.16	5.64

Figure 33: TGA (bold black), DSC (dotted red), and DTG (dashed blue) curves of mortar from 1960s construction showing losses in weight due to various decompositions (loss of water and carbon dioxide) during controlled heating in a Mettler-Toledo's simultaneous TGA/DSC 1 unit from 30ºC to 1000ºC in a ceramic crucible (alumina 70µl, no lid) at a heating rate of 10ºC/min in a nitrogen purge at a rate of 75 mL/min.

Original mortar #3 from 1960s construction showed a rather simple thermogram in Figure 33, which is not so unusual considering the dominant hydrated lime composition in the masonry cement binder of this mortar. The main endotherm found is at 747.47ºC from decarbonation of major amount of limestone fines and subordinate amount of hydrated lime components of the binder. Polymorphic transition of quartz sand at 575.63ºC showed about 68.4 percent quartz, which shows a good resemblance to the quartz content determined (after correction for insoluble residue content) from XRD.

Loss of masses from heating (i) up to 120ºC is 0.46%, which represents losses of free and combined water, (ii) from 120ºC to 200ºC is 0.35%, which represents loss of water from hydrated salts, (iii) from 200ºC to 600ºC is 2.16%, which represents dihydroxylation of structural/hydrate water in various hydraulic components, and finally (iv) 5.64% from 600ºC to 950ºC for decomposition of carbonate phases from limestone fines and fine-grained calcite in carbonated pastes.

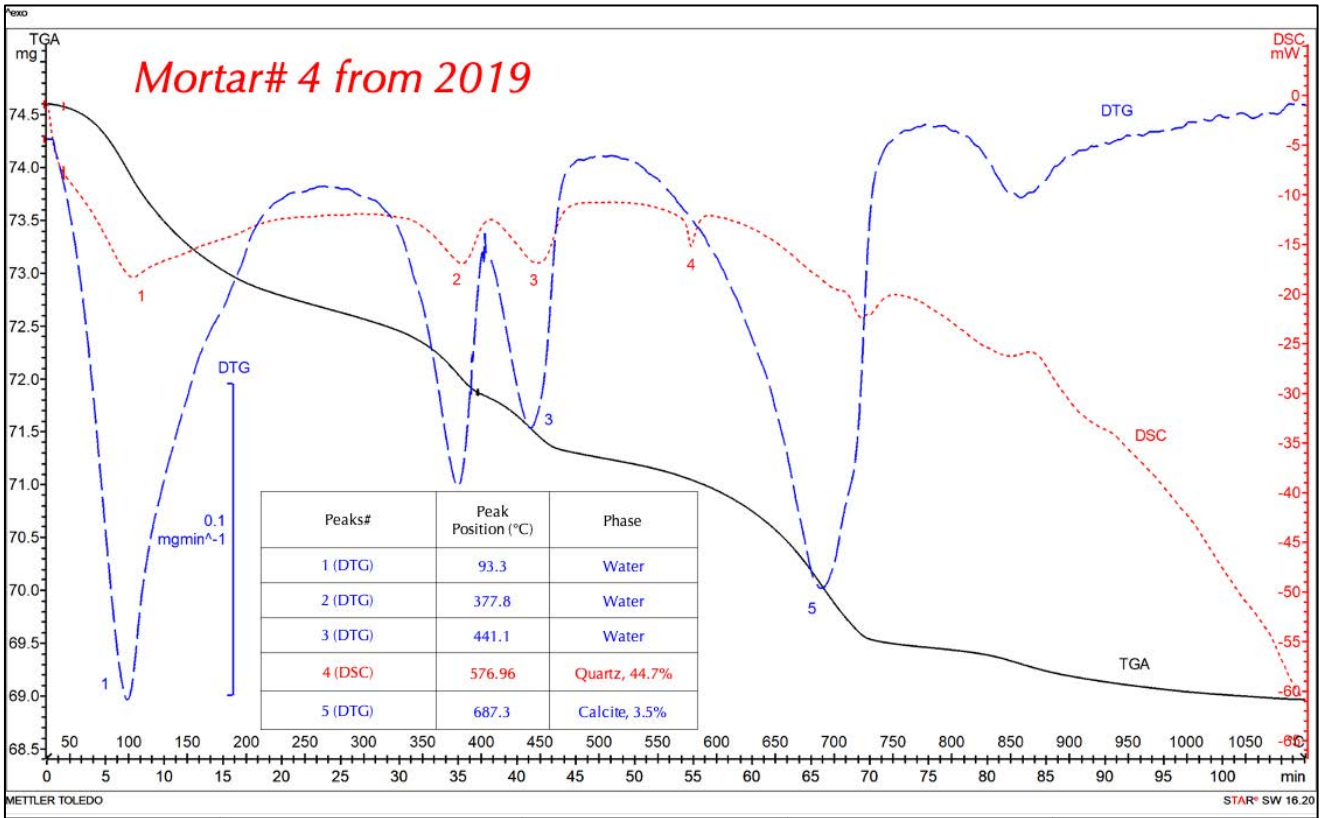

T(°C)	Up to 120°C	120°C to 200°C	200°C to 600°C	> 600°C
Phases	Hygroscopic Water	Water from Hydrated Salts	Structural Water From Hydraulic Components	CO_2 from decomposition of carbonates
Mass Loss (%) from TGA	1.22	1.01	2.63	2.35

Figure 34: TGA (bold black), DSC (dotted red), and DTG (dashed blue) curves of mortar from 2019 construction showing losses in weight due to various decompositions (loss of water and carbon dioxide) during controlled heating in a Mettler-Toledo's simultaneous TGA/DSC 1 unit from 30ºC to 1000ºC in a ceramic crucible (alumina 70µl, no lid) at a heating rate of 10ºC/min in a nitrogen purge at a rate of 75 mL/min.

Recent mortar #4 from 2019 construction showed a rather complex thermogram in Figure 34, due to (i) the presence of noticeable free water and water from hydrated salts resulting in sharp endotherm by 200ºC, (ii) noticeable peaks between 200ºC and 600ºC from dihydroxylation of structural water components in hydraulic phases, (ii) noticeably lower degree of carbonation than the original mortars, and (iv) lower quartz content (<50%) compared to much higher quartz contents (70%) found in the original mortars.

Loss of mass from heating (i) up to 120ºC is 1.22%, which is a factor of 2.5 higher than that from the original mortars due to loss of free water, (ii) from 120ºC to 200ºC is 1%, which is also a factor 2.5 higher than 0.35-0.37% found in the original mortars from loss of water from hydrated salts, (iii) from 200ºC to 600ºC is 2.63%, which is higher than maximum 2.16% found in the original mortars from dihydroxylation of structural/hydrate water in various hydraulic components, and finally (iv) only 2.35% from 600ºC to 950ºC for decomposition of

carbonate phases from limestone fines and fine-grained calcite in carbonated pastes as opposed to 5.64-9.35% found in the original mortars.

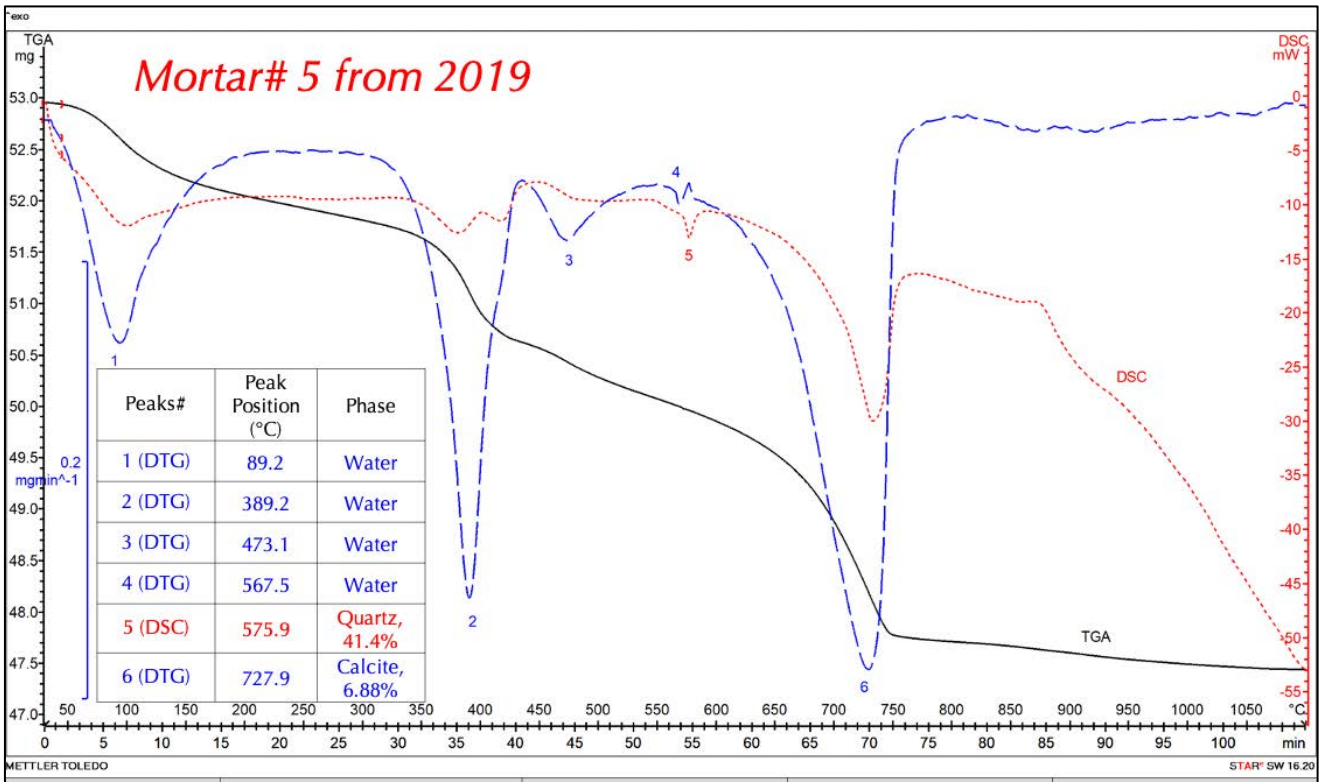

T(°C)	Up to 120°C	120°C to 200°C	200°C to 600°C	> 600°C
Phases	Hygroscopic Water	Water from Hydrated Salts	Structural Water From Hydraulic Components	CO_2 from decomposition of carbonates
Mass Loss (%) from TGA	1.06	0.62	4.14	4.25

Figure 35: TGA (bold black), DSC (dotted red), and DTG (dashed blue) curves of mortar from 2019 construction showing losses in weight due to various decompositions (loss of water and carbon dioxide) during controlled heating in a Mettler-Toledo's simultaneous TGA/DSC 1 unit from 30ºC to 1000ºC in a ceramic crucible (alumina 70µl, no lid) at a heating rate of 10ºC/min in a nitrogen purge at a rate of 75 mL/min.

Recent mortar #5 from 2019 construction again showed another rather complex thermogram in Figure 35, more or less similar to the one found in #4 mortar due to (i) noticeable free water and water from hydrated salts resulting in sharp endotherm by 200ºC, (ii) noticeable peaks between 200ºC and 600ºC from dihydroxylation of structural water components in hydraulic phases, (ii) noticeably lower degree of carbonation than the original mortars, and (iv) lower quartz content (<50%) compared to much higher quartz contents (70%) found in the original mortars.

Loss of mass from heating (i) up to 120ºC is 1.06%, which is a factor of 2 to 2.5 higher than that from the original mortars due to loss of free water, (ii) from 120ºC to 200ºC is 0.62%, which is also a factor 1.5 higher than 0.35-0.37% found in the original mortars from loss of water from hydrated salts, (iii) from 200ºC to 600ºC is 4.14%, which is higher than maximum 2.16% found in the original mortars from dihydroxylation of structural/hydrate

water in various hydraulic components, and finally (iv) only 4.25% from 600ºC to 950ºC for decomposition of carbonate phases from limestone fines and fine-grained calcite in carbonated pastes as opposed to 5.64-9.35% found in the original mortars.

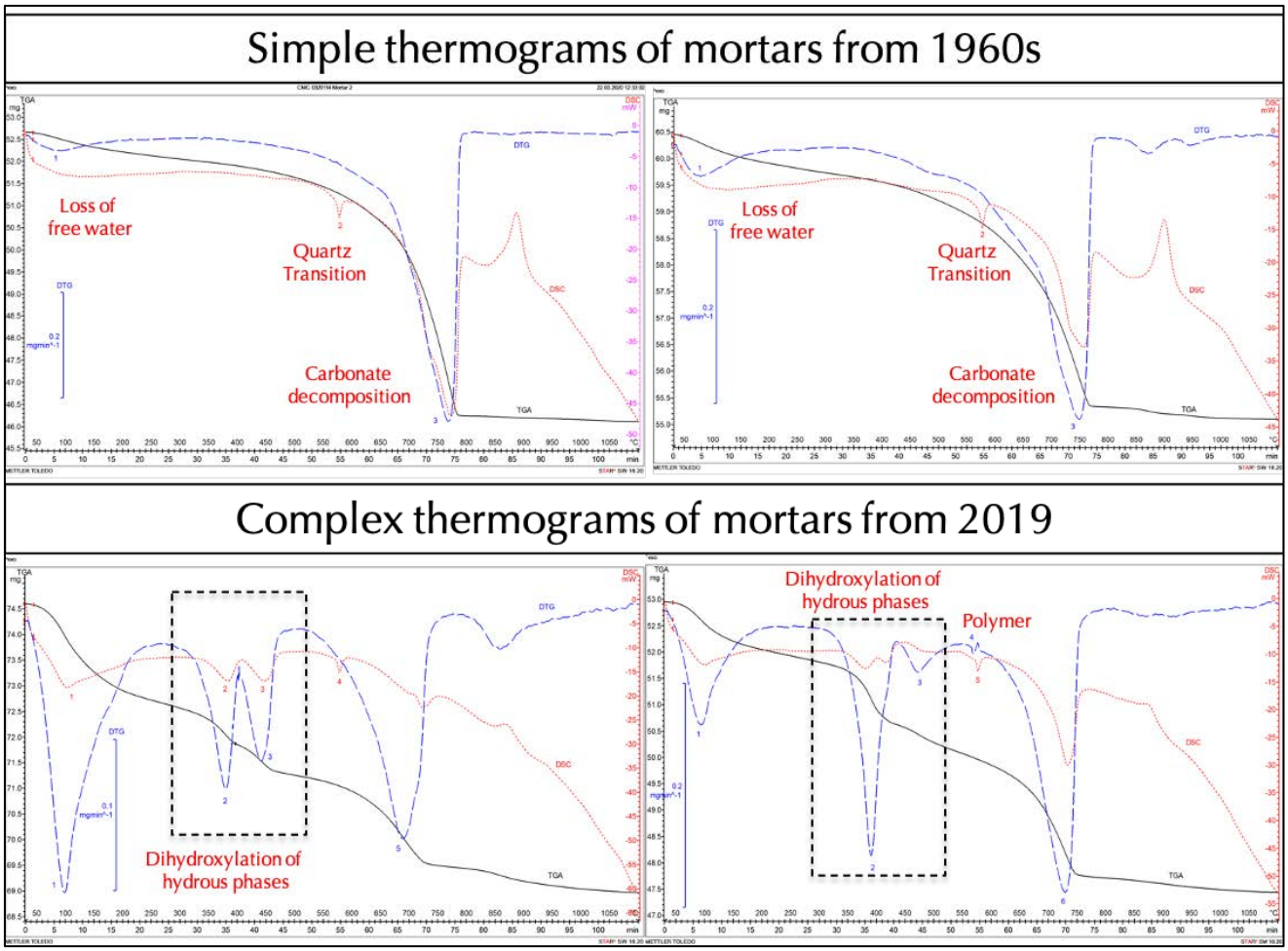

Figure 36: TGA (bold black), DSC (dotted red), and DTG (dashed blue) curves of mortars from 1960s (top) and 2019 (bottom) construction showing losses in weight due to various decompositions (loss of water and carbon dioxide) during controlled heating in a Mettler-Toledo's simultaneous TGA/DSC 1 unit from 30ºC to 1000ºC in a ceramic crucible (alumina 70µl, no lid) at a heating rate of 10ºC/min in a nitrogen purge at a rate of 75 mL/min.

Figure 36 shows comparison of thermograms between the original and recent mortars where recent mortars showed very different rather complex thermograms due to (i) the presence of noticeable structural water components in the 200ºC to 600ºC range resulting in large endotherms (shown within dashed boxes), along with (ii) noticeably larger losses of free water and from hydrated salts at <200ºC, (iii) lower degree of carbonation than the original mortars, and (iv) lower quartz contents in the recent ones (<50%) compared to much high quartz contents (70%) found in the original mortars.

These differences in thermal behaviors of original and recent mortars are consistent with their compositions including types of binders present and sand contents.

Fourier Transform Infrared Spectroscopy (FTIR) of Mortars From 1960s

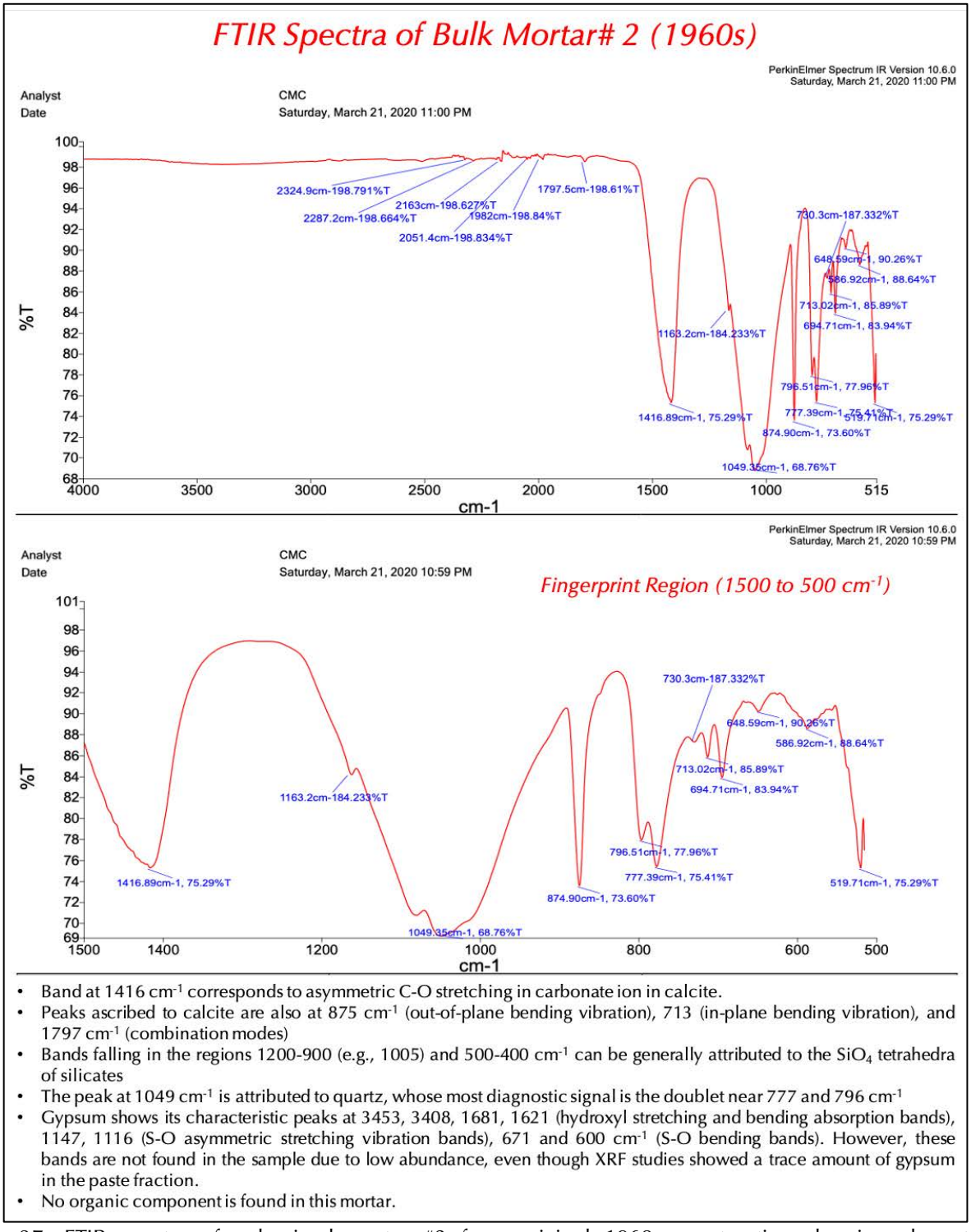

- Band at 1416 cm^{-1} corresponds to asymmetric C-O stretching in carbonate ion in calcite.
- Peaks ascribed to calcite are also at 875 cm^{-1} (out-of-plane bending vibration), 713 (in-plane bending vibration), and 1797 cm^{-1} (combination modes)
- Bands falling in the regions 1200-900 (e.g., 1005) and 500-400 cm^{-1} can be generally attributed to the SiO_4 tetrahedra of silicates
- The peak at 1049 cm^{-1} is attributed to quartz, whose most diagnostic signal is the doublet near 777 and 796 cm^{-1}
- Gypsum shows its characteristic peaks at 3453, 3408, 1681, 1621 (hydroxyl stretching and bending absorption bands), 1147, 1116 (S-O asymmetric stretching vibration bands), 671 and 600 cm^{-1} (S-O bending bands). However, these bands are not found in the sample due to low abundance, even though XRF studies showed a trace amount of gypsum in the paste fraction.
- No organic component is found in this mortar.

Figure 37: FTIR spectra of pulverized mortar #2 from original 1960s construction showing characteristic absorbance bands from calcite in the binder and quartz in the sand. No organic component is detected in this mortar from the lack of any characteristic functional group.

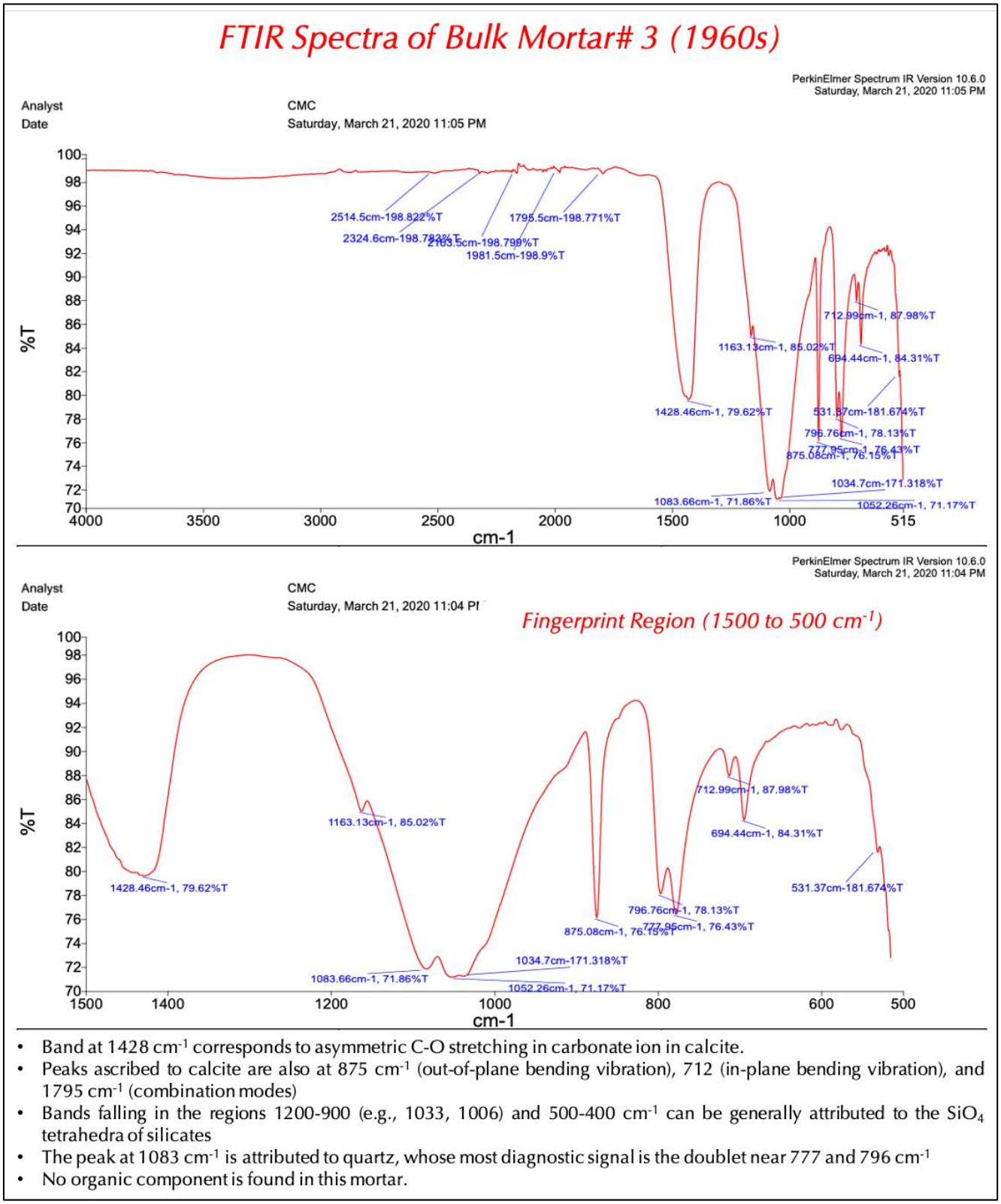

- Band at 1428 cm^{-1} corresponds to asymmetric C-O stretching in carbonate ion in calcite.
- Peaks ascribed to calcite are also at 875 cm^{-1} (out-of-plane bending vibration), 712 (in-plane bending vibration), and 1795 cm^{-1} (combination modes)
- Bands falling in the regions 1200-900 (e.g., 1033, 1006) and 500-400 cm^{-1} can be generally attributed to the SiO_4 tetrahedra of silicates
- The peak at 1083 cm^{-1} is attributed to quartz, whose most diagnostic signal is the doublet near 777 and 796 cm^{-1}
- No organic component is found in this mortar.

Figure 38: FTIR spectra of pulverized mortar #3 from original 1960s construction showing characteristic absorbance bands from calcite in the binder and quartz in the sand. No organic component is detected in this mortar from the lack of any characteristic functional group.

Fourier Transform Infrared Spectroscopy (FTIR) of Mortars From 2019

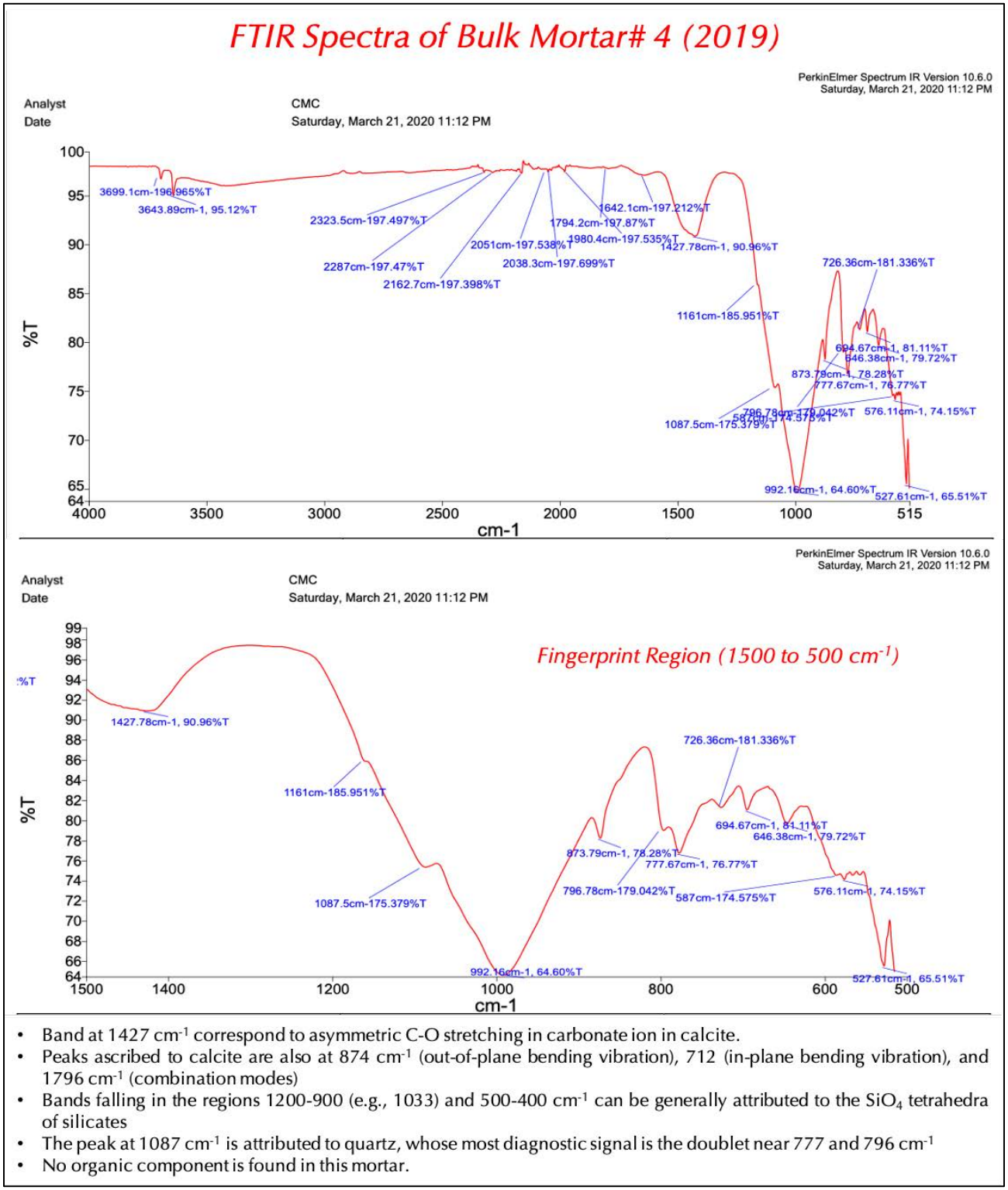

Figure 39: FTIR spectra of pulverized mortar #4 from 2019 construction showing characteristic absorbance bands from calcite in the binder and quartz in the sand. No organic component is detected in this mortar from the lack of any characteristic functional group.

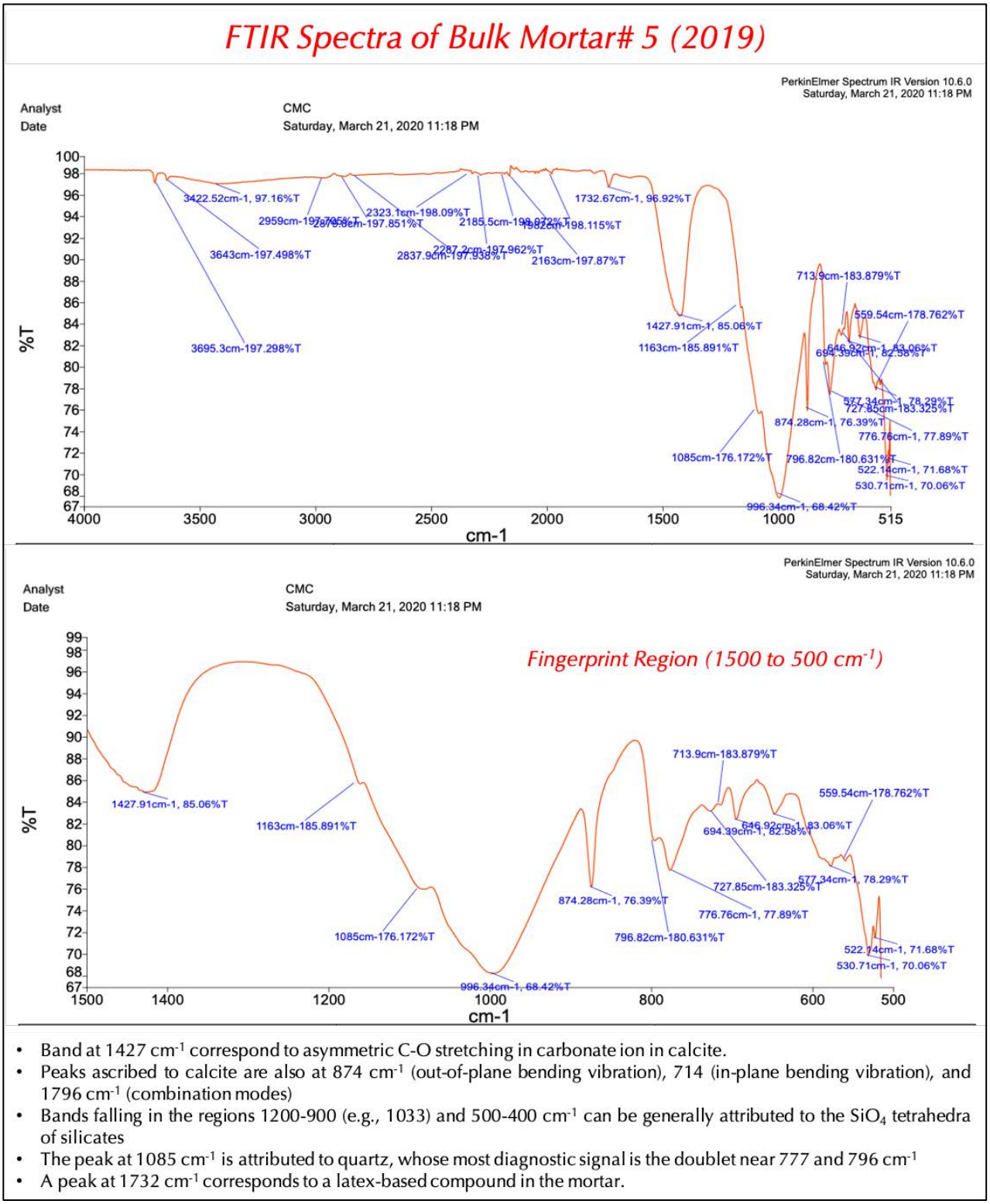

- Band at 1427 cm^{-1} correspond to asymmetric C-O stretching in carbonate ion in calcite.
- Peaks ascribed to calcite are also at 874 cm^{-1} (out-of-plane bending vibration), 714 (in-plane bending vibration), and 1796 cm^{-1} (combination modes)
- Bands falling in the regions 1200-900 (e.g., 1033) and 500-400 cm^{-1} can be generally attributed to the SiO_4 tetrahedra of silicates
- The peak at 1085 cm^{-1} is attributed to quartz, whose most diagnostic signal is the doublet near 777 and 796 cm^{-1}
- A peak at 1732 cm^{-1} corresponds to a latex-based compound in the mortar.

Figure 40: FTIR spectra of pulverized mortar #5 from 2019 construction showing characteristic absorbance bands from calcite in the binder and quartz in the sand. A latex-based polymer component is detected from the characteristic band at 1732 cm^{-1} region.

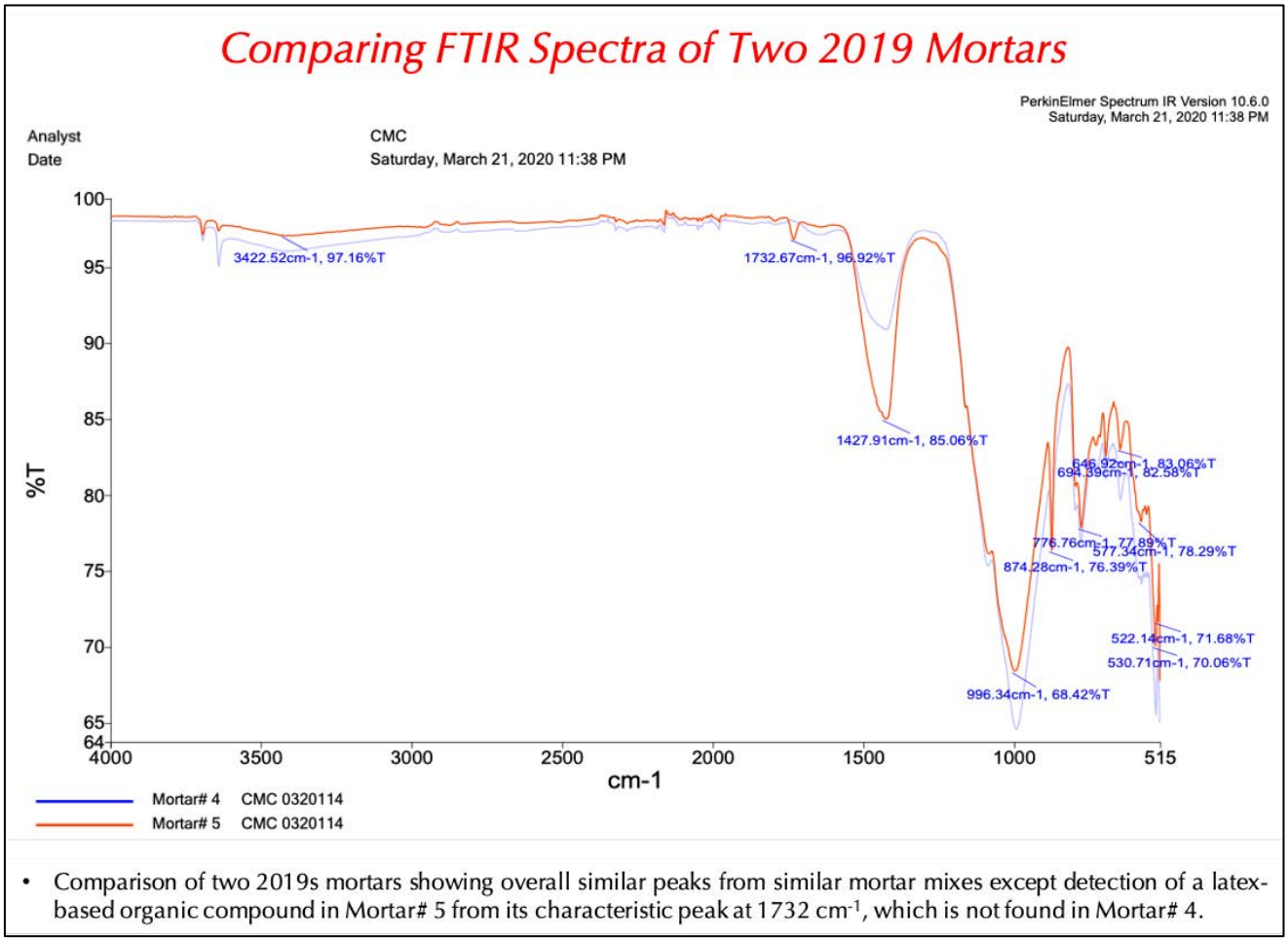

Figure 41: Comparison of FTIR spectra of two recent mortars showing overall similarities in both spectra except a peak at 1732 cm^{-1} region in mortar #5 from the presence of a latex-based polymer in the mortar.

FTIR studies were done essentially to determine the presence of a polymer component in the mortars, which is found only in the #5 mortar from 2019 construction, consistent with the reported latex-based formulation of that mortar. Phases determined from X-ray diffraction and optical microscopy studies are found responsible for most if not all the absorbance bands detected in the FTIR spectra.

Ion Chromatography of Water-Soluble Salts in Masonry Mortars From 1960s

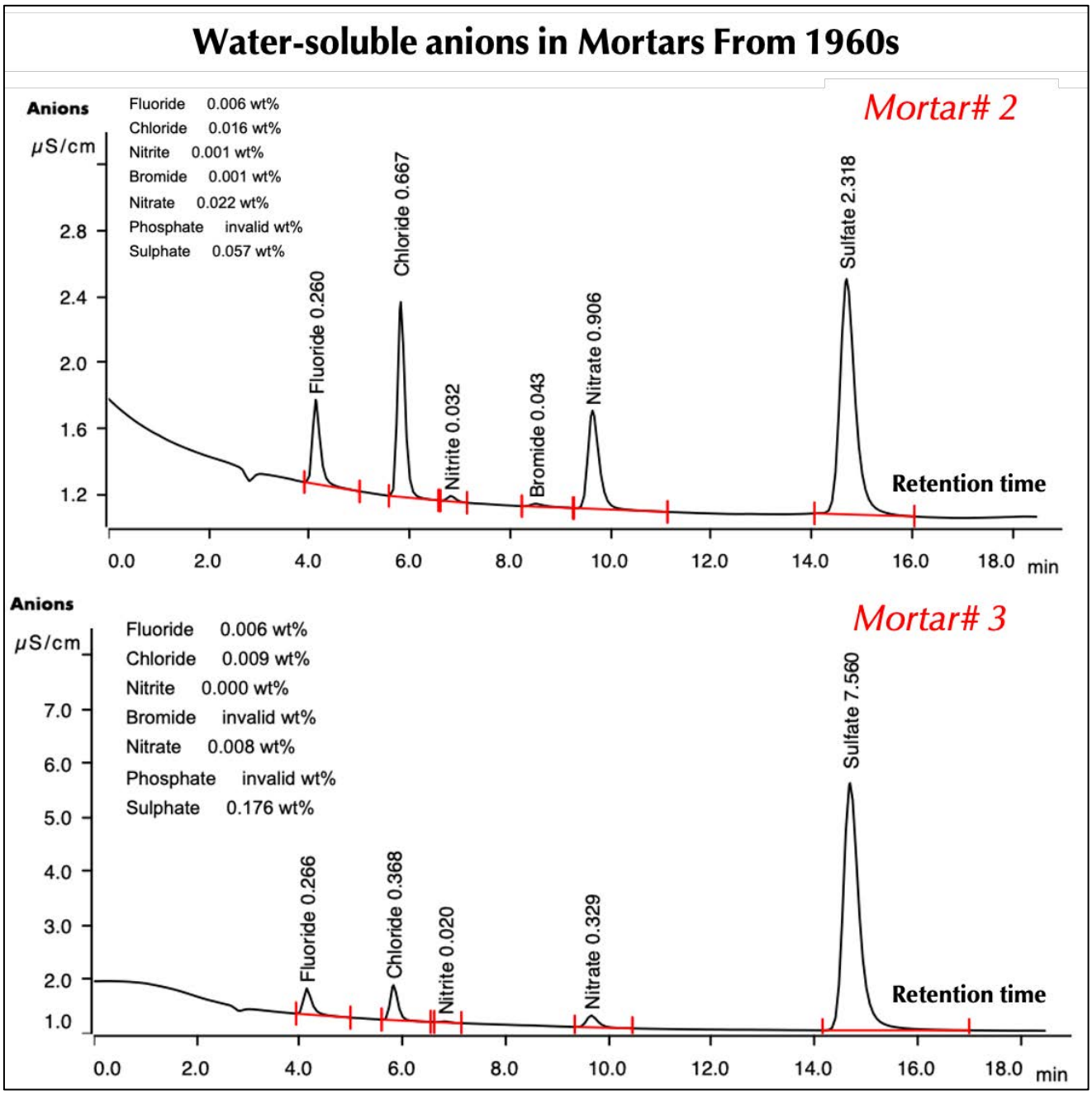

Figure 42: Ion chromatograms of water-soluble anions in two original mortars after digesting representative portions of pulverized mortars (about a gram) in deionized water for 30 minutes at a temperature below boiling, followed by continued digestion in water at the ambient laboratory condition for 24 hours. The digested solution was filtered under vacuum through 0.2-micron filter papers. The final filtrates diluted to 100 ml were analyzed by ion chromatography. Top left insets show results of concentrations of various water-soluble anions, notably water-soluble chloride and sulfate contents in the mortars. Chloride contents in the original mortars are negligible and do not indicate any chloride salts or related distress. However, sulfate contents are noticeable and large variations from 0.057% in #2 (limestone fine rich masonry cement) to 0.176% in #3 (hydrated lime rich masonry cement mortar).

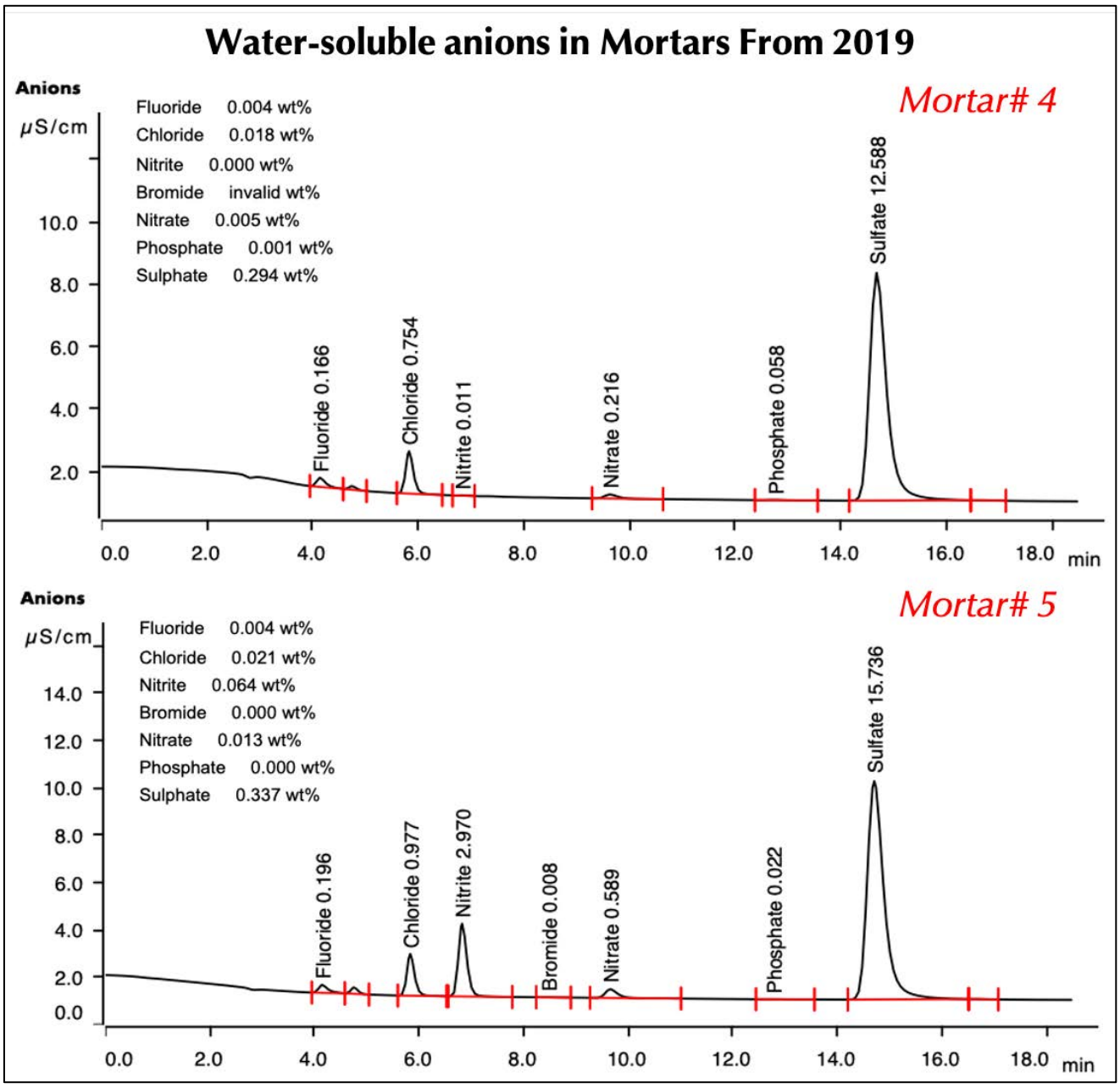

Figure 43: Ion chromatograms of water-soluble anions in two recent mortars after digesting representative portions of pulverized mortars (about a gram) in deionized water for 30 minutes at a temperature below boiling, followed by continued digestion in water at the ambient laboratory condition for 24 hours. The digested solution was filtered under vacuum through 0.2-micron filter papers. The final filtrates diluted to 100 ml were analyzed by ion chromatography. Top left insets show results of concentrations of various water-soluble anions, notably water-soluble chloride and sulfate contents in the mortars. Chloride contents in the recent mortars are negligible (as also found in the original mortars, all four mortars have <0.025% chloride) and do not indicate any chloride salts or related distress. However, sulfate contents are noticeable (from 0.294% to 0.337%) which are higher than the maximum 0.176% sulfate found in #3 original mortar. Presence of Portland cement at a higher amount in the binders of the recent mortars is responsible for the high water-soluble sulfate contents.

Results from Chemical Analyses (Gravimetry, IC, XRF), Thermal, and XRD Studies of Masonry Mortars

Table 6 provides results obtained from chemical analyses (gravimetry), thermal analyses (TGA, DSC, DTG), X-ray diffraction, and X-ray fluorescence showing overall consistencies in results obtained from multiple methods of analyses given the inherent standard errors of estimates for each method, as well as some similarities and noticeable differences between the mortars, all of which are helpful to diagnose not only the types of mortars used but also for calculations of mix proportions of various binders and sands in the mortar mixes. Weight loss during controlled heating experiences in TGA/DSC/DTG unit of milligram levels of pulverized mortars show similarities in results as the ones obtained from losses on step-wise ignition of a gram of pulverized mortar samples in muffle furnace at 110°C, 550°C, and 950°C. Calcite content from XRD correlates with the one from TGA, quartz contents from DSC similarly show consistent results as the ones obtained from XRD after corrections for insoluble residue contents.

All these results showed the following: (i) original mortars have lower free and combined water contents than the recent ones; (ii) carbonate contents from ignition up to 950°C are higher for original mortars than the recent ones; (iii) highest carbonate in mortar #2 correlates well with its highest lime content from XRF, which from petrographic examinations is determined to be due to abundant limestone fine particles in the masonry cement used in this mortar; (iv) volatiles left as balances in XRF are in the same range as the volatiles calculated from total LOI from gravimetry and total LOI from TGA; (v) quartz contents are consistently higher from all methods in the original mortars than the recent ones; (vi) water-soluble chloride contents are negligible in all mortars, but water-soluble sulfates are higher in the recent mortars than the original ones; and (vii) despite different binder types (cement-lime versus masonry cement) in two mortars of 2019 construction, overall chemical compositions of both recent mortars are similar.

Correlations of Results From Thermal Analyses (TGA, DSC), Gravimetry (LOI), XRD, IC, and XRF

Mortar Types	TGA Wt. Loss Up to 120°C	LOI from up to 110°C	TGA Wt. Loss 120°C to 200°C	TGA Wt. Loss 200°C to 600°C	LOI from 110°C to 550°C	TGA Wt. Loss > 600°C	LOI from 550°C to 950°C	Calcite Content From TGA	Calcite Content From XRD	CaO Content From XRF	LOI From XRF	Total LOI From Gravimetry	Total LOI From TGA	Sulfate Content From XRF	Water-Soluble Sulfate From IC	Quartz Content From DSC	Quartz Content From Insoluble Residue & XRD
	Free Water		Combined Water			Carbonates		Calcite		Lime	Volatiles ($H_2O + CO_2$)			Sulfate		Quartz	
Masonry cement Mortar# 2 circa 1960s	0.47	0.40	0.37	2.08	1.90	9.35	10.10	17.2	8.3	14.7	7.11	12.4	12.3	ND	0.057	71.1	62.0
AE Cement-Lime Mortar# 3 circa 1960s	0.46	1.60	0.35	2.16	2.10	5.64	6.30	9.34	7.9	9.35	6.55	10.0	8.6	0.019	0.176	68.4	68.9
Cement-lime Mortar# 4 2019	1.22	3.60	1.01	2.63	3.10	2.35	2.50	3.5	2.9	11.4	8.59	9.2	7.2	0.062	0.294	44.7	43.3
Masonry cement Mortar# 5 2019	1.06	-	0.62	4.14	-	4.25	-	6.88	-	11.6	9.71	-	10.1	0.007	0.337	41.4	-

Table 6: Summary of results obtained from chemical analyses (gravimetry), thermal analyses (TGA, DSC, DTG), X-ray diffraction, and X-ray fluorescence.

Mix Proportions of Masonry Mortars from Petrographic and Chemical Data

Mortars' Compositions & Mix Proportions	Mortar #2 from circa 1960s	Mortar #3 from circa 1960s	Mortar #4 from 2019
Chemical Compositions			
Soluble Silica, SiO_2 (%)	2.16	1.12	2.57
Calcium Oxide, CaO (%)	14.7	9.35	11.4
Acid-Insoluble Residue (%)	67.6	74.8	68.8
Loss on Ignition: From 0°C to 110°C (Free Water) (%)	0.4	1.6	3.6
Loss on Ignition: From 110-550°C (Combined Water) (%)	1.9	2.1	3.1
Loss on Ignition: From 550-950°C (Carbonation, CO_2) (%)	10.1	6.3	2.5
Assumed Compositions & Densities			
Portland Cement Silica (SiO_2) %	21	21	21
Hydrated Lime – From CO_2, CaO, MgO, Brucite, or Soluble Silica (SiO_2) for hydraulic lime (%)	-	-	From CaO content, after assigning CaO for Portland Cement and assuming 63.5% CaO in Portland Cement, and converting the residual CaO to lime $Ca(OH)_2$ by multiplying the residual CaO with the factor 1.322 (mol. wt. of lime to CaO = 74.03/56 = 1.322)
Bulk Density of Cement, (lbs./ft.^{3})	70 (Type N), 75 (Type S), 80 (Type M)	70 (Type N), 75 (Type S), 80 (Type M)	94 (Portland Cement)
Bulk Density of Hydrated Lime, (lbs./ft.^{3})	-	-	40
Bulk Density of Sand, (lbs./ft.^{3})	80	80	80
Calculated Volumetric Proportions			
Portland or Masonry Cement Contents (%)	Portland Cement (PC) = 100(2.16/21.0) = **10.28**; Masonry Cement (MC) = 100 – [Free water + Combined water + Sand] = 100 – (0.4+1.9+67.6) = **30.1** **PC/MC = 0.34, Type N masonry cement**	Portland Cement (PC) = 100(1.12/21.0) = **5.3**; Masonry Cement (MC) = 100 – [Free water + Combined water + Sand] = 100 – (1.6+2.1+74.8) = **21.5** **PC/MC = 0.24, Type N masonry cement**	Masonry cement content = 100(2.57/21.0) = **12.2**
Hydrated Lime Content (%)	-	-	1.322 × [11.4 – (12.2 × 0.635)] = 4.79
Sand Content (%) = Acid Insoluble Residue Content (%), For Siliceous Sand	**67.6**	**74.8**	**68.8**
Sand Content (%) = 100 – [Free Water + Combined Water + Binder], or, 100 – [Cement + Lime] For Siliceous-Calcareous Sand			
Cement Volume	30.1/70 (Type N masonry cement) = **0.430**	21.5/70 (Type N masonry cement) = **0.307**	12.2/94 = **0.129**
Hydrated Lime Volume	-	-	4.79/40 = 0.119
Sand Volume	67.6/80 = 0.845	74.8/80 = 0.935	68.8/80 = 0.860
Relative Volumes of Binder Phases : Sand	Masonry Cement : Sand = 0.430 : 0.845 = **1-part masonry cement to 2-part sand, similar to an ASTM C 270 Type N masonry cement mortar**	Masonry Cement : Sand = 0.307 : 0.935 = **1-part masonry cement to 3-part sand, similar to an ASTM C 270 Type N masonry cement mortar**	Portland Cement : Lime : Sand = 0.129: 0.119 : 0.860 = **1-part Portland cement to 1.1-part lime to 6.6-part sand (sand 3.2 times the sum of separate volumes of cement and lime, similar to an ASTM C 270 Type N cement-lime mortar**

Table 7: Calculations of mix proportions of original and recent masonry mortars from petrographic and chemical data.

DISCUSSIONS

Type of Mortar & Its Ingredients

Optical microscopy has determined the masonry cement-based composition of both original mortars from their characteristic: (i) carbonated natures of pastes in both mortars, (ii) air entrainment in mortar #3, (iii) presence of limestone fines as microfiller in abundance in mortar #2 and much lesser extent in mortar #3, (iv) presence of hydrated lime in abundance in mortar #3 and in subordinate proportion to limestone fines in mortar #2. For the two recent mortars from 2019 construction, optical microscopy has determined Portland cement-lime composition for mortar #4 from its non-carbonated nature of paste containing many residual Portland cement particles and fine-grained, porous hydrated lime with occassional lime patches. Hydrated lime component in masonry cements and in cement-lime mortar were all dolomitic lime manufactured from slaking quicklime produced from calcination of a magnesian limestone since subsequent SEM-EDS studies have detected appreciable magnesia in the pastes.

For the sand used in two original mortars from 1960s construction, both mortars (#2 and 3) showed use of compositionally similar sands, which are crushed siliceous sands consisting of major amounts of crushed silica (quartz) and minor amounts of quartzite, feldspar, and other siliceous components. Sands extracted from original mortars showed grain-size distributions having abundance of finer grain sizes that were concentrated from the crushing operations, which do not conform to grain size distribution of ASTM C 144 masonry sand. By contrast, sands used in the recent 2019 construction, though also siliceous, contain a noticeable amount of feldspar (albite), quartzite, mica and other siliceous components at subordinate amounts after quartz as the dominant siliceous constituent. Since sand constitutes the dominant volume fraction of mortars, such variabilities in and mineralogies between original and recent mortars is reflected in their bulk chemical (oxide) compositions as well. Grain size distribution of sand extracted from a recent 2019 mortar after acid digestion showed dominance of finer size fractions as also seen in the sands from the original mortars, having sand finer than the grain size distribution of sands recommended for ASTM C 144 masonry sands. Grain size distribution plots of sands from two original mortars and one recent mortar are very similar showing excessive fines and deviation of ranges of size distribution recommended for ASTM C 144 masonry sands. Excessive fines in the sands increases the water requirements of mortar, thereby increases the overall water-cementitious materials ratios, makes mortar more permeable to moisture, and reduces long-term moisture tightness of mortar joints. Sand particles are dense, hard, clear to off-white to light brown, and present in sound conditions without any evidence of potentially deleterious alkali-aggregate reactions in the mortars.

The two original mortars contained masonry cement as the binder. Pastes in both mortars showed the characteristic carbonated nature. In mortar #2, masonry cement contained a significant amount of limestone fines, which has given an overall granular appearance of mortar as noticed in optical and electron microscopy. By contrast, masonry cement used in mortar #3 had major amount of dolomitic hydrated lime, which has given an

overall very fine-grained porous and carbonated appearance of paste as opposed to coarser granular appearance from limestone fine particles seen in mortar #2.

Mortar #2 shows marginal air entrainment but has numerous irregular-shaped entrapped voids between sand particles as well as pore spaces between individual calcite grains of limestone fines, which have resulted in an overall porous microstructure of this mortar susceptible to moisture penetration. By contrast, mortar #3 shows excellent air entrainment in having numerous fine, discrete, spherical and near-spherical entrained air voids of sizes 1 mm or less, as well as many coarse voids, all of which, in fact, have given an excessive air entrainment appearance in the mortar. Even though masonry cement mortars are characteristically air entrained in having 16 to 18 percent air, air content in mortar #3 is found to be at the high end of this range, which is detrimental to development of good bond to the adjacent masonry units. Abundant irregular-shaped voids and interstitial capillary pore spaces in mortar #2 and abundant spherical entrained air bubbles in mortar #3 both are detrimental to development of a good bond to adjacent masonry units as well as their resistance to moisture transmission. Therefore, both original mortars are found to be candidates to have weak bond to their adjacent masonry units and have high moisture permeabilities.

Mortar #4 from the recent 2019 construction showed use of Portland cement and dolomitic hydrated lime as the two essential binder components. Therefore, paste in this mortar is non-carbonated, and contains abundant residual Portland cement particles, cement hydration products including coarser patches of calcium hydroxide crystals of cement hydration mixed with finer-grained porous hydrated lime, which is still not carbonated enough due to limited interaction with atmospheric carbon dioxide. By contrast, mortar #5 showed use of masonry cement as found in the original mortars, but masonry cement in mortar #5 used in 2019 construction is very different from two masonry cements found in the 1960s construction. In mortar #5, masonry cement does not show any noticeable abundance of either limestone fines (as found in #2) or hydrated lime (as found in #3) but more reasonable proportions of cement, lime, and limestone fines commonly found in many modern-day well-proportioned masonry cement mortars. Mortar #5 showed another difference in paste from the rest of the mortars in having a polymer component, which has densified the paste more than other mortars. Such polymer-induced added densification of paste beyond carbonated lime and cement hydration products is not only detected in optical microscopy but more so during SEM-EDS studies. FTIR analysis of this mortar detected a latex-based polymer addition, consistent with reported latex-modified nature of this mortar.

SEM-EDS studies of paste *per se* in two original and two recent mortars showed overall enrichment of silica in siliceous sand grains and interstitial lime-based paste reflected in elemental (Ca-Si-Al-Mg-etc.) maps. Use of dolomitic lime in all mortars is reflected from the high magnesia contents of pastes in SEM-EDS studies. Cementation indices of pastes (paste-CI after Eckel 1922) show wide range within and between the mortars which is not unexpected considering proprietary mix composition of masonry mortars as well as variable degrees of mixing of cement, lime, and limestone fine components in the paste. A systematic trend in compositional plots of

silica and lime contents of pastes against paste-CI from SEM-EDS studies demonstrated their lime, limestone fines and Portland cement based compositions of original binders.

Optical microscopy and scanning electron microscopy showed evidence of leaching of lime paste from around sand grains in mortar #2 from original 1960s construction, which is responsible for overall porous microstructure of original mortar.

Compositional analyses of original and recent mortars by XRF showed overall similar oxide compositions of two original mortars (despite their differences in compositions of masonry cements used), which are very different from the two recent mortars. Two recent mortars from 2019 construction showed overall similarities in oxide compositions. Two original mortars are found richer in silica mostly due to higher sand contents and quartz-rich composition of sands as opposed to many feldspar particles found in the sands in recent mortars, which are responsible for elevated alumina contents in the recent mortars compared to the original ones. High feldspar content of sand in the recent mortars also elevated the potassium contents in these mortars compared to the original ones. Since sand constitutes bulk volume of the mortar, changes in the sand mineralogies between the 1960s and 2019 mortars are reflected in their bulk chemistries. Oxide compositions of all four mortars reflect their similarities and differences in the mineralogies of sands used, as well as compositions of binder phases.

Mineralogical compositions of mortars determined from X-ray diffraction studies showed simple quartz-based mineralogy of sand in original mortars, more complex quartz-feldspar-mica based mineralogy of sand in recent mortars, dominance of quartz in the sand in all four mortars, and subordinate amount of calcite from carbonated paste and calcite fine particles of masonry cements. XRD studies of soft, white, efflorescence powder on mortar #5 showed calcium carbonate (calcite) composition of the efflorescence due to moisture-induced leaching of lime and cement hydration products from mortar followed by evaporation, precipitation of dissolved salts on the mortar's outer surface, and atmospheric carbonation of precipitated salts.

Thermal analyses of all four mortars show simple thermograms for original mortars mostly from loss of free water and water in hydrate salts during heating up to 200ºC, polymorphic transition of quartz at 575ºC, and major endothermic peak from decarbonation of carbonated lime and calcite fine particles. Both original mortars showed very similar thermograms having a minimal loss of free water (<0.5%) and water from hydrated salts (<0.5%) at up to 200ºC followed by a measurable loss (2 to 2.2%) of hydrate water from 200ºC to 600ºC. Degree of carbonation is higher in the #2 mortar (9.3% due to abundant limestone fine component along with hydrated lime) than 5.6% found in #3 mortar mostly from hydrated lime component in the latter. Quartz contents in both mortars are around 70 percent determined from polymorphic transition of quartz around 575ºC. Two recent mortars from 2019 construction, however, showed very different rather complex thermograms due to (i) the presence of noticeable structural water components in the 200ºC to 600ºC range, along with (ii) noticeably larger losses of free water and from hydrated salts at <200ºC, (iii) lower degree of carbonation than the original mortars, and (iv) lower quartz contents in the recent ones (<50%) compared to much high quartz contents (70%) found in the original mortars.

FTIR studies of all four mortars showed the simple inorganic phases (e.g., quartz, calcite) that are detected in microscopy and XRD studies and lack of any polymer component in the mortars except in mortar #5 from 2019 construction that showed absorbance peak from a latex-based polymer.

Ion chromatography (IC) of water-soluble salts showed negligible chloride contents in the original mortars (0.016% and 0.009% chlorides by mass of mortars in #2 and #3), which do not indicate ingress of any chloride salts or related distress. However, sulfate contents are noticeable and large variations in sulfate contents are found from 0.057% in #2 (limestone fine rich masonry cement) to 0.176% in #3 (hydrated lime rich masonry cement mortar). Chloride contents in the recent mortars are also negligible (0.018% and 0.021% chlorides by mass of mortars in #4 and #5) to confirm lack of any chloride salts or related distress. However, as in the original mortars, sulfate contents in 2019 mortars are noticeable (from 0.294% to 0.337%) which are higher than the maximum 0.176% sulfate found in #3 original mortar. Presence of Portland cement at a higher amount in the binders of the recent mortars is responsible for the high water-soluble sulfate contents. The highest Portland cement content detected from optical microscopy in mortar#5 correlated with its highest water-soluble sulfate from IC.

White efflorescence deposits on the surface of mortar# 5 is determined to be calcium carbonate, which is a testament of moisture penetration through the masonry joints at the location of #5. This is rather unusual considering dense polymer-impregnated microstructure of #5 as well as its Portland cement-rich composition with the impression of the best mortar of all examined in this study. This indicates that other factors beyond the mortar type (compatibility with adjacent masonry units, design, improper flushing, etc.) are also important to control the overall moisture tightness of masonry facades.

Mix Calculations

Information obtained from: (a) petrographic examinations to determine the sand compositions, binder types, as well as overall mortar types, and (b) chemical analyses of mortars to determine the soluble silica contents, water contents, and insoluble residue contents are used to calculate the volumetric proportions of mortars' ingredients. Mix calculations of mortars showed the two original mortars to be made using 1-part masonry cement to 2 to 3-part sand (mortar #3 has higher sand content than #2), whereas recent cement-lime mortar (#4) to be made using 1-part Portland cement to 1.1-part dolomitic hydrated lime to 6.6-part sand (which is 3.2 times the sum of separate volumes of cement and lime). All these proportions are indicative of use of ASTM C 270 Type N masonry cement for original mortar and Type N cement-lime mortar for the #4 recent mortar.

Mortar Condition

Mortar #2 from the original construction showed evidence of leaching of lime leaving empty spaces between calcite fine particles. Two recent mortars are free from any potentially deleterious atmospheric alterations. However, calcium carbonate efflorescence deposits in mortar #5 indicate moisture penetration through masonry joints.

Stone Type

Optical microscopy of the stone sample has determined its type to be diabase, which is a medium-grained intrusive, basic igneous rock consisting of subhedral plagioclase feldspar laths, anhedral equant pyroxene grains, and small dark opaque minerals, where pyroxene crystals partially enclosed plagioclase laths to create the characteristic subophitic textural arrangement of crystals that are common in diabase.

Tuckpointing Mortar

Based on the determined masonry mortar compositions of original mortars having 1-part masonry cement to 2 to 3-part sand similar to ASTM type N type of masonry cement mortar, and the diabase stone for masonry units, an appropriate masonry mortar should be an ASTM C 270 Type S or M cement-lime mortar, or, an ASTM C 270 Type S or M masonry/mortar cement mortar. A cement-lime mortar is preferable due to well-controlled proportions than a proprietary masonry cement binder. Air content of the mortar should be carefully controlled to provide the necessary workability and freeze-thaw durability without compromising the bond strength. Sand used should not be crushed too fine to increase the water demand of mortar mixes. Mortar ingredients to use should be in full conformance to their ASTM specifications (e.g., ASTM C 91/C1329 for masonry/mortar cement, C 144 for sand, C 150 for Portland cement, C 207 for hydrated lime, etc.).

REFERENCES

ASTM C 10, "Standard Specification for Natural Cement," In Annual Book of ASTM Standards, Section Four Construction, Vol. 04.01 Cement; Lime; Gypsum; ASTM Committee C01 on Cement, 2017.

ASTM C 91, "Standard Specification for Masonry Cement," In Annual Book of ASTM Standards, Section Four Construction, Vol. 04.01 Cement; Lime; Gypsum; ASTM Committee C01 on Cement, 2017.

ASTM C 144, "Standard Specification for Aggregate for Masonry Mortar," In Annual Book of ASTM Standards, Section Four Construction, Vol. 04.05 Chemical-Resistant Nonmetallic Materials; Vitrified Clay Pipe; Concrete Pipe; Fiber-Reinforced Cement Products; Mortars or mortars and Grouts; Masonry; Precast Concrete; ASTM Committee C12 on Mortars or mortars for Unit Masonry, 2017.

ASTM C 1324, "Standard Test Method for Examination and Analysis of Hardened Masonry Mortar," In Annual Book of ASTM Standards, Section Four Construction, Vol. 04.05 Chemical-Resistant Nonmetallic Materials; Vitrified Clay Pipe; Concrete Pipe; Fiber-Reinforced Cement Products; Mortars or mortars and Grouts; Masonry; Precast Concrete; ASTM Committee C12 on Mortars or mortars for Unit Masonry, 2017.

ASTM C 270, "Standard Specification for Mortar for Unit Masonry," In Annual Book of ASTM Standards, Section Four Construction, Vol. 04.05 Chemical-Resistant Nonmetallic Materials; Vitrified Clay Pipe; Concrete Pipe; Fiber-Reinforced Cement Products; Mortars or mortars and Grouts; Masonry; Precast Concrete; ASTM Committee C12 on Mortars or mortars and Grouts for Unit Masonry, 2017.

ASTM C 1713, "Standard Specification for Mortars or mortars for the Repair of Historic Masonry," In Annual Book of ASTM Standards, Section Four Construction, Vol. 04.05 Chemical-Resistant Nonmetallic Materials; Vitrified Clay Pipe; Concrete Pipe; Fiber-Reinforced Cement Products; Mortars or mortars and Grouts; Masonry; Precast Concrete; ASTM Committee C12 on Mortars or mortars and Grouts for Unit Masonry, 2017.

ASTM C 51, "Standard Terminology Relating to Lime and Limestone (as used by the Industry)'" In Annual Book of ASTM Standards, Section Four Construction, Vol. 04.01 Cement; Lime; Gypsum; ASTM Committee C07 on Lime, 2017.

ASTM C 856, "Standard Practice for Petrographic Examination of Hardened Concrete," In Annual Book of ASTM Standards, Section Four Construction, Vol. 04.02; ASTM Subcommittee C 9.65, 2017.

ASTM C 1723, "Standard Guide for Examination of Hardened Concrete Using Scanning Electron Microscopy," In Annual Book of ASTM Standards, Section Four Construction, Vol. 04.02; ASTM Subcommittee C 9.65, 2017.

ASTM C 1329, "Standard Specification for Mortar Cement," In Annual Book of ASTM Standards, Section Four Construction, Vol. 04.01; ASTM Subcommittee C01.11, 2016.

ASTM C 150, "Standard Specification for Portland Cement," In Annual Book of ASTM Standards, Section Four Construction, Vol. 04.01; ASTM Subcommittee C01.10, 2018.

ASTM C 1489, "Standard Specification for Lime Putty for Structural Purposes," In Annual Book of ASTM Standards, Section Four Construction, Vol. 04.01; ASTM Subcommittee C07.02, 2015.

ASTM C 207, "Standard Specification for Hydrated Lime for Masonry Purposes," In Annual Book of ASTM Standards, Section Four Construction, Vol. 04.01; ASTM Subcommittee C07.02, 2011.

ASTM C 979 "Standard Specification for Pigments for Integrally Colored Concrete,' In Annual Book of ASTM Standards, Section Four Construction, Vol. 04.01; ASTM Subcommittee C07.02, 2011.

Bartos, P. Groot, C., and Hughes, J.J. (eds.), "Historic Mortars or mortars: Characteristics and Tests", Proceedings PRO12, RILEM Publications, France, 2000.

Boynton, R., *Chemistry and Technology of Lime and Limestone, 2nd edition*, John Wiley & Sons, Inc. 1980.

Brosnan, Denis, A., Characterization of Rosendale Mortars or mortars For Fort Sumter National Monument and Degradation of Mortars or mortars by Sea Water and Frost Action, Final Report, April 19, 2012.

Callebaut, K., Elsen, J., Van Balen, K., and Viaene, W., "Nineteenth century hydraulic restoration mortars or mortars in the Saint Michael's Church (Leuven, Belgium) Natural hydraulic lime or cement?" Cement and Concrete Research, V 31, pp 397-403, 2001.

Callebaut, K., Elsen, J., Van Balen, K., and Viaene, W., Historical and scientific study of hydraulic mortars or mortars from the 19th century. In International RILEM workshop on historic mortars or mortars: Characterization and Tests; Paisley, Scotland, 12th to 14th May 1999, Edited by Barton, P., Groot, C., and Hughes, J.J., Cachan, France, RILEM Publications, 2000.

Charloa, A.E., "Mortar analysis: A comparison of European procedures." US/ICOMOS Scientific Journal: Historic Mortars or mortars & Acidic Deposition on Stone, 3 (1), pp. 2-5, 2001.

Charola, A.E., and Lazzarin, L., Deterioration of Brick Masonry Caused by Acid Rain, ACS Symposium Series, Vol. 318, pp. 250-258, 2009.

Chiari, G., Torraca, G., and Santarelli, M.L., "Recommendations for Systematic Instrumental Analysis of Ancient Mortars or mortars: The Italian Experience", *Standards for Preservation and Rehabilitation*, ASTM STP 1258, S.J. Kelley, ed., American Society for Testing and Materials, pp. 275-284, 1996.

Doebley, C.E., and Spitzer, D., "Guidelines and Standards for Testing Historic Mortars or mortars", *Standards for Preservation and Rehabilitation*, ASTM STP 1258, S.J. Kelley, ed., American Society for Testing and Materials, pp. 285-293, 1996.

Eckel, Edwin, C., *Cements, Limes, and Plasters*, John Wiley & Sons, Inc. 655pp, 1922.

Edison, M.P. (Editor), *Natural Cement*, ASTM STP 1494, American Society for Testing and Materials, 2008.

Elsen, J., "Microscopy of Historic Mortars or mortars – A Review", *Cement and Concrete Research 36*, 1416-1424, 2006.

Elsen, J., Mertens, G., and Van Balen, K., Raw materials used in ancient mortars or mortars from the Cathedral of Notre-Dame in Tournai (Belgium), Eur. J. Mineral., Vol. 23, pp. 871-882, 2011.

Elsen, J., Van Balen, K., and Mertens, G., Hydraulicity in Historic Lime Mortars or mortars: A Review, In, Valek, J, Hughes, J.J., and Groot, W.P. (Eds.), Historic Mortars or mortars Characterisation, Assessment and Repair, RILEM Book series, Volume 7, pp. 125-139, Springer, 2012.

Erlin, B., and Hime, W.G., "Evaluating Mortar Deterioration", *APT Bulletin*, Vol. 19, No. 4, pp. 8-10+54, 1987.

Goins E.S., "Standard Practice for Determining the Components of Historic Cementitious Materials," National Center for Preservation Technology and Training, Materials Research Series, NCPTT 2004.

Goins, E.S., "A standard method for the characterization of historic cementitious materials." US/ICOMOS Scientific Journal: Historic Mortars or mortars & Acidic Deposition on Stone, # (1), pp. 6-7, 2001.

Groot, C., Ashall, G., and Hughes, J., Characterization of Old Mortars or mortars with Respect to their Repair, State-of-the-art Report of RILEM Technical Committee 167-COM, 2004.

Hughes, D.C., Jaglin, D., Kozlowski, R., Mayr, N., Mucha, D., and Weber, J., "Calcination of Marls to Produce Roman Cement", pp. 84-95, In, Edison, M.P. (Editor), *Natural Cement*, ASTM STP 1494, American Society for Testing and Materials, 2007.

Hughes, J.J., Cuthbert, S., and, Bartos, P., "Alteration Textures in Historic Scottish Lime Mortars or mortars and the Implications for Practical Mortar Analysis", *Proceedings of the 7th Euroseminar on Microscopy Applied to Building Materials*, Delft, pp. 417-426, 1999.

Hughes, R.E., and Bargh, B.L., The weathering of brick: Causes, Assessment and Measurement, A Report of the Joint Agreement between the U.S. Geological Survey and the Illinois State Geological Survey, 1982.

Jana, D., "Application of Petrography In Restoration of Historic Masonry Structures", In: Hughes, J.J., Lesie, A.B. and Walsh, J.A., eds. *Proceedings of 10th Euroseminar on Microscopy Applied to Building Materials*, Paisley, 2005.

Jana, D., "Sample Preparation Techniques in Petrographic Examinations of Construction Materials: A State-of-the-art Review", *Proceedings of the 28th Conference on Cement Microscopy*, International Cement Microcopy Association, Denver, Colorado, pp. 23-70, 2006.

Jedrzejewska, H., Old mortars or mortars in Poland: a new method of investigation, Studies in Conservation 5, pp. 132-138, 1960.

Langley, W.S., Report to CRH Canada on Investigation of Failed Mortar, W.S. Langley Concrete & Materials Technology, Inc. Project No. 191271, June 2019.

Leslie, A.B., and Hughes, J.J., "Binder Microstructure in Lime Mortars or mortars: Implications for the Interpretation of Analysis Results", *Quarterly Journal of Engineering Geology & Hydrogeology*, V. 35, No. 3, pp. 257-263, 2001.

Lubell, B., van Hees, Rob. P.J., and Groot, Casper J.W.P., The role of sea salts in the occurrence of different damage mechanisms and decay on brick masonry, Construction and Building Materials, Vol. 18, pp. 119-124, 2004.

Martinet, G., Quenee, B., Proposal for a useful methodology for the study of ancient mortars or mortars, Proceedings of the International RILEM workshop "Historic Mortars or mortars: Characteristics and tests," Paisley, pp. 81-91, 2000.

Mack, Robert, and Speweik, John P., *Preservation Briefs 2*, U.S. Department of the Interior, National Park Service Cultural Resources, Heritage Preservation Services, pp. 1-16, 1998.

Middendorf, B., Baronio, G., Callebaut, K, and Hughes, J.J., "Chemical-mineralogical and physical-mechanical investigation of old mortars or mortars, Proceedings of the International RILEM workshop "Historic Mortars or mortars: Characteristics and tests," Paisley, pp. 53-61, 2000.

Middendorf, B., Hughes, J.J., Callebaut, K., Baronio, G., and Papayanni, I., Mineralogical characterization of historic mortars or mortars, In. Groot, C., et al. (eds), Characterisation of Old Mortars or mortars with Respect to their Repair, State-of-the-art Report of RILEM Technical Committee 167-COM, pp. 21-36, 2004a.

Middendorf, B., Hughes, J.J., Callebaut, K., Baronio, G., and Papayanni, I., Chemical characterization of historic mortars or mortars, In. Groot, C., et al. (eds), Characterisation of Old Mortars or mortars with Respect to their Repair, State-of-the-art Report of RILEM Technical Committee 167-COM, pp. 37-53, 2004b.

Middendorf, B., Hughes, J.J., Callebaut, K., Baronio, G., and Papayanni, I., "Investigative Methods for the Characterization of Historic Mortars or mortars – Part 1: Mineralogical Characterization," *Materials and Structures*, Vol. 38, 2005a.

Middendorf, B., Hughes, J.J., Callebaut, K., Baronio, G., and Papayanni, I., "Investigative Methods for the Characterization of Historic Mortars or mortars – Part 2: Chemical Characterization," *Materials and Structures*, Vol. 38, pp 771-780, 2005b.

Sarkar, S.L., Aimin, Xu, and Jana, Dipayan, Scanning electron microscopy and X-ray microanalysis of Concretes, pp. 231-274, In, Ramachandran, V.S. and Beaudoin, J.J. Handbook of Analytical Techniques in Concrete Science and Technology, Noyes Publications, Park Ridge, New Jersey, 2000.

Speweik, J.P., *The History of Masonry Mortar in America 1720-1995*, 2010.

Stewart, J., and Moore, J., Chemical techniques of historic mortar analysis, Proceedings of the ICCROM Symposium "Mortars or mortars, Cements, and Grouts used in the Conservation of Historic Buildings," Rome, ICCROM, Rome, pp. 297-310, 1981.

Valek, J., Hughes, J.J., and Groot, C. (eds.), *Historic Mortars or mortars: Characterization, Assessment and Repair*, Springer, RILEM Book series Vol. 7, p. 464, 2012.

Valek, J., Hughes, J.J., and Groot, C. (eds.), Historic Mortars or mortars: Characterization, Assessment and Repair, Springer, RILEM Book series Vol. 7, 2012.

Van Balen, K., Toumbakari, E.E., Blanco, M.T., Aguilera, J., Puertas, F., Sabbioni, C., Zappia, G., Riontino, C., and Gobbi, G., "Procedures for mortar type identification: A proposal." In International RILEM workshop on historic mortars or mortars: Characteristics and Tests; Paisley, Scotland, 13th to 14th May 1999, edited by Barton, P., Groot, C., and Hughes, J.J., Cachan, France: RILEM Publications, 2000.

Vyskocilova, R., W. Schwarz, D. Mucha, D. Hughes, R. Kozlowski, and J. Weber, "Hydration processes in pastes of roman and American natural cements," *ASTM STP*, vol. 4, no. 2, 2007.

Weber, J., Gadermayr, N., Kozlowski, R., Mucha, D., Hughes, D., Jaglin, D., and Schwarz, W., Microstructure and mineral composition of Roman cements produced at defined calcination conditions, Materials Characterization, Vol. 58, pp. 1217-1228, 2007.

✪□✪□✪ END OF TEXT ✪□✪□✪

APPENDIX –
LABORATORY TESTING OF MASONRY MORTARS

Introduction[1]

Until 1970s characterization of masonry mortars were mostly based on traditional wet chemical analyses (Jedrzejewska, 1960, Stewart and Moore, 1981), where interpretation of results were often difficult if not impossible without a good knowledge of the nature of different sand and binder components in mortars. The majority of later mortar characterization proposed optical microscopy (Erlin and Hime 1987, Middendorf et al. 2000, Elsen 2006) as the first step in identification of different components of mortar based on which other analytical techniques including the wet chemistry are performed. Examples include scanning electron microscopy and X-ray microanalysis, X-ray diffraction, X-ray fluorescence, atomic absorption, thermal analysis, infrared spectroscopy, etc. (Bartos et al. 2000, Elsen 2006, Callebaut et al. 2000, Erlin and Hime 1987, Goins 2001, 2004, Groot et al. 2004, Doebley and Spitzer 1996, Chiari et al. 1996, Middendorf et al. 2000, 2004, 2005, Leslie and Hughes 2001, Martinet and Quenee 2000, Valek et al., 2012, Jana 2005, 2006). The choices of appropriate techniques depend mainly on the questions that have to be addressed, and, on the amount of material available.

Purposes of laboratory testing are: (a) to document an in place mortar by examining its sand and binder components, proportions of various ingredients, and their effects on properties and performance of the mortar, (b) evidence of any chemical or physical deterioration of the mortar from unsoundness of its ingredients to effects of potentially deleterious agents from the environment (e.g., salts), (c) records of later repointing events and their beneficial or detrimental effects on the performance of the original mortar and masonry units, and finally, (d) an assessment of an appropriate restoration mortar to ensure compatibility with the existing structure.

Currently there are two standardized procedures available that describe various laboratory techniques for analyses of masonry mortars with special emphasize to historic mortars. One is from the USA, the ASTM C 1324 "Standard Test Method for Examination and Analysis of Hardened Masonry Mortar," which includes detailed petrographic examinations, followed by chemical analyses, along with various other analytical methods to test masonry mortars as described in various literatures, e.g., XRD, thermal analysis, and infrared spectroscopy. The second one is from European studies and described in RILEM (Middendorf et al. 2004 and b, and 2005 a and b).

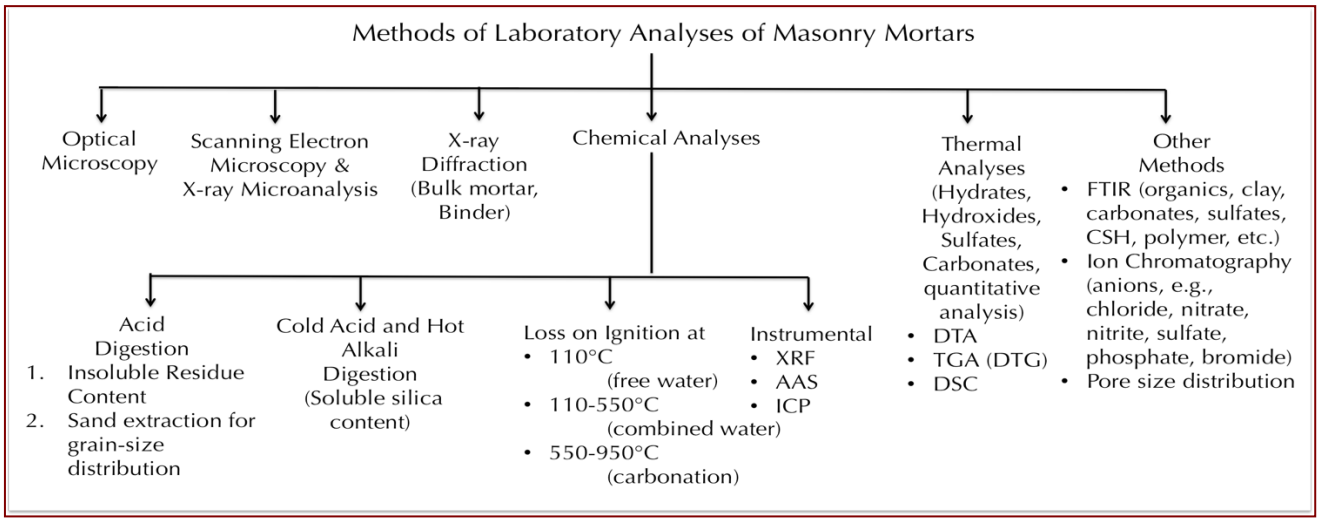

Figure A1: Various methods of laboratory analyses of masonry mortars. Optical microsocpy is the first method that provides many useful information about the mortar and its ingredeints, and dictates the subsequent methods to follow. Electron microscopy, X-ray diffraction, and various chemical analyses are commonly followed after optical microcopy to further determine the composition, microstructure, and mineralogy of sand and binder(s).

[1] For various analytical facilities for laboratory testing of mortars, please visit our website at www.cmc-concrete.com.

Sample Selection and Steps of Laboratory Analyses

Mortar samples are first photographed with a digital camera, scanned on a flatbed scanner, and examined in a low-power stereomicroscope for the preliminary examinations, e.g., to screen any unusual pieces having different appearances, e.g., representing contaminants from prior pointing episodes.

Four (4) subsets of the pieces of interest are then selected from the original amount for: (1) optical microscopy, scanning electron microscopy, and X-ray microanalysis of a representative sizable amount to cover as much of an entire 50 mm × 75 mm thin section per sample with multiple pieces as possible for chemical and mineralogical compositions, and microstructures of sand, paste, and mortar, (2) extraction of masonry sand by acid digestion for grain size distribution of sand (preferably from an un-pulverized or gently pulverized mortar), (3a) loss on ignition for water and carbonate contents, (3b) acid digestion for determination of insoluble residue content, and (3c) cold-acid then hot-alkali digestion for soluble silica content from hydraulic binders – all three after pulverizing the 3rd subset mortar to finer than 0.3 mm size and collecting aliquots of 1 gram, 1 gram, and 5 grams, respectively, and, (4) ultrafine pulverization (finer than 44-micron particle size) of 10 grams of mortar from the 4th subset for XRD, XRF, and thermal analyses. Any additional analyses, if needed, e.g., water digestion for determination of soluble salts by ion chromatography, or, infrared spectroscopy are done from the 4th subset. Organic analysis (e.g., paint or surface coating on masonry) by FTIR is done on the coating of interest from the original mortar pieces.

After preliminary visual examinations, optical microscopy is the first detailed examination that is most crucial in mortar analysis to determine the types of sand and binder used from mineralogical and textural characteristics of mortar, based on which subsequent chemical analyses are done to determine the chemical compositions of binders and proportions of sand, and binder components. Information obtained from petrographic examinations is crucial to devise the appropriate guidelines to follow for chemical methods, and to properly interpret the results of chemical analyses. For example, detection of siliceous versus calcareous versus argillaceous natures of aggregates in mortar, or the presence of any pozzolan in the binder (slag, fly ash, ceramic dusts, etc.) from petrography restricts which chemical method to follow, and how to interpret the results of such analyses, e.g., acid-insoluble residue contents. Therefore, a direct chemical analysis e.g., acid digestion of a mortar without doing a prior petrographic examination to determine the types of aggregates and binder used could lead to highly erroneous results and interpretation. Armed with petrographic and chemical data, and based on assumed compositions and bulk densities of the sand and the binder(s) similar to the ones detected from petrographic examinations volumetric proportions of sand and various binders present in the examined mortar can be calculated. The estimated mix proportions from such calculations can provide at least a rough guideline to use as a starting mix during formulation of a tuck pointing mortar to match with the existing mortar.

Optical Microscopy For Mineralogy & Microstructure of Mortar

After preliminary non-destructive examinations, e.g., from visual examinations, photographing as-received sample with a digital camera, scanning mortar pieces on a flatbed scanner, and examining in a low-power stereomicroscope, subsequent destructive sample preparation steps are followed for examinations of detailed mineralogical and microstructural compositions of mortar sand and binders in thin sections (25 to 30 micron thickness) in (a) a higher power Stereozoom microscope from 5X to 100X, and then in a research-grade petrographic microscope from 40X to 1000X both microscopes are equipped with transmitted, reflected, polarized, and fluorescent light facilities, as well as photo-micrographic capabilities with advanced high-resolution microscope cameras.

The main purposes of optical microscopy of masonry mortar are characterization of: (a) aggregates, e.g., type(s), chemical and mineralogical compositions, nominal maximum size, shape, angularity, grain-size distribution, soundness, alkali-aggregate reactivity, etc. (b) paste, e.g., compositions and microstructures to diagnose various type(s) of binder(s) used, (c) air, e.g., presence or absence of air entrainment, air content, etc., (d) alterations, e.g., lime leaching, carbonation, staining, etc. due to interactions with the environmental agents during service, and effects of such alterations on properties and performance of mortar; and (e) deteriorations, e.g., chemical and/or physical deteriorations during service, cracking from various mechanisms, salt attacks, possible reasons for the lack of bond if reported from the masonry unit, etc.

Four essential steps followed during optical microscopy are: (1) visual examination of as-received, fresh fractured, and sectioned surfaces of mortar in a stereo-microscope, (2) preparation of a large-area (50 × 75 mm) thin section of homogeneous thickness (25-30 micron), (3) observation of thin section in a transmitted-light stereo-zoom microscope from 5X to 100X preferably with polarized-light facilities to observe large-scale distribution of sand and mortar microstructure, and finally (4) observation of thin section in a petrographic microscope from 40X to 600X equipped with transmitted and reflected polarized and fluorescent-light facilities for examinations of sand and binder compositions and microstructures.

For thin section preparation, representative fragments are oven-dried at 40°C to a constant mass and placed in a flexible (e.g., molded silicone) sample holder, then encapsulated with a colored dye (e.g., blue dye commonly used in sedimentary petrography, or, fluorescent dye, Elsen 2006) mixed low-viscosity epoxy resin under vacuum to impregnate the capillary pore spaces of mortar, improve the overall integrity of sample during sectioning by the cured epoxy, highlight porous areas of mortar, alterations, cracks, voids, reaction products, etc. The epoxy-encapsulated cured solid block of sample is then de-molded and processed through a series of coarse to fine grinding on metal and resin-bonded diamond grinding discs with water or a lubricant, eventually a perfectly flat clean ground surface is glued to a large-area (50 × 75 mm) glass slide. Careful precision sectioning and precision grinding of the sample is then done in a thin-sectioning machine (e.g., Buehler, Logitech, Ingram-Wards, Microtrim, Struers) till the thickness is down to 50-60 micron. Final thinning down to 25-30 micron thickness is done on a glass plate with fine (5-15 micron) alumina abrasive. Thin section is eventually polished with various fine (1 micron to 0.25 micron size) diamond abrasives on polishing wheels for examinations in a petrographic microscope, and eventually in SEM-EDS. Sample preparation steps are described in detail in Jana (2006).

Steps followed during light optical microscopical examinations of a mortar sample include:

a. Visual examinations of mortar fragments, as received, to select fragments for detailed optical microscopy; initial digital and flatbed scanner photography of mortar as received;
b. Low-power stereomicroscopic examinations of saw-cut and freshly fractured sections of mortar for evaluation of variations in color, grain-size and appearances of sand, and the nature of the mortar paste;
c. Examinations of oil immersion mounts for special features and materials from mortar in a petrographic microscope;
d. Examinations of colored (blue or fluorescent) dye-mixed epoxy-impregnated polished thin sections of mortar fragments in a transmitted-light Stereozoom microscope for determination of size, shape, angularity, and distribution of sand, as well as abundance and distribution of void and pore spaces that are highlighted by the colored dye-mixed epoxy;
e. Image analyses of photomicrographs of mortar thin sections for estimations of pores, voids, intergranular open spaces, and shrinkage microcracks by using Image J or other image analysis software where multiple photomicrographs are collected in plane polarized light mode by using a high-resolution Stereozoom microscope equipped with transmitted and polarizing light facilities and stitched to get a representative coverage;
f. Examinations of colored (blue or fluorescent) dye-mixed epoxy-impregnated polished thin sections of mortar fragments in a petrographic microscope for detailed compositional, mineralogical, textural, and microstructural analyses of aggregates and binders in mortars, along with diagnoses of evidence of any deleterious processes and alterations (e.g., lime leaching, precipitation of secondary deposits and alteration products, salts);
g. Examinations of polished thin or solid section in reflected-light (epi-illumination) mode of petrographic microscope after etching the surface with acid to identify various non-hydrated hydraulic phases (e.g., C_2S, C_3S, C_3A, etc. Middendorf et al., 2005);
h. Examinations of any physical or chemical deterioration of mortar or signs of improper construction practices from microstructural evidences;
i. Stereo-microscopical examinations of size, shape, and color variations of sand extracted after hydrochloric acid digestion; and finally,
j. Selection of areas of interest to be examined by scanning electron microscopy.

CMC has a large assortment of optical microscopes from early 20th century to many latest advanced Nikon, Olympus, Leitz, Zeiss stereozoom and petrographic microscopes and several petrographic sample preparation and photomicrography facilities that can be found in our website at www.cmc-concrete.com.

Figure A2: Top - Optical microscopy laboratory in CMC which houses a variety of optical microscopes including low-power stereomicroscopes, high-power transmitted, reflected, fluorescent, and polarized-light stereozoom microcope, metallurgical microcopes, petrographic microcopes with reflected, transmitted, fluoescent, and polarized light facilities, fluoreccent microscopes, inverted microscopes, comparison microscopes, etc. Mortar examinations are done on stereomicroscopes, fluorescent light microscopes, and petrographic microscopes. Bottom – Thin sectioning equipments from Buehler and Microtec that prepare 25 to 30 micron thick thin-sections impregnted in clear, blue, or fluorescent dye-mixed epoxy for observations in petrographic and stereozoom microscopes (left), Nikon Eclipse E600 POL petrographic micorscope (2nd from left), Nikon SMZ-10A stereomicroscope (3rd from left) and Olympus SZX-12 transmitted-light stereozoom microscope (rightmost) all having photomicrographic capabilities with advanced high-resolution microscope cameras (e.g., Jenoptik Progres Gryphax, Luminera Infinity series) for documenting compositional and microstructural features from optical microsocpical examinations of masonry mortar.

Scanning Electron Microscopy & X-Ray Microanalyses For Mineralogy, Microstructure, and Microchemical Compositions of Mortar

Figure A3: CamScan Series 2 scanning electron microscope in CMC that is attached to a backscatter detector, a secondary electron detector and an energy-dispersive X-ray detector.

Methods followed in scanning electron microscopy and energy-dispersive X-ray fluorescence spectroscopy (SEM-EDS) include: (a) secondary electron imaging (SEI) to determine the surface texture, microstructure and morphology of the examined surface, (b) backscatter electron (BSE) imaging to determine compositions of various phases from various shades of darkness/grayness from average atomic numbers of phases from the darkest pore spaces to brightest iron minerals (via minerals e.g., thaumasite, periclase, ettringite, quartz, dolomite, monosulfate, gypsum, calcite, C-S-H, aluminate, calcium hydroxide, belite, alite, free lime, and ferrite having progressively increasing average atomic numbers and brightness in BSE image), (c) X-ray elemental mapping (dot mapping) of an area of interest to differentiate various phases, (d) point-mode or area (raster)-mode analysis of specific area/phase of interest on a polished thin or solid section, and (e) average compositional analysis of a specific phase or an area on a polished thin or solid section or small subset of a sample.

The main purposes of SEM-EDS analyses of mortar are to: (a) observe the morphology and microstructure of various phases of sand and binder, (b) characterize the typical fine-grained microstructure of hydrated hydraulic components that are too fine to be examined by optical microscopy and not well crystallize to be detected by XRD; (c) determine the major element oxide compositions, and compositional variations of paste, and from that determine the type of binder used, especially to differentiate non-hydraulic calcitic and dolomitic lime mortars from hydraulic lime varieties, natural cements, pozzolans, slag cements, Portland cements, etc. all from their characteristic differences in compositions and hydraulicities (e.g., cementation index of Eckel 1922); (d) determine composition of residual hydraulic phases to assess the raw feed and calcination processes used in binder manufacturing; (e) assess hydration, carbonation, and alteration products of binders, (f) investigate effects of various environmental alterations of paste and its role on properties and performance of mortar, (g) detect salts

and other potentially deleterious constituents, (h) detect pigments and fillers, (i) examine compositional variations across multiple coats of binder installed, etc.; and eventually (i) complement and confirm the results of optical microscopy.

Due to characteristic difference in compositions of pastes made using various binders, e.g., non-hydraulic lime (CaO dominants over all other oxides), variably hydraulic lime (CaO with variable SiO_2 contents depending on hydraulicity), dolomitic lime (high CaO and MgO), natural cement (CaO, SiO_2, Al_2O_3, and MgO contents are high, high MgO and FeO contents are characteristic), and Portland cement (CaO and SiO_2 contents are higher than all other oxides), SEM-EDS analysis of paste is a powerful method for detection of the original binder components in the mortar. Effects of chemical alterations and various chemical deteriorations of a mortar (e.g., lime leaching, secondary calcite precipitates, gypsum deposits, etc.) can also be detected effectively by SEM-EDS.

SEM-EDS analysis is done in a CamScan Series 2 scanning electron microscope (Figure A3) equipped with a high-resolution column 40Å tungsten, 40 kV electron optics zoom condenser 75° focusing lens operating at 20 kV, equipped with a variable geometry secondary electron detector, backscatter electron detector, EDS detector for observations of microstructures at high-resolution, compositional analysis, and quantitative determinations of major element oxides from various areas of interest, respectively. Revolution 4Pi software is used for digital storage of secondary election and backscatter electron images, elemental mapping, and analysis along a line, a point, or an area of interest.

Portion(s) of interest on the polished 50 mm × 75 mm size thin section used for optical microscopy are subsequently coated with a thin conductive carbon or gold-palladium film and placed on a custom-made aluminum sample holder to fit inside the large multiported chamber of CamScan SEM equipped with the eucentric 50 × 100 mm motorized stage. Procedures for SEM examinations are described in ASTM C 1723. Sarkar et al. (2000) described various applications of SEM-EDS in concrete and other construction materials.

Acid Digestion for Siliceous Sand Content and Size Distribution of Sand

Acid digestion is perhaps the most commonly used test of masonry mortar, which is done to: (a) extract sand from mortar by dissolving the binder fractions so that grain-size distribution of sand can be done by sieve analysis, and (b) assess sand content in the mortar. Sand content after acid digestion is determined both from: (a) 1.00 gram of pulverized mortar (finer than 0.3 mm size) digested in 50-ml dilute (1+3) HCl (heated rapidly but below boiling), and, (b) from digesting a representative bulk mortar *per se* (for harder mortars perhaps with light pulverization) in multiple fresh batches of (1+3) HCl at ambient temperature. The former usually gives better result due to small amount, pulverization to easily remove the binder fraction for digestion, and use of rapidly heated acid, whereas latter method requires multiple episodes of digestion in fresh acid and is time-consuming. Acid digestion is also done as the first step to determine soluble silica content in a mortar as described below, which is contributed from the hydraulic components in binder.

All these goals of acid digestion depend on the assumptions that: (i) sand is siliceous in composition and does not contain any acid-soluble constituents (e.g., carbonates), and, (ii) binder entirely dissolves in acid and does not contain any acid-insoluble constituents (gypsum, clay, etc.). Applicability of acid digestion to assess these tasks should therefore be first verified by optical microscopy to confirm the siliceous nature of sand without any appreciable acid-soluble constituents, and calcareous nature of binder, and none without any appreciable argillaceous (clay) constituents.

For grain-size distribution of sand (for mortar found from optical microscopy to contain siliceous sand), a few representative fragments of (preferably not pulverized or lightly pulverized in a porcelain mortar and pestle for harder mortars to break down to smaller size fraction without crushing the sand to retain the original sand size) are selected for digestion in multiple fresh batches of (1+3) dilute hydrochloric acid to dissolve away all binder fractions and extract, wash, and oven-dry the acid-insoluble component of aggregate. Usually multiple episodes of acid digestion in fresh batches of acid and filtration of residues are needed to entirely remove the binder fractions without losing the finer fractions of sand. Sand particles thus extracted are washed, oven-dried, and sieved in an automatic mini sieve shaker (e.g., from Gilson) through various U.S. Sieves from No. 4 (4.75 mm) through 8 (2.36 mm), 16 (1.18 mm), 30 (0.6 mm), 50 (0.3 mm), 100 (0.15 mm), and 200 (0.075 mm) for determination of the size, shape, angularity, and color of sands retained on various sieves. Grain-size distribution

of sand is then compared with ASTM C 144 specifications for masonry sand. Photomicrographs of sand retained on each sieve are then taken with a stereomicroscope to record the sand color. For low amount of mortar, or, for mortar having calcareous sand, image analysis (e.g., ImageJ) on stitched photomicrographs of thin sections taken from multiple areas can be done to determine the sand-size distribution (Elsen et al. 2011).

Cold-Acid & Hot-Alkali Digestion For Soluble Silica Content

Digestion of a pulverized sample of mortar in a cold acid followed by further digestion of residue in a hot alkali hydroxide solution are done to determine the soluble silica content contributed from the hydraulic component of binder, where cold acid digestion usually dissolves most of the binder without affecting the sand, followed by hot alkali hydroxide digestion to dissolve remaining soluble silica from calcium silicate hydrate component of paste or in mortars containing hydraulic binders. The soluble silica content corresponds to the silica mostly contributed from the hydraulic binder components (and a minor amount from any soluble silica component in the aggregates).

For determination of soluble silica content (modified from ASTM C 1324), 5.00 grams of pulverized mortar (finer than 0.3 mm size, without excessive fines) is first digested in 100-mL cold (at 3 to 5°C) HCl and filtered through two 2.5-micron filter papers (filtrate#1). The residue with filter papers is then digested again in hot (below boiling) 75-ml NaOH, and filtered through two 2.5-micron filter papers (filtrate# 2). The two filtrates from acid and alkali digestions are then combined, re-filtered twice with 2.5-micron and then through 0.45-micron filter paper to remove any suspended silica fines, brought to 250 mL volume with distilled water, and then used for soluble silica determination by an analytical method, such as atomic absorption spectroscopy (AAS), inductive coupled plasma optical emission spectroscopy (ICP-OES), or X-ray fluorescence spectroscopy (XRF). Multiple steps of filtrations from 2.5-micron to submicron (0.2-micron pore size) filter papers are necessary to remove any suspended silica that can skew the result. Instrument to be used for such determination must be calibrated with several silica standards in matrices similar to the one used in mortar analysis. CMC uses an XRF unit that is calibrated with filtrates from a series of laboratory-prepared standards of Portland cement and silica sand mortars (moist cured at *w/c* of 0.50 for at least 30 days) having various proportions of cements (SiO_2 contents of standards ranging from 1 to 10%) for determining SiO_2 Kα X-ray intensities from known stoichiometric silica (cement) contents of standards (using exact 5.00 grams as samples) prepared by the same procedure of cold HCl-digestion/filtration/hot NaOH-digestion/2nd filtration/combination of two filtrates/re-filtration steps followed for mortars. Hydraulic binder content is then calculated as: [(soluble SiO_2, weight percent in sample as calculated above) divided by assumed soluble SiO_2 content in binder] ×100, where assumed SiO_2 contents of binders varies, e.g., 21% in Portland cement, 20% in natural cement, 27% in slag cement, 7 to 10% in hydraulic lime, etc., or, more preferably, from the average paste-SiO_2 content determined from SEM-EDS for binder content.

Losses on Ignition For Free & Combined Water Contents, and, Carbonate Content

Losses in weight of a mortar on step-wise heating from ambient to 110°C, 550°C, and 950°C temperatures liberate free water from capillary pore spaces by 110°C, combined water from dehydroxylation of various hydrous phases (calcium silicate hydrate, calcium hydroxide, etc.) by 550°C, and liberation of carbon dioxide from decomposition of carbonated paste and carbonate minerals by 950°C. Such losses in weight are measured by following the procedures of ASTM C 1324 by heating 1.00 gram of pulverized mortar (finer than 0.3 mm) in an alumina crucible in a muffle furnace in a controlled step-wise heating at a heating rate of 10ºC/min. Mortars having hydraulic binders and hydration products of such provide measurable combined water contents after calcination to 550°C whereas those having high calcareous components (high-calcium lime, mortar having calcareous sand) produce high weight loss during ignition to 950°C. Usually, a good correlation is found between weight losses at 550°C from dehydration of combined water and soluble silica contents contributed from hydraulic binders amongst series of mortars containing variable amounts of hydraulic phases.

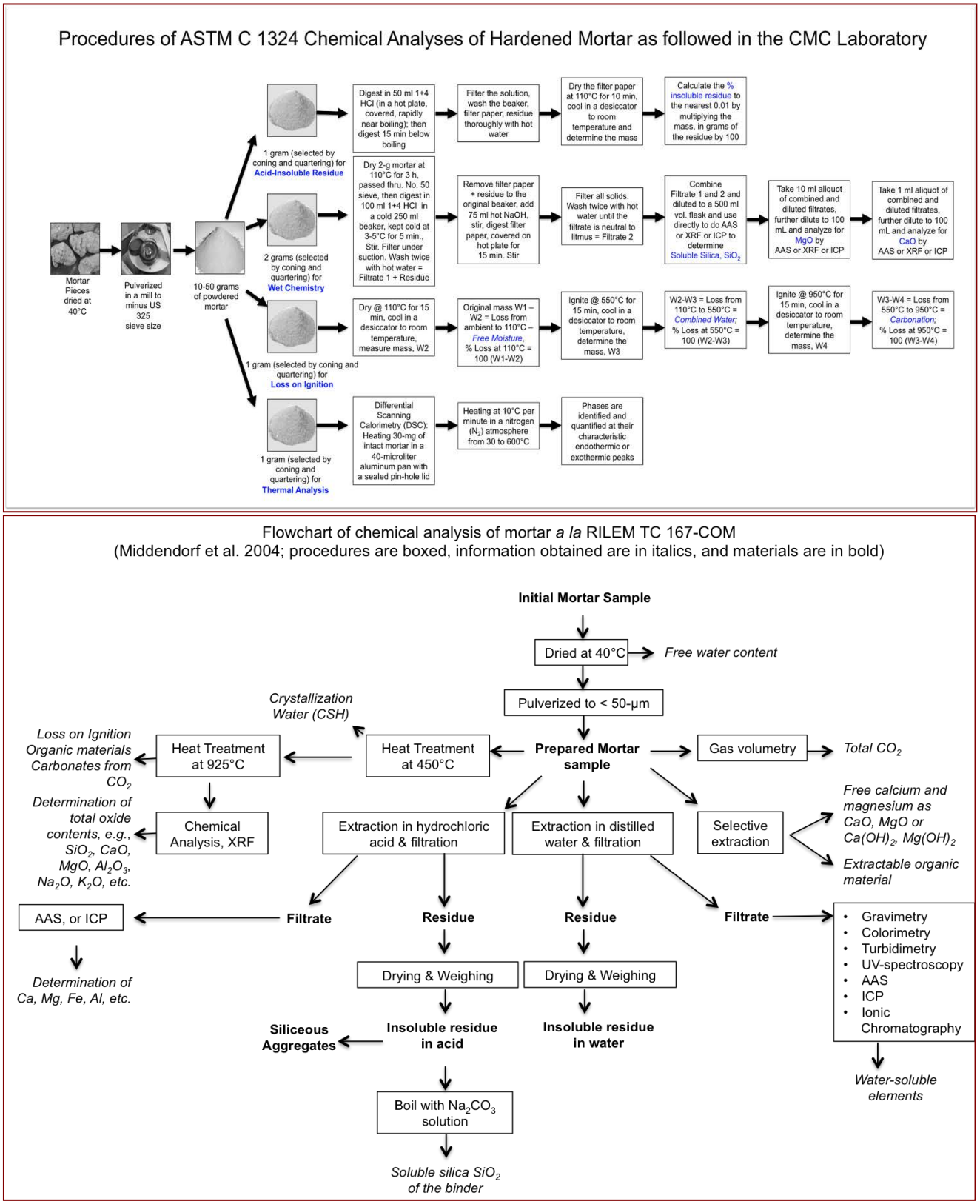

Figure A4: Flow charts for various chemical analyses of masonry mortar according to the US (top, ASTM C 1324) and European (bottom, RILEM) standards.

X-Ray Diffraction For Mineralogy of Mortar

X-ray diffraction (XRD) is a powerful method for: (a) determination of bulk mineralogical composition of mortar, including its aggregate and binder mineralogies (e.g., quartz in sand from major diffraction peaks at 26.65º, 20.85º, 50.14º 2θ, or calcite in sand or carbonated lime binder from major peaks at 29.41º, 39.40º, 43.15º 2θ, or Portlandite in binder from major peaks at 34.09º, 18.09º, 47.12º 2θ); (b) individual primary mineralogy and alteration products of aggregate at various size fractions, and binder phases; (c) detection of dolomitic lime binder from brucite in the mortar from major peaks at 38.02º, 18.59º, 50.86º 2θ; (d) detection of use of lime (portlandite), gypsum (11.59º, 20.72º, 29.11º 2θ), or cement binders from their characteristic mineralogies; (e) detection of any potentially deleterious constituents, e.g., deleterious salts, or efflorescence deposits; (f) detection of a mineral oxide-based pigmenting component in the mortar; and (g) detection of components that are difficult to detect by microscopical methods.

X-ray diffraction can be done on: (i) pulverized (to finer than 45 micron) portion of bulk mortar, or (ii) on the sand extracted from the mortar by acid digestion, if sand has a complex mineralogy, or also (iii) on the binder-fraction by separating the sand from the binder from a carefully ground mortar (in a mortar and pestle) and passing the ground mass through US 200 sieve (75 micron) to collect the fraction rich in binder. Since sands used in mortars are commonly siliceous, XRD pattern of bulk mortar shows quartz as the dominant mineral that surpasses peaks for all other phases (e.g., calcite, dolomite, clay, secondary deposits); hence binder separation is sometimes useful to detect minor minerals of interest (e.g., salts or pigments). For binder mineralogy, mortar is first dried at 40°C to a constant mass, then carefully crushed without pulverizing the sand, and sieved through a 75-micron opening screen to retain sand-rich fraction on the sieve and obtain the passed binder-rich fraction for further pulverization down to finer than 45 micron. Salts and other soft components can also be analyzed from binder fraction. Efflorescence salts on masonry walls are also analyzed routinely in XRD.

For sample preparation, a Rocklab (Sepor Mini-Thor Ring) pulverizer is used to grind mortar sample down to finer than 100 microns. Usually, a few drops of anhydrous alcohol are added to reduce decomposition of hydrous phases from the heat generated from grinding. Approximately 10 grams of sample is ground first in the pulverizer, from which about 8.0 grams of sample is selected, mixed with an appropriate binder (e.g., three Herzog grinding aid pellets from Oxford Instruments having a total binder weight of 0.6 gram for 8 grams of sample for a fixed binder proportion of 7.5 percent); the mixture is then further ground in Rocklab pulverizer and in a McCrone micronizing mill with anhydrous alcohol down to finer than 45-micron size. Approximately 7.0 grams of binder-mixed pulverized sample thus prepared is weighed into an aluminum sample cup and inserted in a stainless steel die press to prepare the sample pellet. A 25-ton Spex X-press is used to prepare 32 mm diameter pellet from the pulverized sample (see Figure A5 for sample preparation). The pressed pellet is then placed in a custom-made circular sample holder for XRD and excited with the copper radiation of 1.54 angstroms. Sample holders made with quartz or silicon are best for working with very small quantities of sample because these holders create no diffraction peaks between 2° and 90° 2θ (Middendorf et al. 2005).

XRD is carried out in a Siemens D5000 Powder diffractometer (θ-2θ goniometer) employing a long line focus Cu X-ray tube, divergent and anti-scatter slits fixed at 1 mm, a receiving slit (0.6 mm), diffracted and incident beam Soller slits (0.04 rad), a curved graphite diffracted beam monochromator, and a sealed proportional counter. Siemens D5000 is equipped with (a) a horizontal stage (fixed), (b) an X-ray generator with CuKα, fine focus sealed tube source, (c) large diameter goniometer (600 mm), low divergence collimator, and Soller slits, (d) fixed detector slits 0.05, 0.2, 0.6, 1.0, 2.0, and 6.0, and (e) Scintillation detector. Generator settings used are 40 kV and 30 mA. Tests are usually run at 2θ from 4° to 64° with a step scan of 0.02° and a dwell time of one second.

The resulting diffraction patterns are collected by DataScan 4 software of Materials Data, Inc. (MDI), analyzed by Jade software of MDI with ICDD PDF-4 (Minerals 2019) diffraction data. Phase identification, and quantitative analyses were carried out with MDI's Search/Match, Easy Quant, and Rietveld modules, respectively.

Figure A5: Siemens D5000 X-ray diffractometer in CMC that is connected to PC through MDI Datascan to collect diffraction data. XRD results are analyzed with MDI Jade software with search-match, easy quant, and Rietveld modules. The bottom row shows sample preparation for XRD where a Sepor Ring pulverizer (2nd from left) followed by McCrone micronizing mill (leftmost one) pulverized the sample to finer than 45-micron size. The pulverized sample is mixed with an appropriate binder and pressed in a 25-ton Spex press to form a 32-mm diameter pellet. Small amount of sample (i.e. not enough to prepare a pellet) is pulverized and spread over a quartz plate coated with a thin film of Vaseline.

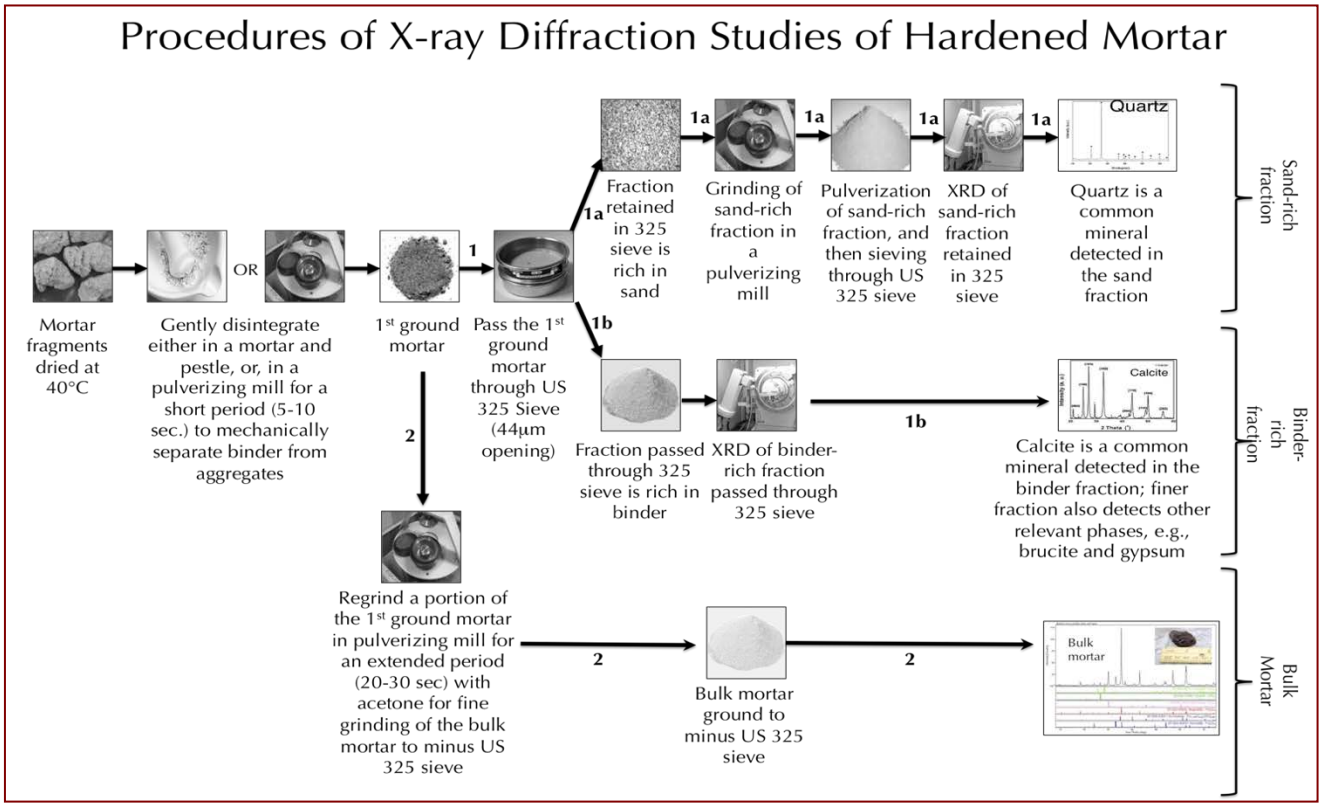

Figure A6: Various procedures for X-ray diffraction analysis of bulk mortar, and sand and/or binder fraction extracted from mortar.

X-Ray Fluorescence Spectroscopy For Chemical Composition of Mortar

X-ray fluorescence (XRF) is used for determining: (a) major element oxide composition of mortar, and (b) soluble silica content of filtrate after digestion of mortar in cold-HCl and hot-NaOH. Major element oxide compositions provide clues about the siliceous sand content of mortar from silica content, type of binder used (e.g., a dolomitic lime or natural cement based binder gives a characteristically higher magnesia than a calcitic lime or Portland cement based binder), calculation of lime content in a cement-lime mortar from bulk CaO content from XRF, effect of alterations and deteriorations (e.g., salt ingress in a mortar from marine environment can be diagnosed from excessive sodium, sulfate, etc.), etc. A series of standards from Portland cements, lime, gypsum, to various rocks, and masonry mortars of certified compositions (e.g., from USGS, GSA, NIST, CCRL, Brammer, or measured by ICP) are used to calibrate the instrument for various oxides and empirical calculations are done from such calibrations to determine oxide compositions of mortars. For mortars with highly unusual compositions (e.g. severely salt-contaminated mortar) a standardless FP calculation is done to determine the best possible composition.

An energy-dispersive bench-top X-ray fluorescence unit from Rigaku Americas Corporation (NEX-CG) is used (Figure A7). Rigaku NEX CG delivers rapid qualitative and quantitative determination of major and minor atomic elements in a wide variety of sample types with minimal standards. Unlike conventional EDXRF analyzers, the NEX CG was engineered with a unique close-coupled Cartesian Geometry (CG) optical kernel that dramatically increases signal-to-noise. By using monochromatic secondary target excitation, instead of conventional direct excitation, sensitivity is further improved. The resulting dramatic reduction in background noise, and simultaneous increase in element peaks, result in a spectrometer capable of routine trace element analysis even in difficult sample types. The instrument is calibrated by using various certified (CCRL, NIST, GSA, and Brammer) reference standards of cements and rocks. The same pellet used for XRD for mineralogical compositions is used for XRF to determine the chemical composition.

Figure A7: Rigaku NEX-CG in CMC, which can perform analyses of 9 pressed pellet or fused bead of mortar. Samples are prepared either as pressed pellet (usually the one already prepared for XRD) or can also accommodate fused bead with proper calibrate of standard beads.

Thermal Analyses For Determination of Hydrous, Carbonate, and Sulfate Phases in Mortar

Thermal analyses encompass: (1) thermogravimetric analysis (TGA), which measures the weight loss in a mortar as it is heated, where weight loss can be related to specific physical decomposition of a phase of interest at a specific temperature that is characteristic of the phase from which both the phase composition and the abundance can be determined; (2) differential thermal analysis (DTA, or first derivative of TGA i.e. DTG) measuring temperature difference between the sample and an inert standard (Al_2O_3) both are heated at the same rate and time where endothermic peaks are recorded when the standard continues to increase in temperature during heating but the sample does not due to decompositions (e.g., dehydration of hydrous or decarbonation of carbonate phases); the endothermic or exothermic transitions are characteristic of particular phase, which can be identified and quantified using DTA (or DTG); and (3) differential scanning calorimetry (DSC), which follows the same basic principle as DTA, whereas temperature differences are measured in DTA, during heating using DSC energy is added to maintain the same and the reference material (Al_2O_3) at the same temperature; this energy use is recorded and used as a measure of the calorific value of the thermal transitions that the sample experiences; this is particularly useful for detection of quartz that undergoes polymorphic (α to β form) transitions and no weight loss.

Thermal analyses are done to determine the presence and quantitative amounts of: (a) hydrates (e.g., combined water liberated from paste dehydration during decomposition of calcium-silicate-hydrate component in paste at 180-190ºC); (b) sulfates (gypsum from decompositions at 125ºC, and 185-200ºC, ettringite at 120-130ºC, thaumasite at 150ºC); (c) brucite from its dehydroxylation at 300-400ºC to confirm the presence of dolomitic lime; (d) hydrate water from decomposition of Portlandite component of paste at 400-600ºC; (e) quartz from

polymorphic transformation (α to β form) at 573ºC; (f) cryptocrystalline calcite in the carbonated lime matrix from decomposition at 620-690ºC, or magnesite at 450-520ºC, or (g) coarsely crystalline calcite e.g., in limestone by decomposition at 680-800ºC or (h) dolomite at 740-800ºC and 925ºC, and (i) phase transition of belite (C_2S) at 693ºC, etc. Phases are determined from their characteristic decomposition temperatures occurring mostly as endothermic peaks or polymorphic transition temperatures as for quartz.

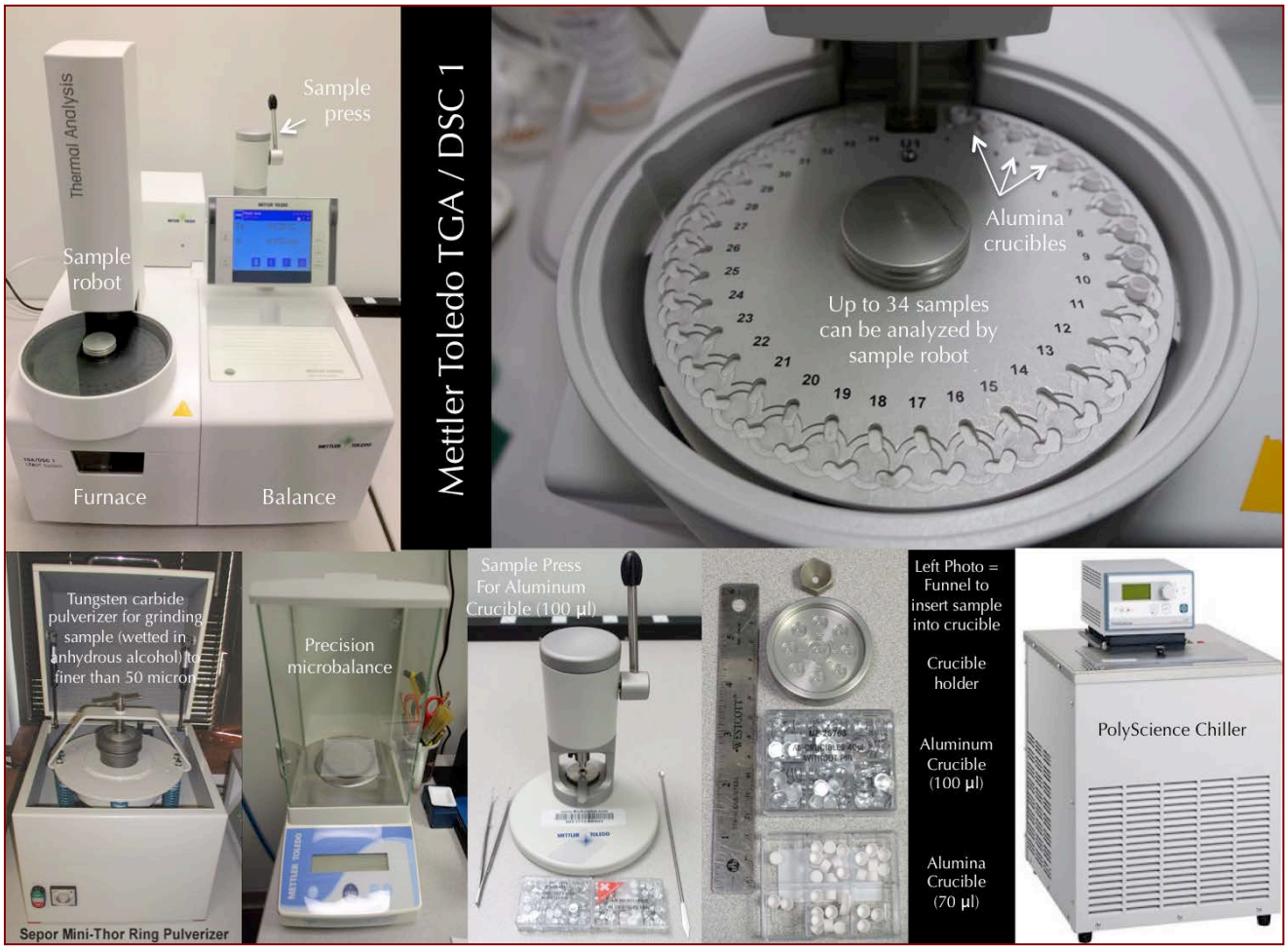

Figure A8: Mettler-Toledo simultaneous TGA/DSC1 unit in CMC that can accommodate 32 samples. The top left photo shows the TGA/DSC1 unit with sample robot for automation as well as the sample holder for pressing aluminum sample holders. Sample is pulverized in a ring pulverizer shown in the bottom left, then a small amount (usually 30-70 mg) is weighed in a precision balance (shown 2nd from left in bottom row) and taken in an alumina sample holder (without lid). For DSC measurements up to 600°C, sometimes sample is taken in an aluminum holder and pressed in sample press (3rd from left in bottom row) and pierced with a needle for release of volatiles from decomposition. A PolyScience chiller (rightmost one in the bottom row) is used to cool the furnace. An ultrapure nitrogen gas is purged through the system during analyses.

Simultaneous TGA and DSC analyses are done in a Mettler Toledo TGA/DSC 1 unit (Figure A8) on 30-70 mg of finely ground (<0.6 mm) mortar in alumina crucible (70 µl, no lid) from 30°C to 1000°C at a heating rate of 10°C/min with high purity nitrogen as purge gas at a flow rate of 75.0 ml/min. By using one of the three removable sensor types the TGA/DSC 1 simultaneously measures heat flow in addition to weight change. The instrument offers high resolution (ultra-microgram resolution over the whole measurement range), efficient automation (with a reliable sample robot for high sample throughput), wide measurement range (measure small and large sample masses and volumes) broad temperature scale (analyze samples from ambient to 1100°C), superior ultra-micro balance, simultaneous DSC heat flow measurement (for simultaneous detection of thermal

events, e.g., polymorphic alpha-to-beta transition of quartz and quartz content), and a gastight cell (ensures a properly defined measurement environment).

Infrared Spectroscopy For Determination of Organic Components in Mortar

Fourier-transform infrared spectroscopy (FT-IR) measures interaction between applied infrared radiation and the molecules in the compounds of interest (Middendorf et al. 2005). Bonds between atoms have distinctive geometrics and natural states of rotation and vibration. Incident infrared radiation will excite these vibrations and rotations when a critical wavelength is reached that can impart energy to the bond. At this point the atomic bond that is being excited will absorb that wavelength of infrared radiation. If the sample is placed between the source of radiation and a detector these times of absorption of infrared radiation can be recorded as reduced intensity and can be related to specific types of atomic bonds characteristic of particular functional groups in compounds (e.g., CO^{3-}group in carbonates). FT-IR is particularly useful for detection of admixture, additives, and polymer resins. FT-IR is used mainly to identify various organic components (functional groups) in mortar (e.g., methyl CH_3, organic acids CO-OH, carbonates CO_3) from their characteristic spectral fingerprints in FT-IR spectrum. FT-IR can also be used for detection of main mineral phases in a hydraulic binder, CSH, carbonates, gypsum, and clays (Middendorf et al. 2005). Organic compounds such as synthetic (e.g., acrylics, polyesters) and natural resins, carbohydrates, colorants, oils and fats, proteins, waxes as well as inorganic compounds, e.g., corrosion products, minerals, pigments, paints, fillers, stone, glass, and ceramics can be detected by this technique.

FT-IR measurements are done in a Perkin Elmer Spectrum 100 FT-IR spectrophotometer (Figure A9) running with Spectrum 10 software. Samples were measured using attenuated total reflection (ATR) on a single bounce diamond/ZnSe ATR crystal. Sample was measured between a frequency range of 4000 to 650 cm^{-1}. Each run was collected at 4 cm^{-1} resolution with Strong Beer-Norton apodization. Data were collected with a temperature-stabilized deuterated triglycine sulfate (DTGS) detector by placing the sample in contact with the ATR crystal and by applying force from the pressure applicator supplied with the ATR accessory. The application of pressure enabled the sample to be in intimate contact with the ATR crystal, ensuring a high-quality spectrum was achieved. Additionally, more conventional KBr pellet is also used for samples on as-needed basis.

Figure A9: Perkin Elmer Spectrum 100 FT-IR unit in CMC with Universal ATR and Liquid Sipper attachments. The FT-IR unit can analyze a sample as-received in the Universal ATR (left), or as a pressed pellet after mixing with KBr powder in a KBr press (middle), or as a liquid either directly in Universal ATR or in Liquid Sipper unit (right).

Ion Chromatography For Determination of Water-Soluble Cations and Anions in Mortar

Salts can cause various deteriorations in masonry from: (a) mere aesthetic issues of surface efflorescence by precipitation from evaporation of leachates on the masonry wall surfaces followed by atmospheric carbonation of the precipitates where salts deposit as individual crystals or as crust to (b) more serious internal distress in mortar and masonry units from crystallization inside the pores (sub-fluorescence or crypto-fluorescence) from expansive forces associated with crystallization of salt from supersaturated solutions. Some common salts in masonry are calcium carbonates (e.g., calcite, vaterite), magnesium carbonate (magnesite), sodium carbonate hydrate and bicarbonate (thermonatrite, trona, nahcolite), sulphates (gypsum, thenardite, epsomite, melanterite, mirabilite, glauberite, or ettringite and thaumasite from oxidation of sulfides or cement hydrates), and chlorides (halite, sylvite, calcium oxychloride from deicing salts, salt-bearing aggregates, ground water). X-ray diffraction and SEM-EDS can determine many of these salts as long as they are present in detectable amounts.

Ion chromatography is an established technique for analyses of various water-soluble anions and cations in salts (e.g., chloride, sulfate, and nitrate anions, and magnesium, calcium, alkali, ammonium cations) to assess magnitude of environmental impacts on masonry units and mortars, and subsequent effects of such salt ingress. Masonry samples are pulverized, digested in ultrapure deionized water to dissolve all water-soluble salts, then solid residues are filtered out, and finally water-digested filtrates are analyzed by an ion chromatograph.

Procedures followed in Ion chromatography are described in ASTM D 4327 "Standard Test Method for Anions in Water by Chemically Suppressed Ion Chromatography." Briefly, an aliquot of 1 gram of pulverized sample (passing No. 50 sieve) is digested in 50 ml distilled water for 6 to 8 hours on a magnetic stirrer at a temperature below boiling point of water; then the digested sample is filtered through two 2.5-micron filter papers using vacuum, followed by a second filtration through micro-filter (0.2 micron) paper, then the filtrate is either used directly or diluted to 100 to 250 ml with distilled water depending on the concentration of ions, and used for analysis to get ppm-level cations (calcium, magnesium, sodium, potassium, lithium, ammonium), and anions (fluoride, chloride, nitrite, bromide, nitrate, phosphate, and sulfate) in the water-digested sample in Metrohm IC units (Figure A10). The instruments are calibrated against multiple custom-made Metrohm standard solutions having all the ions of interest from 0.1-ppm to 100-ppm levels. To check the accuracy of the instrument, a 50-ppm standard solution was run first prior to the analysis of samples.

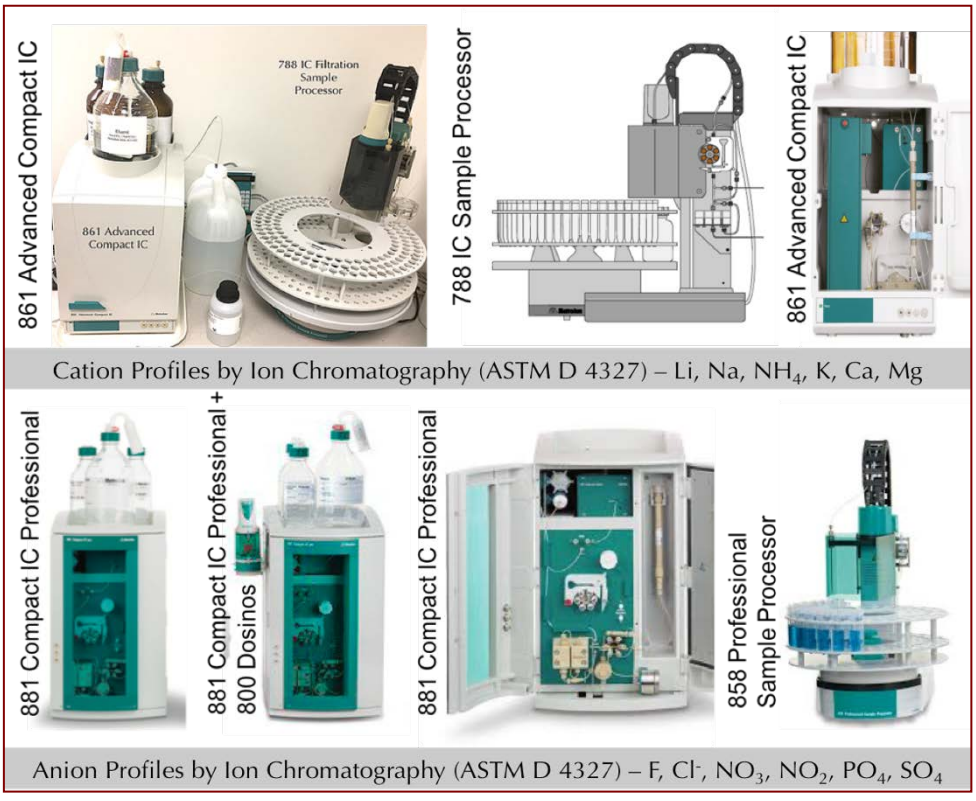

Figure A10: Various ion chromatography units used in CMC for determination of water-soluble ions after digestion of pulverized masonry mortar in deionized water to determine various anions (sulfate, chloride, nitrate, nitrite, phosphate, bromide) extracted from mortar.

Information Obtained from Various Laboratory Methods

Information	Optical Microscopy	SEM-EDS	XRD	XRF	Chemical (Gravimetry)	Chemical (Titration & IC)	Sieve Analyses of Sand	Thermal	FTIR
Mortar Sand Type	X	X	X	X					
Sand Composition	X	X	X	X					
Sand Mineralogy	X	X	X						
Sand Soundness	X	X							
Sand Fineness	X						X		
Sand Grading & Color	X						X		
Mortar Binder Type(s)	X	X	X					X	
Binder Composition	X	X	X					X	
Binder Microstructure	X	X							
Portland Cement	X	X	X	X				X	
Hydrated Calcitic Lime	X	X						X	
Dolomitic Lime	X	X	X					X	
Hydraulic Lime	X	X						X	X
Masonry Cement	X	X							
Natural Cement	X	X							
Carbonation	X	X	X					X	X
Carbonated Paste vs. Carbonate Sand	X							X	
Fillers	X	X						X	
Organic Components		X						X	X
Surface Treatments	X	X				X			X
Clay Contaminants	X		X					X	X
Mortar Type	X	X			X				
Masonry Discoloration	X	X	X	X		X		X	
Masonry Cracking	X	X	X						
Mortar Softening	X	X			X				
Mortar Crumbling	X	X	X		X				
Mortar Cracking	X	X	X	X			X	X	
Mortar Discoloration	X	X	X	X		X			
Mortar Shrinkage, Stiffening	X	X							
Bond to Masonry	X	X							
Masonry Efflorescence	X	X	X	X					

Information	Optical Microscopy	SEM-EDS	XRD	XRF	Chemical (Gravimetry)	Chemical (Titration & IC)	Sieve Analyses of Sand	Thermal	FTIR
Salt Attack	X	X	X			X		X	
Lime Leaching	X	X				X			
Polymer		X						X	X
Mix Proportion	X	X	X	X	X				
Tuckpointing Mortar Suggestions	X	X	X	X	X		X	X	X
Miscellaneous Failure Analysis	X	X	X	X	X			X	X

Table 8: Information obtained from various laboratory methods.

Steps Followed in Laboratory Analyses

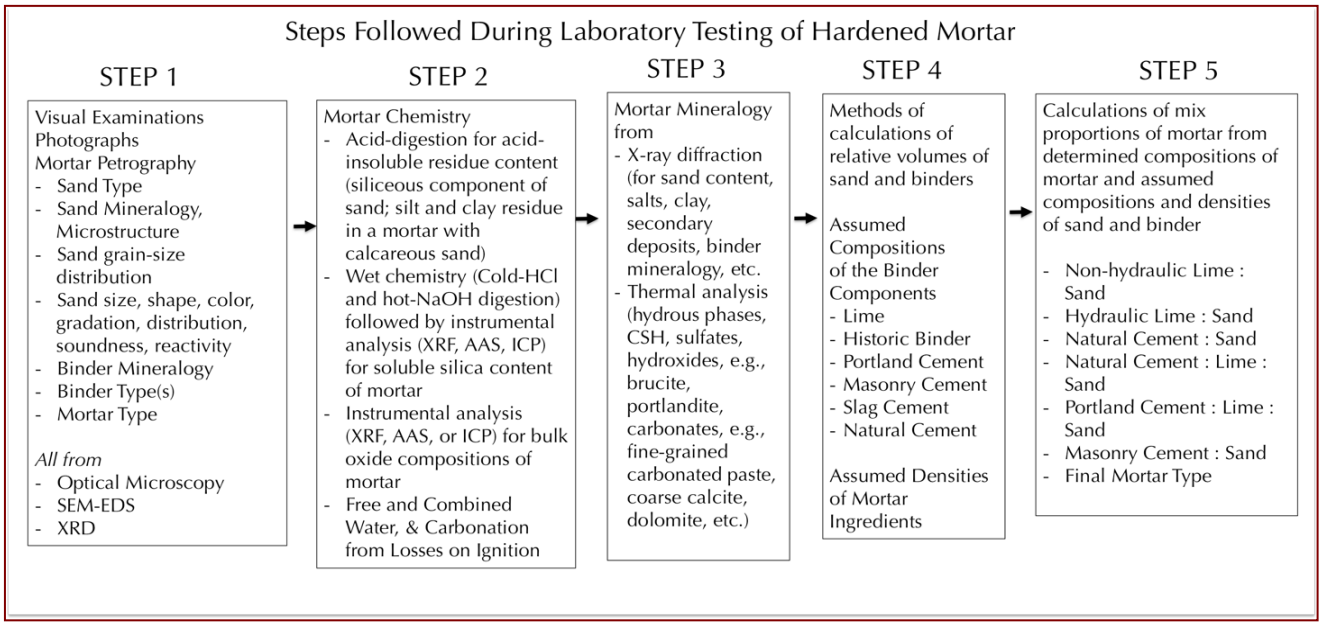

Figure A11: Sequence of steps commonly followed during laboratory analyses of masonry mortars.

Mix Calculations From Petrography & Chemical Analyses of Mortar

ASTM C 1324 provides procedures of calculations of volumetric proportions of Portland cement, lime, and sand in a modern cement-lime mortar containing siliceous or calcareous sand, and proportion of Portland cement in a masonry cement and masonry cement to sand proportion in a masonry cement mortar. Such approaches can be extended for other mortars having other binder types from non-hydraulic lime, to hydraulic lime, to natural cement, slag cement etc. These approaches, however, are based on many underlying assumptions that are important to know and verify against the results of laboratory tests to validate for a particular mortar, especially of historic nature. For example, for mix calculations in a common modern-day Portland cement-lime-silica sand mortar, such approach assumes fixed composition of cement (21% silica and 63.5% lime), fixed composition of magnesian or dolomitic lime (brucite), negligible effect of pozzolanic and other cementitious materials, negligible soluble silica or lime contribution from sand, etc. The following Figure provides examples of various approaches of mix calculations for mortars containing a wide range of sand and binder.

Binders and Sand	Assumed Compositions and Methods of Calculation	Assumed Bulk Density (lbs./ft^3)
High-Calcium Non-hydraulic Lime	[CO_2 data from loss on ignition at 950°C divided by 0.594], where 0.594 is ratio of molecular weights of CO_2 to $Ca(OH)_2$ i.e. 44/74.09	40
Magnesian Non-hydraulic Lime	[100 times (brucite content in mortar from TGA/DSC/5.8)], assuming magnesian lime has 71% CaO and 4% MgO, or 5.8% brucite, since ratio of molecular weights of brucite to MgO (58.32 / 40.32) is 1.447	40
Dolomitic Non-hydraulic Lime	[100 times (brucite content in mortar from TGA or DSC divided by 42)], assuming dolomitic lime has 41% CaO and 29% MgO, or 42% brucite, since ratio of molecular weights of brucite to MgO (58.32 / 40.32) is 1.447	40
Calcitic or Magnesian Hydraulic Lime	[100 times (soluble silica in mortar/0.07] assuming hydraulic lime has 7% SiO_2, or average SiO_2 content calculated from SEM-EDS data of paste	40
Dolomitic Hydraulic Lime	[100 times (soluble silica in mortar/0.07] assuming hydraulic lime has 7% SiO_2, or average SiO_2 content calculated from SEM-EDS data of paste Or [100 times (brucite content in mortar from TGA/DSC/38)], assuming lime has 38% CaO and 26% MgO, or 38% brucite, since ratio of molecular weights of brucite to MgO (58.32 / 40.32) is 1.447	40
Portland Cement in Cement-Lime Mortar	100 × [Soluble silica in mortar / 21.0], assuming 21% silica in Portland cement	94
Calcitic Lime in Portland Cement-Lime Mortar	Lime content = 1.322 × CaO assignable to Lime, which is [CaO content of Mortar – (CaO assignable to portland cement, which is portland cement content × 0.635, assuming 63.5% CaO in portland cement)], where the factor 1.322 comes from ratio of molecular weights of $Ca(OH)_2$ to CaO i.e. 74.09/56.03	40
Dolomitic Lime in Portland Cement-Lime Mortar	100 times (brucite content in mortar from TGA/DSC/42)], assuming dolomitic lime has 41% CaO and 29% MgO, or 42% brucite, since ratio of molecular weights of brucite to MgO (58.32 / 40.32) is 1.447	40
Slag Cement	100 × [Soluble silica in mortar / 27.0], assuming 27% silica in slag cement, or average SiO_2 content determined from SEM-EDS data	90
Natural Cement	100 × [Soluble silica in mortar / 20.0], assuming 20% silica in natural cement, or average SiO_2 content determined from SEM-EDS data	75
Masonry Cement	(i) 100 – [Sand + Total Water], if sand is all siliceous and hence sand content is obtained directly from the acid-insoluble residue content; (ii) PC content (from the soluble silica data) divided by factor 0.50, 0.66, or 0.75 with an assumed masonry cement type of N, S, or M, respectively. MC Type (M, S, N) is determined from PC/MC = 0.75 (for M), 0.66 (for S), or 0.50(for N) – if sand has calcareous component	70 (Type N) 75 (Type S) 80 (Type M)
Gypsum Plaster	Gypsum content from XRD or thermal analysis times 0.843 (ratio of molecular weight of plaster to gypsum)	70
Sand	If sand contains acid-soluble component (carbonates), Sand content = 100 – [Total Binder + Total Water from LOI to 550°C i.e. free plus hydrated water]; If sand has no acid-soluble component (i.e. all siliceous sand) Sand content is directly obtained from the acid-insoluble residue content	80

Figure A12: Various procedures followed for calculations of binder-to-sand volumetric proportions from (a) the determined sand and binder, (b) calculated contents of ingredients, and (c) assumed bulk densities of sand and binders.

Flow Chart of Procedures Followed in Laboratory Analyses of Masonry Mortars

Finally, Figure A13 provides step-by-step procedures followed during laboratory analyses of masonry mortars.

Laboratory Analyses of Masonry Mortars

Initial Mortar (50 to 100 grams) [Photographed with digital camera & flat-bed scanner, As-received condition, total weight, and dimensions of largest piece are documented]

Intact Pieces (20+ g)

1. *Optical Microscopy*

I. Perform visual examination of mortar as received, then saw-cut and fractured surfaces and with a low-power stereomicroscope,
II. Take digital and flat bed scanner photos of intact piece(s),
III. Encapsulate the piece for thin section microscopy in a flexible mold with a low-viscosity colored or fluorescent dye-mixed epoxy to highlight voids, pores, cracks, etc.,
IV. Prepare thin section (< 30 micron thickness) and polish the thin section for optical and SEM-EDS analyses,
V. Scan the thin section on a flat-bed scanner with the thin section residue,
VI. Take transmitted light high-power stereo-zoom photomicrographs of thin sections from different areas to be stitched to determine volumes and size distributions of pore spaces and sand grains by Image J,
VII. Take plane and crossed polarized-light photomicrographs of sand and binder fractions in thin section from a petrographic microscope and determine areas for further studies by SEM-EDS,
VIII. Do detailed petrographic examinations to determine the sand and binder compositions, sand mineralogy and texture, binder phases, residual binders, alterations, and products of any deleterious reactions, immersion mounts of specific areas of interest, etc.

2. *SEM-EDS*

I. Put conductive coating only on the portion of polished thin section intended for SEM-EDS studies from optical microscopy,
II. Take backscatter and/or secondary electron images, and if needed X-ray elemental maps,
III. Select multiple areas on paste to determine oxide compositions and Eckel's cementation indices,
IV. Tabulate the paste composition variations across the backscatter/secondary electron image.
V. Determine chemical compositions of resides left from the original components of the binders, as well as the hydration and carbonation and other alteration products

Lightly hand-ground in a Mortar & Pestle (30+ g)

3. *Acid Digestion - Sand Color & Sand Size Distribution* (10 g)

I. Take 10 g. of mortar lightly ground in mortar & pestle and digest in HCl (1+3) in a 250 ml beaker on a magnetic stirrer until all sand separates and settles at the bottom of beaker,
II. Filter all through two 2.5 micron filter paper, wash the beaker, filter paper, and all sand residue with dist. water,
III. Dry the residue at 110°C in an oven for 10 min., gently brush out from the filter paper and collect, then sieve the entire sand residue through No. 4 through 200 sieves in a mini sieve shaker (e.g., from Gilson),
IV. Determine the mass retained on each sieve, and on the pan (finer than No. 200 sieve),
V. Take photomicrographs of sand particles retained on each sieve for sand color variations in a stereomicroscope.

4. *Acid & Alkali Digestion – Soluble Silica for Hydraulic Binder* (5 g)

I. Grind 10 g of lightly ground fraction from mortar & pestle in a WC pulverizer for 30 sec.
II. Sieve thru. No. 50 sieve, collect the fraction passing the sieve,
III. Re-grind the residue retained on sieve for 15 sec. and mix thoroughly with the previous fraction;
IV. Use 5.00 g of thus prepared powder (passing No. 50 sieve) for digestion in 100 ml cold (3-5°C/38-41°F) HCl (1+4) in a 250 ml beaker for 15 min. on a magnetic stirrer,
V. Filter thru. two 2.5 micron filter paper and keep the filtrate# 1,
VI. Digest the residue with filter paper in 75 ml hot NaOH (below boiling) on hot plate for 15 min. on magnetic stirrer,
VII. Cool down to room temp. and filter thru. two 2.5 micron filter paper and collect filtrate# 2,
VIII. Combine these two filtrates, filter the combined filtrates thru. two 2.5 micron filter paper to remove any suspended silica (especially for sand-rich mortars, or if mortar is grounded too long); then dilute to 250 ml in a volumetric flask with dist. water, an aliquot (about 10 ml) is then used for XRF for soluble silica determination against the calibrations with standard PC mortars of known soluble silica contents prepared in the same way.

5. *Acid Digestion – Acid-Insoluble Residue Content for Siliceous Sand Content* (2 g)

I. Take 1-2 g of prepared mortar powder from Step 4 iii (passing No. 50 sieve) and digest in 50 ml HCl (1+3) in a 250 ml beaker (covered) on a hot pate rapidly near boiling, then 15 min. at a temp. below boiling, then cool down to room temperatures,
II. Filter thru. two pre-weighed 2.5 micron filter papers, washing the beaker, paper, and residue thoroughly with hot water,
III. Dry the filter paper at 110C for 10 min, cool in a desiccator to room temp. and measure the weight.
IV. Subtract from mass of dry filter paper to determine acid-insoluble residue content.

6. *Chemical Analysis – Loss On Ignition for Free and Combined Water Content, and Carbonate plus Carbonation* (2 g)

I. Take 1-2 g (W_1) of prepared mortar powder from Step 3 iii (passing No. 50 sieve) in a tarred porcelain crucible (keep a record of mass of the empty crucible),
II. Dry at 110°C for 15 min in a muffle furnace pre-set to 110°C, cool in a desiccator to room temp. and measure the mass (W_2) by subtracting the empty crucible mass from the total mass,
III. Ignite at 550°C for 15 min. in the muffle furnace pre-set to 550°C, cool in a desiccator to room temp. and measure the mass (W_3) by subtracting the empty crucible mass from the total mass,
IV. Ignite at 950°C for 15 min. in the muffle furnace pre-set to 950°C, cool in a desiccator to room temp. and measure the mass (W_4) by subtracting the empty crucible mass from the total mass,
V. Calculate the losses on ignition at 110°C, 550°C, and 950°C for free water, combined water, and carbonate plus degree of carbonation, respectively.

7. *Mineralogy of Bulk Mortar, Extracted Sand, Extracted Binder, or Salt from XRD* (at least 8 g)

I. Weigh 8.00 g of mortar (or extracted sand or binder as needed) lightly ground in a mortar & pestle, add three grinding/pelletizing aid tablets (e.g., from Oxford Instruments) and pulverize in a suitable mill to minimize contamination (e.g., Rocklab pulverizer with WC bowl or McCrone Micronizing Mill with agate) for 3 min. with anhydrous alcohol to get <45 micron size particles passing U.S. No. 325 sieve,
II. Take 6.8 to 7.0 g. of ground <45 micron prepared mass in an aluminum sample holder inside a stainless steel die to prepare a 32 mm pellet with 25 ton pressure for 1 min,
III. Use the prepared pellet for XRD and then use the same pellet for XRF.
IV. Do XRD on the binder-rich fraction, or salt either on a shallow-depth sample holder or preferably on a zero background quartz plate for small volume of sample.

8. *Bulk Mortar's Composition from X-Ray Fluorescence (XRF)* (same pellet used in XRD)

I. Use the same pellet prepared for XRD in the XRF, or, use a fused bead if sample volume is low to prepare a pellet. In either method, have calibrations of measured oxides with adequate standard.
II. XRF can also be used with proper calibrations for soluble silica determination on the filtrates after acid and alkali digestions, as described in Section 3.

9. *Thermal Analyses* (0.1 g), TGA, DTG, DSC, DTA, for quantitative analysis of various hydrous, sulfate, and carbonate phases in mortar, content of dolomitic lime added from the brucite content in mortar as determined from TGA or DSC, etc.

I. Simultaneous TGA and DSC analyses can be done on 30-70 mg of finely ground (<0.6 mm) mortar in alumina crucible (70 µl, no lid) from 30°C to 1000°C at a heating rate of 10°C/min with high purity nitrogen as purge gas at a flow rate of 75.0 ml/min .

10. *Infrared Spectroscopy,* for determination of various organic additives, and clays in mortar

I. Take an aliquot of powder prepared for thermal analysis and use that in Universal ATR of FTIR.
II. Alternately, digest a pulverized mortar in acetone to extract the organic additive and analyze the liquid in FTIR for characteristic functional groups.

11. *Ion Chromatography of Water-Soluble Salts* (1 g)

I. Take an aliquot of 1 gram powder prepared for chemical analysis (i.e. passing U.S. No. 50 sieve), digest in distilled or deionized water for at least 24 hours in a beaker on a magnetic stirrer, filter the solid residues out to collect the filtrate and analyze the filtrate for soluble salts (chloride, sulfate, nitrate, nitrite, phosphate, etc.) by ion chromatography.

Figure A13: Step-by-step procedures followed for various laboraotry analyses of masonry mortars.

END OF REPORT[2]

[2] The CMC logo is made using a lapped polished section of a 1930's concrete from an underground tunnel in the U.S. Capitol.